TECHNICAL REPORT NO. 8641

DEVELOPMENT AND FABRICATION OF RING LASER SYSTEMS

P. H. LEE

FACILITY FORM 602
N67-35629 (ACCESSION NUMBER)
178 (PAGES)
CR-88193 (NASA CR OR TMX OR AD NUMBER)
(THRU) 1
(CODE) 16
(CATEGORY)

THE PERKIN-ELMER CORPORATION

CONTRACT NO. NAS 8-11669

DECEMBER 1966

National Aeronautics and Space Administration
G. C. Marshall Space Flight Center
Huntsville, Alabama

TECHNICAL REPORT NO. 8641

DEVELOPMENT AND FABRICATION OF RING LASER SYSTEMS

P. H. LEE

THE PERKIN-ELMER CORPORATION

CONTRACT NO. NAS 8-11669

DECEMBER 1966

National Aeronautics and Space Administration
G. C. Marshall Space Flight Center
Huntsville, Alabama

APPENDIX III

THE PERKIN-ELMER CORPORATION

NEW TECHNOLOGY INTERIM REPORT

October 14, 1965

TABLE OF CONTENTS

Section	Title	Page
I	THEORY AND OPERATION OF RING LASER ROTATION SENSOR	1
II	OPTICAL COMPONENTS AND MECHANICAL STRUCTURE	13
	A. Pressure Tight Housing	13
	B. Invar Supporting Frame	13
	C. Adjustable Mirror Mounts	13
	D. Plasma Tubes	16
	E. Plasma Tube Supports And Heat Shields	16
	F. Variable Loss Control	18
	G. PZT Mirror Pusher	19
	H. Mirror And Beam Extractor Prism	19
	I. Shovel Nose Prism And Interferometer Prism	19
	J. Nonreciprocal Transmission Element	20
	K. Nonreciprocal Bias Element	22
III	ELECTRONIC SYSTEMS	25
	A. Laser Tuning Servo	25
	B. Laser Intensity Servo	26
	C. Laser Filament Supply And Plasma Voltage Source	29
	D. Plasma Current Control	29
	E. Beat Frequency Offset And Measurement	29
	F. Temperature Control Servo	30
IV	RESULTS OBTAINED	31
	A. Earth's Rotation	31
	B. Magnetic Field Sensitivity	31
	C. Beat Stability	32
	D. Beat Pushing	32
	E. Bias Current Calibration	33
	F. Plasma Current Balance	33
V	CONCLUSIONS AND RECOMMENDATIONS	37

LIST OF APPENDICES

Appendices	Title	Page
I	OPERATION MANUAL, ELECTRONIC CIRCUITS, AND PARTS LIST	I-i
II	MEASUREMENT OF SATURATION INDUCED OPTICAL NONRECIPROCITY IN A RING LASER PLASMA	II-i
III	INTERIM NEW TECHNOLOGY REPORT	III-i

LIST OF ILLUSTRATIONS

Figure	Title	Page
1	Beat Frequency Variation vs. Resonator Tuning, for Different Beam Power Ratios (Curve A, ratio = .81; Curve B, ratio = .59)	3
2	Ring Laser Optical Configuration	6
3	Laser Total Output vs. Frequency	10
4	Laser Output in Automatic Control Mode	10
5	Optical Components	14
6	Adjustable Mirror Mount	15
7	Plasma Tubes Used In Ring Laser	17
8	(No Title)	18
9	(No Title)	20
10	(No Title)	21
11	(No Title)	22
12	Nonreciprocal Bias Element and Mount	23
13	(No Title)	26
14	System Block Diagram	27/28
15	Representative Scans of Length Versus Analog Conversion of Beat Frequency Output, Nonreciprocal Gain Set So Sum Intensity in Order A Goes Negative, In Order B Goes Positive.	34
16	Representative Scans of Length Versus Analog Conversion of Beat Frequency Output, Nonreciprocal Gain Set so Sum Intensity in Order A Goes Negative, In Order B Goes Nearly Constant.	35
17	Beat Frequency vs. Nonreciprocal Bias Element Current	36

ABSTRACT

This report covers the development and fabrication of a new ring laser system. Our approach was based in part on the desire to make the instrument itself a successful rotation sensor, and with the hope of discovering or measuring effects important to the advancement of the state-of-the-art.

The theory and operation of the Ring Laser Rotation Sensor is presented. The instrument and its component parts are described in detail. The laser embodies a complex optical resonator having controls for gain, nonreciprocal time delay, nonreciprocal transmission, and overall loss. The report also gives the system performance and our Conclusions and Recommendations.

SECTION I

THEORY AND OPERATION OF RING LASER ROTATION SENSOR

In the first paper suggesting the use of a ring laser for angular rotation sensing, Rosenthal[1] showed that the sensitivity to be expected will be:

$$\Delta F = \frac{4A}{P\lambda} \Omega$$

where

A is the ring area normal to the axis of rotation

P is the perimeter of the ring

λ is the wavelength of light

(all above measured in the same units of length)

Ω is the angular rotation rate in rad/sec

ΔF is the beat frequency between the counter-rotating laser modes in Hz

In the same paper, Rosenthal suggested the use of a ring laser for the measurement of any and all other forms of optical nonreciprocity, including those effects on the beams resulting from the Fizeau Drag of a moving dielectric medium and the Faraday Effects of optical materials in a magnetic field.

---

[1] A.H. Rosenthal, "Regenerative circulatory multiple-beam interferometry for the study of light-propagation effects," Journal of the Optical Society of America, Vol. 52, pp. 1143-1148, October 1962.

These various, nonreciprocal effects each contribute to the beat frequency output from an angular rotation sensor and could cause significant errors in the rotation rate measurement. An example of such an extraneous effect error is the beat contribution resulting from the nonreciprocity in the index of refraction of the gas laser plasma itself. This inherent nonreciprocal effect was first discovered at Perkin-Elmer some months before this contract was started and was subsequently measured carefully. A description of the measurement procedure, and a comparison of results with laser theory, was published recently[2]. A copy of that publication is bound with this report as Appendix II.

The nonreciprocity in index of refraction of the excited gas causes an error in the beat frequency which is independent of the rotational bias--no matter how large. It is sometimes called a "pushing" effect and should not be confused with "pulling" or "locking" errors which can be completely eliminated by a large rotational bias. In normal operation, the laser is biased to give a beat frequency of 40 kHz.

The nonreciprocal dispersion error varies as the resonant cavity is tuned across the Doppler gain line with characteristic dispersion curve shapes drawn at the top of Figure 1. The bottom of Figure 1, drawn on the same horizontal frequency axis, shows a typical power output curve at corresponding cavity tuning frequencies.

---

[2] P.H. Lee and J.G. Atwood "Measurement of Saturation Induced Optical Nonreciprocity in a Ring Laser Plasma," IEEE Quantum Electronics, Vol. QE-2, pp. 235-243, August 1966.

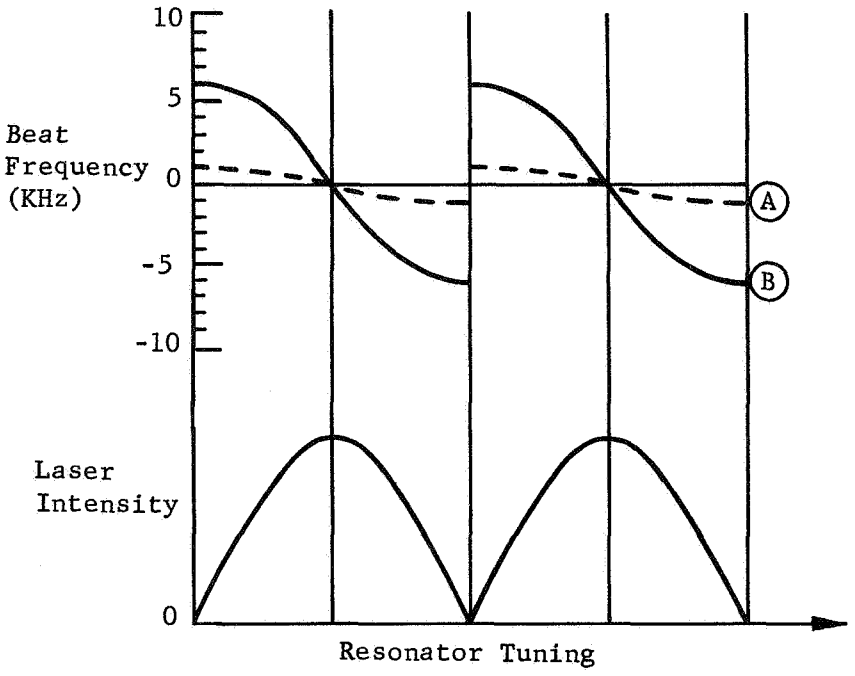


Figure 1. Beat Frequency Variation vs. Resonator Tuning, for Different Beam Power Ratios (Curve A, ratio = .81; Curve B, ratio = .59)

In addition to variation with cavity tuning, the nonreciprocal dispersion error also varies with the difference in power, ΔI, between the clockwise and the counterclockwise going beams as shown by the dotted curves in Figure 1.

The angular rate accuracy goal specified by this contract is 1 arc-sec/sec. The sensitivity of a He-Ne ring laser of the size contemplated is approximately 2 Hz/arc-sec/sec. In the early experimental ring lasers used for the measurement of the nonreciprocal dispersion effect, we were never able to reduce the random error attributed to noise in ΔI to less than 50 Hz across a full frequency scan. As Figure 1 shows, errors as large as 12 kHz were measured for large and intentionally unequal beam intensities.

Because this nonreciprocal dispersion error could be so large, we felt it necessary to minimize its effect in the design of a sensitive and stable laser rotation sensor. To do so, we chose to build a ring laser using isotopically pure Ne and to control the following three parameters in the design:

F - the optical frequency referred to the atomic line center

I - the average laser output power in both beams

ΔT - the nonreciprocal difference in cavity transmission for the clockwise and counterclockwise beams

To eliminate mode locking or pulling, it was necessary also to provide a large simulated rotational bias. This Faraday effect bias was a fourth controlled and stable laser-design parameter:

Δn - The nonreciprocal difference in index of refraction for the clockwise and counterclockwise beams in the absence of any physical rotation

The first two of these parameters, F and (I), are reciprocal properties which we chose to control with interlocking servo mechanisms which will be described in detail later. The second two parameters, ΔT and Δn, are nonreciprocal properties which we preset using two orthogonal Faraday effect devices. Thereafter, we relied on good mechanical, thermal and current stability to hold these parameters fixed.

The ring laser which we designed has the optical configuration shown in Figure 2. The optical path lies largely in a horizontal plane. The design is intended to provide good rotation sensitivity by maintaining a large area-to-perimeter ratio within the confines of a square case.

Competing effects from gain in the infrared line at 3.39μ are removed by dispersion from the prisms located at (A) and (B). These prisms are modified to act as Faraday effect nonreciprocal control elements, one affecting the transmission difference, ΔT; and the other, the index of refraction difference, Δn. The first element is called a nonreciprocal transmission control. The second element is called a nonreciprocal time delay, nonreciprocal bias element, or "bizarre bar." These elements are described later in detail.

Optical tuning is effected by varying the cavity length using a piezoelectrically driven mirror pusher shown at (C). A second piezoelectrically driven element controls the cavity loss, by varying the gap in a frustrated total internal reflection (TIR) prism, shown at (D).

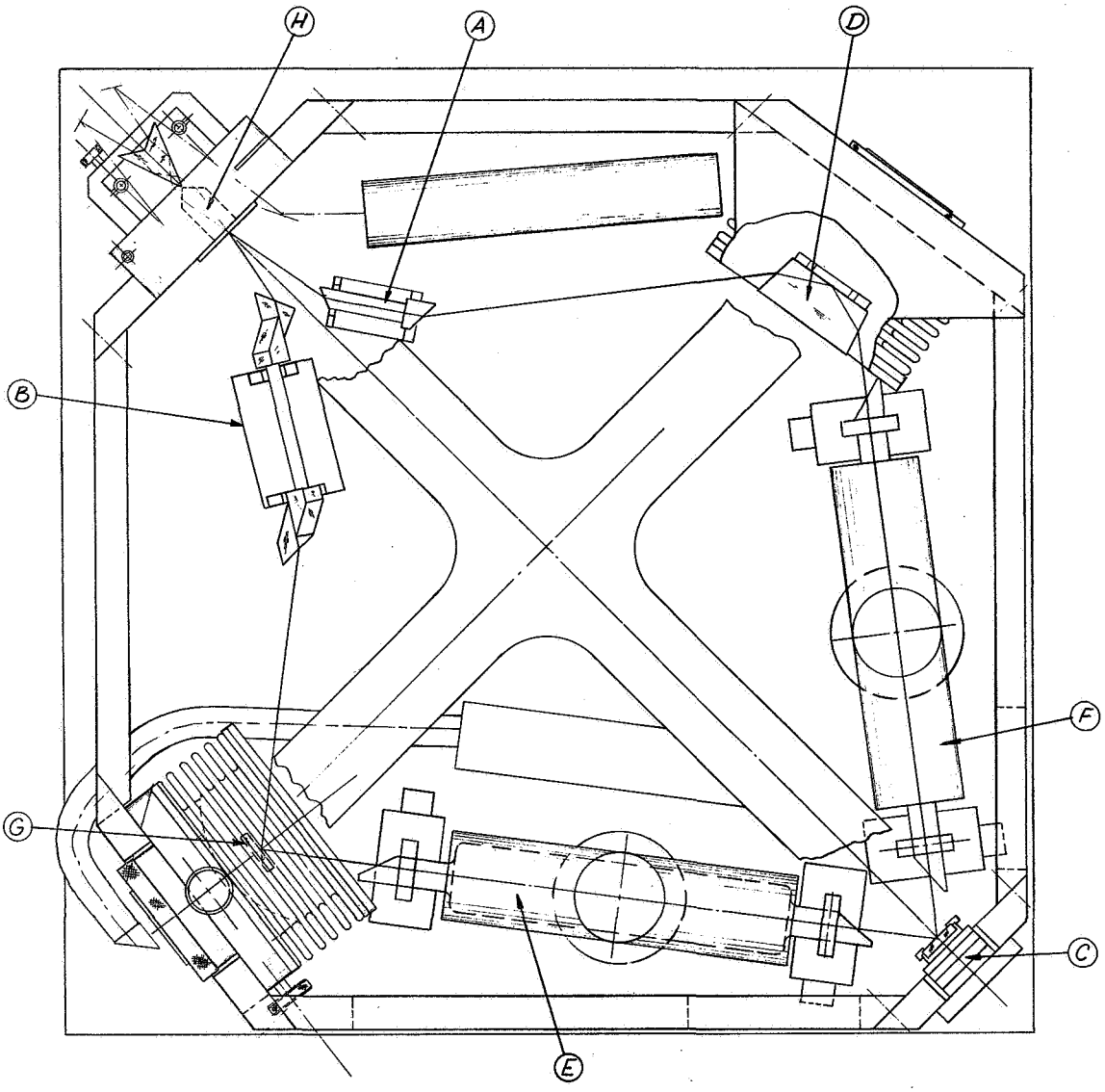


Figure 2. Ring Laser Optical Configuration

It is also possible to control the laser gain by varying the dc plasma anode current, but this current will not usually be changed during a run to avoid introducing thermal transients. Two plasma tubes are used as shown at (E) and (F). Each tube has a central heated cathode and two independently ballasted anodes, one at each end, to cancel out plasma drift bias. These tubes have Brewster-angle end windows. Their anode and cathode supply circuitry are described in detail later.

The laser frame is a heavy Invar box structure with a solid bottom and a webbed top plate. The rails and plates were first ground flat and then solidly bolted together to form a stiff structure, free from residual strain. One mirror shown at (G) and the prism (D) may be tilted to align the laser. These reflectors are carried in ground ball and socket joints which can be friction locked when the adjustment is complete. These locking mounts are described in detail later.

The laser frame is kinematically supported in a thick walled cast aluminum case, split symmetrically in the horizontal plane. The joint is hermetically sealed to isolate the laser from barometric pressure changes.

The case also serves as an oven wall which, together with an active temperature control system, isolates the laser from ambient temperature changes. A separate aluminum heat shield surrounds each plasma tube. These shields carry heat directly from the tubes to the outer case and thereby eliminate thermal gradients in the Invar laser frame.

An unusually compact beam combiner is fastened to the symmetrically placed output mirror mount shown at (H). The beam combination scheme and hardware are described later.

The combined output beam is directed to a photomultiplier tube within the case. Its beat frequency signal is amplified externally and then actuates a precise electronic counter. A second photomultiplier reads the sum of the cw and ccw output power from the mirror at (G) through an incoherent fiber bundle. This summed light power output signal carries all the information normally used to control automatically both the laser power level and the optical frequency with respect to the atomic gain curve.

The method by which this signal is used for control may be understood most easily step by step:

First, the total laser output signal is displayed on the vertical axis of an oscillograph while a sawtooth laser tuning drive is displayed on the horizontal. See Figure 3. The TIR loss control is manually adjusted to match the center trace in the figure where the dashed upper trace displays too much gain, and the lower trace too little.

Having established this gain level, the tuning sweep is removed and the laser is manually tuned to a frequency near the cross marked "1". The tuning servo is then engaged and adjusted to hold the laser to the frequency marked by sensing changes in output power.

The laser could be operated indefinitely under this control condition but with relatively poor long-term frequency stability because

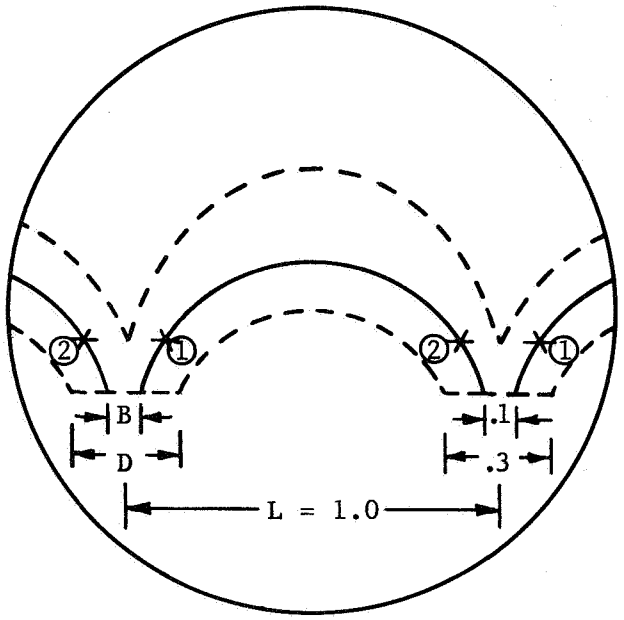
the basic frequency reference is simply the measured power output. Under these conditions, the frequency is dependent on the laser output stability and on the photomultiplier gain.

Note that by reversing the sign of the error signal in the servo loop the laser can also be set to lock to the point marked "2" which has an equal output power level. This fact is used in the automatic frequency control mode to provide sequential operating conditions symmetrically displaced from the center of the Doppler broadened atomic line.

When using this automatic control mode, the oscilloscope gain and centering controls are reset to display the pattern shown in Figure 4. An internal digital logic system commands the transition repeatedly from servo position 1 to position 2, and vice versa. In each position, cycles of the beat frequency between cw and ccw waves are counted for precisely 1 second. No beat counting is done during the 40 millisecond transition intervals between servo positions 1 and 2.

The beat count is totaled following each 1-second interval and can be read directly from the counter display. The laser logic system also includes an internal digital-to-analog converter for recording each count on a strip chart with an expanded scale and offset zero.

If the beat frequency is consistently different between position 1 and position 2, this indicates the presence of saturation-induced nonreciprocity in the laser plasma. Therefore the laser nonreciprocal transmission control is adjusted manually to remove the difference by equalizing the cw and ccw beam intensities. The control is then locked for the duration of the run.



Solid Curve is the Normal Laser Operating Condition and the Crosses are Normal Servo Control Points.

Figure 3. Laser Total Output vs Frequency

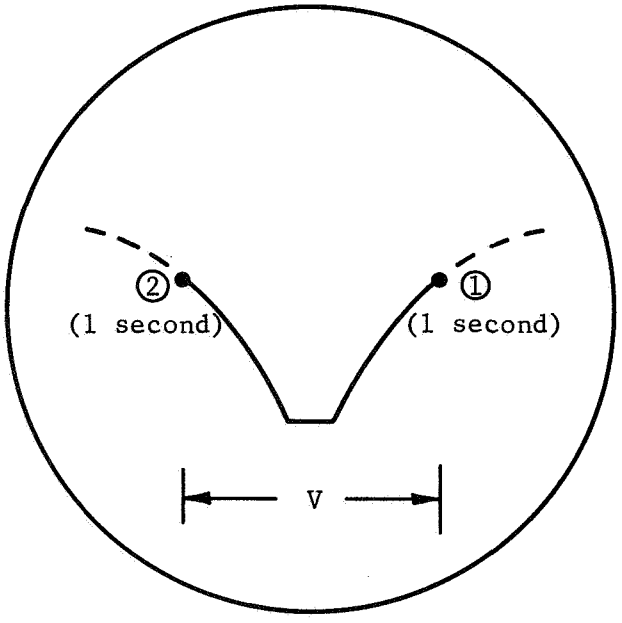


Figure 4. Laser Output in Automatic Control Mode

This beat difference measurement is the only practical measure of small but very important differences between cw and ccw transmission in the laser cavity. The concomitant differences in power output between the cw and ccw beams are so small (10^{-5} to 10^{-7}) that they cannot be measured photometrically with adequate accuracy to use for control of the saturation induced nonreciprocity.

To keep the output powers in the cw and ccw beams from changing, and thus deranging the automatic frequency control system, the ring laser also has an automatic intensity control system. In this system, the voltage difference V required at the piezoelectric tuning pusher to tune from position 1 to position 2 is averaged over several preceding cycles. The averaged value is used as a reference for a second loss control servo which adjusts the cavity loss to hold the required voltage difference to a preset value. This in effect controls the laser frequency difference between positions 1 and 2.

When the loss and frequency control servos are both operating at the same time, the end result is that the laser frequency with respect to the atomic line is controlled by the preset voltage V. The effective frequency offset reference then becomes the voltage sensitivity of the piezoelectric pusher. Thus, with both of these laser stabilization servos in operation, frequency control stability is independent of laser output power and photomultiplier gain variations.

The details of these servo controls and of the logic system which commands them are fully shown in the circuit diagrams in Appendix I and are briefly described in the text.

SECTION II

OPTICAL COMPONENTS AND MECHANICAL STRUCTURE

A. PRESSURE TIGHT HOUSING

The ring laser is housed in a heavy-walled, cast aluminum case with a gasketed cover. Hermetically sealed connectors are used for all electrical inputs, and the entire case can be sealed to reduce acoustic and barometric pressure changes. A temperature control servo, consisting of a thermistor sensor, amplifiers, and a group of resistors distributed about the inside of the base and cover sections, maintains the temperature constant.

B. INVAR SUPPORTING FRAME (See figure 5.)

The optical components of the ring laser which determine its geometry are supported by Invar mounts designed to lock securely in position after being adjusted for maximum resonator Q. The component mounts are attached to either the bottom or sides of a heavy, very rigid, Invar box structure. This structure rests on three Bakelite studs inside the cast aluminum case. Lateral freedom is provided at these three points to prevent strains which would otherwise occur because of the differing thermal expansion of case and frame. The studs are made from Bakelite to give thermal isolation between frame and case.

C. ADJUSTABLE MIRROR MOUNTS

Figure 6 shows a sectional view of the mounts used for the adjustable mirror and prism at diagonal corners of the ring. The mirror or prism

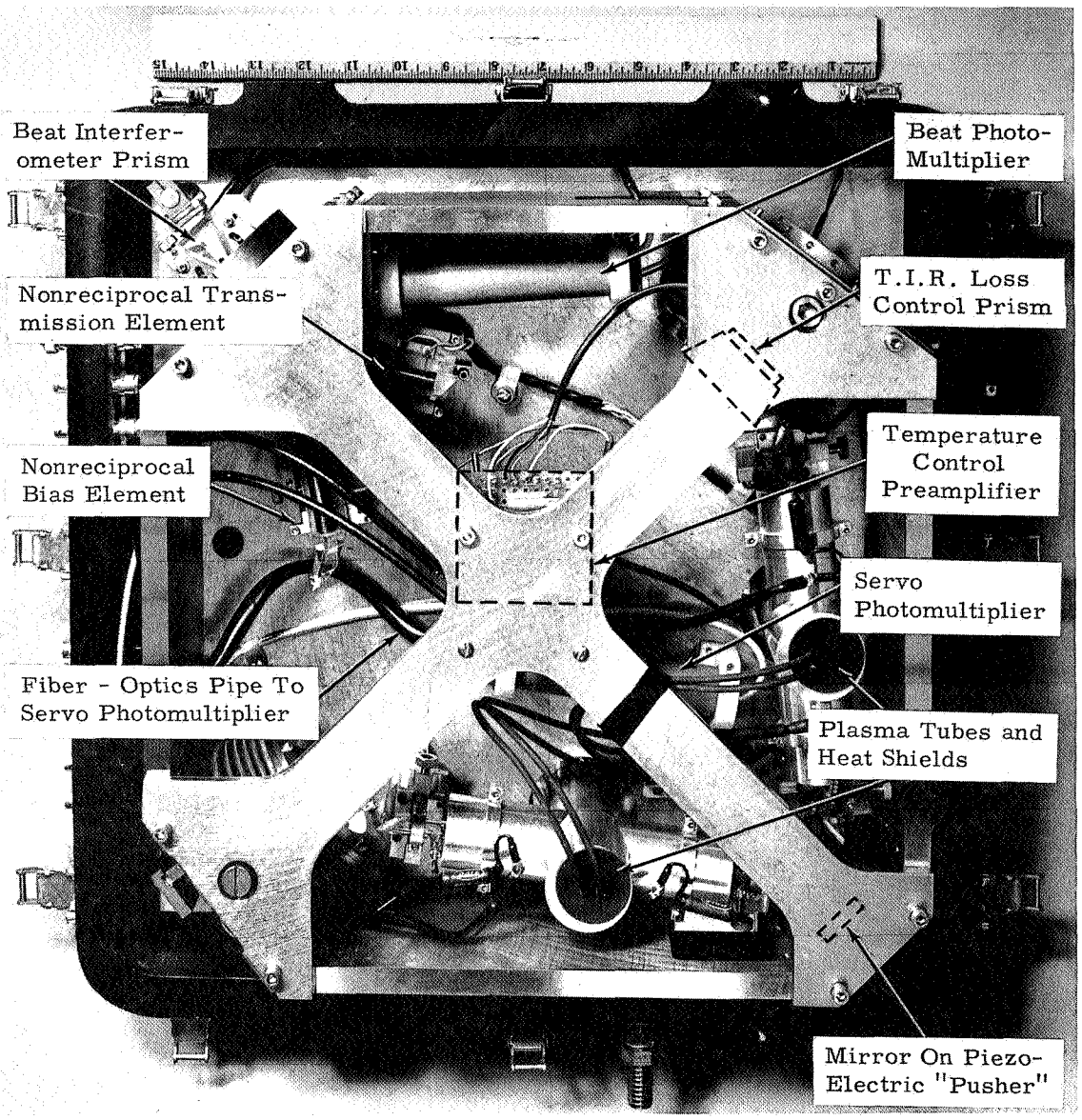


Figure 5. Optical Components

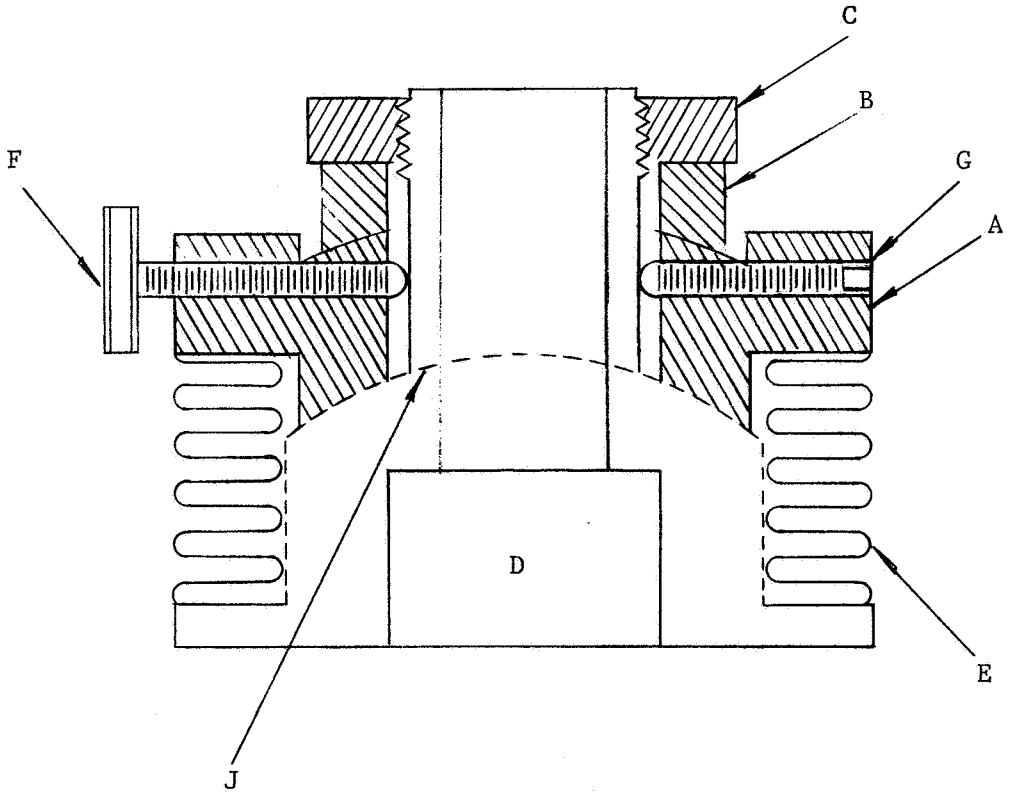


Figure 6. Adjustable Mirror Mount

is mounted in an Invar cup (D) having a spherical surface at (J). Surface J is ground and lapped to fit the base A, to which it can be locked by tightening nut C on spherical washer B. Rotation of part D is prevented by a bellows (E) connecting it to the base A. To adjust this mirror mount, the locking nut is released slightly and screws (F and G) bearing against the rear extension of (D) are loosened or tightened as required. Another pair of screws, not shown, moves the mount in a vertical plane. When the desired adjustment is obtained, the locking nut is tightened firmly.

D. PLASMA TUBES

Figure 7 shows a sectional view of one of the plasma tubes used in the ring laser. It consists basically of a thick-walled 1.5 mm ID capillary tube with an anode at each end. The cathode and getter assemblies are contained in a short side tube, which communicates with the capillary through a small hole at the center. An outer reservoir of larger diameter tubing serves to stiffen the assembly, in addition to providing a sufficient volume of gas. Glass is used throughout for structure. The windows, at Brewster's angle, are made of fused silica. These tubes were filled with a 7:1 mixture of He^3:Ne^{22} to a total pressure of 3 Torr. The active length is about 15 cm.

E. PLASMA TUBE SUPPORTS AND HEAT SHIELDS

Locking adjustments are provided in both the vertical and horizontal directions for each end of the plasma tubes. To minimize heat conduction and consequent thermal gradients in the base plate, the tube is clamped at the ends to the mount through rubber "O" rings. In addition, each tube is surrounded, but not touched, by a close fitting thick walled aluminum shield which clears the base plate and makes good thermal contact with the outer case.

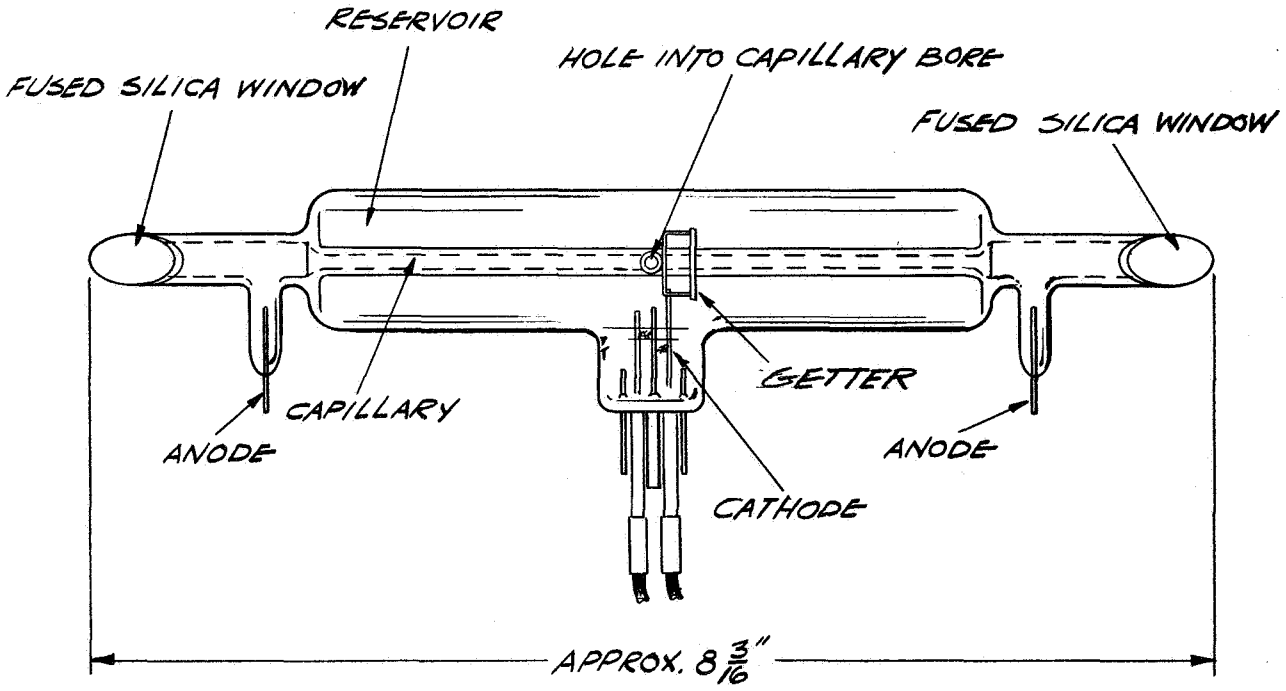


Figure 7. Plasma Tubes Used In Ring Laser

F. VARIABLE LOSS CONTROL

Figure 8 illustrates the layout of the frustrated total internal reflection variable loss prism used to control transmission of the ring laser cavity. The beam enters surface 1 or 2 at Brewster's angle, and is internally reflected at surface 3. The angle is such that the internal reflection would be total except that another surface, C, is moved into close proximity.

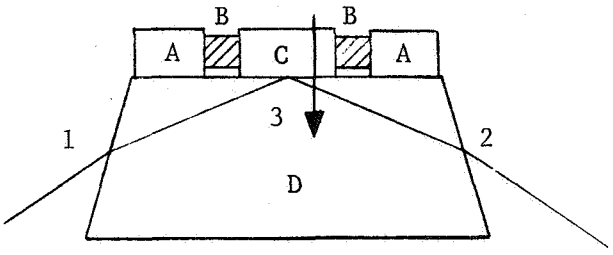


Figure 8.

The transmittance across the gap (T) is then theoretically:

$$T = \exp - d/\lambda \sqrt{\sin^2\theta_i - n}$$

n = index of the material

d = width of the gap

λ = wavelength of the light

θ_i = angle of incidence

The device uses parts A as mounting blocks made of fused silica. Parts B are activator blocks of piezoelectric ceramic which deform, in shear in the direction of the arrow, when an actuating voltage is applied. C is a fused silica loss plate. Parts A, B, and C are first cemented together, then ground and polished to an optically flat surface across A, C, A. Dielectric spacers of about 1λ thickness are evaporated onto prism D in the areas adjacent to parts A, then the assembly of A, B, and C is placed in optical contact with

the coated area. This technique insures that the plate C will be spaced 1λ away from the prism surface at 3 when no voltage is applied to the piezoelectric material, because the area under C was masked during evaporation. Range of the device is sufficient so that the laser can be extinguished at maximum current in the plasma tube.

G. PZT MIRROR PUSHER

Perimeter tuning of the ring laser is done by moving the mirror at the corner opposite the beam combining interferometer. The mirror is mounted in an aluminum cell cemented to the top of a stack of four piezoelectric discs. Electrodes on each surface of the discs permit them to be driven in parallel electrically to reduce the voltage requirement of the driving electronics. The four-layer pusher tunes the ring resonator through about 2-1/2 orders with the 450V output of the driver. The sensitivity is 1.24 MHz per volt calculated for an order spacing of 261 MHz and 210V required to tune through one order.

H. MIRROR AND BEAM EXTRACTOR PRISM

One mirror in a movable mount is backed by a prism which makes use of two total internal reflection surfaces to divert the transmitted beams onto a right angle prism at the rear of the mount. The right angle prism reflects the two beams onto a fiber-optics flexible light pipe which in turn carries the light energy to the photomultiplier at the input to the servo tuning system.

I. SHOVEL NOSE PRISM AND INTERFEROMETER PRISM

To obtain a beat between the two counter-rotating beams, they must be combined in an interferometer. The combining optics must not reflect

energy from one beam into the other, and paths in air should be short. The combination of prisms shown in Figure 9 accomplishes these functions.

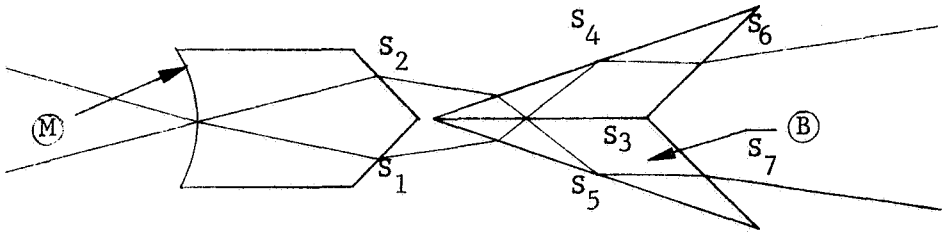


Figure 9.

A prism integral with the mirror M can be rotated without effect on the laser alignment to refract both beams so that they intersect. Surfaces S_1, S_2, S_4, S_5, S_6, and S_7 are at Brewster's angle, for minimum reflection. In prism (B) surface S_3 is coated for equal transmission and reflection, and the beams are combined here. Each pair of combined beams is totally internally reflected at S_4 and S_5 and then exits diverging.

Three adjustments are required to align the interferometer. A translation of the prism perpendicular to the beam divider surface places the surface at the point of intersection of the beams. Rotation about two perpendicular axes then serves to make the direction of the beam collinear. The mount used provides these three motions.

J. NONRECIPROCAL TRANSMISSION ELEMENT

The element used, which has a differing transmission for a beam traveling toward the right than for one going toward the left, is shown in Figure 10 . Beams enter the device at 1 and 2 at Brewster's angle.

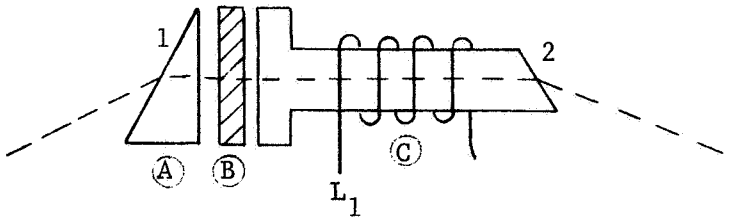


Figure 10.

A is a birefringent crystal quartz prism, part (B) is a plate of crystal quartz with its optic axis parallel to the light beam. It is cut to the 0.214mm thickness required to give a 4° rotation of the plane of polarization. Part (C) is a cylinder of fused silica, wound with a solenoid, L_1. Longitudinal magnetic field in the solenoid rotates the plane of polarization due to Faraday effect in the fused silica. Faraday rotation is nonreciprocal and changes sign with the direction of the light, as viewed along the direction of propagation of the light beam. The reciprocal rotation independent of direction produced by plate (B) is thus augmented for one direction of light, and diminished for the other. (The quartz prism (A) transmits only one polarization orientation along the cavity axis. The orthogonal orientation is refracted away.) The combination thus forms an element which has differential transmission, the amount being proportional to the current in L_1.

The unit is mounted on an adjustable Invar base having motions vertically and horizontally with respect to the beam. Locking clamps are provided for each adjustment. The optical element is mounted in a fused silica V-block to prevent transmission of strains from the base. The solenoid is wound on a longitudinally split fused silica tube, which is shimmed at each end to fit snugly around the optical element. The shims provide enough clearance so that strains from heating of the winding are not transmitted to the optics on the axis of the solenoid.

K. NONRECIPROCAL BIAS ELEMENT

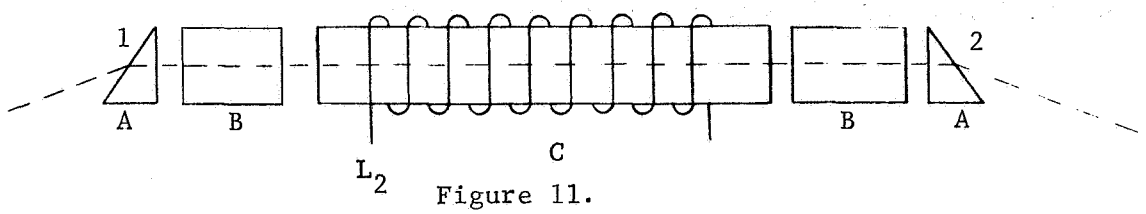


Figure 11.

The nonreciprocal bias element introduces a nonreciprocal time delay into the resonator, allowing the beat frequency to be offset from zero when the ring laser is not being rotated. It is shown schematically in Figure 11 and photographically together with its mount in Figure 12. The entire optical element is made of fused silica.

The light enters at 1 and 2 at Brewster's angle. Sections B are circular polarizers, in this case Fresnel rhombs, which produce circular polarization through two total internal reflections at 45° to the plane of incidence. Section C is a Faraday rotator, with solenoid winding L_2. Under these circular polarization conditions, current in the coil produces nonreciprocal time delay for opposing directions of light propagation.

The nonreciprocal bias element is mounted (in a fashion similar to the nonreciprocal transmission control above) on a fused silica V-block supported by a locking adjustable Invar base. Here again, the coil is tightly wound on a split silica tube shimmed away from the coaxial optics, and the combination of stable coil geometry and stable current supply insures a stable field in the rotator element.

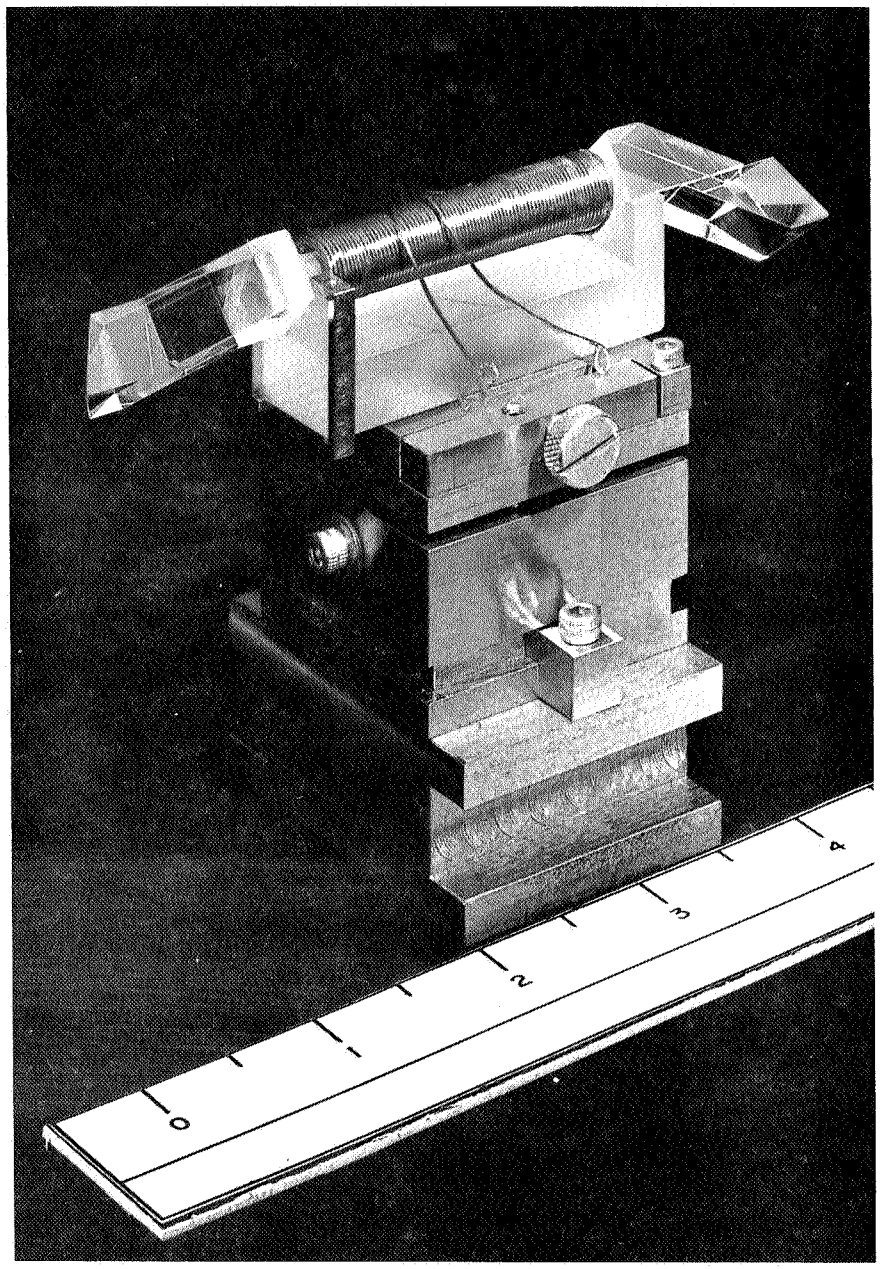


Figure 12. Nonreciprocal Bias Element and Mount

Mechanical, thermal, and electrical stability of the bias element is essential to laser rotation sensor engineering because, in practice, instability of bias will appear directly as an error in the rotation rate reading.

SECTION III

ELECTRONIC SYSTEMS

Controls and outputs for the various modes of operation of the ring laser rotation sensor are centralized in an electronic equipment console. A block diagram of the console, together with elements located in the laser housing, is shown in Figure 14. In this figure, the optical paths in the housing are indicated by dotted lines, electrical connections by solid lines.

A. LASER TUNING SERVO

The laser tuning servo switches the length of the ring laser cavity between two positions of equal intensity on the Doppler-broadened gain curve (on adjacent cavity orders). It also regulates the intensity at a predetermined level at each position. For proper operation of the servo, the overall intensity must remain so low that the laser is out, or nearly out, between orders. For such a condition, laser output as a function of cavity length would be as shown in Figure 13.

The tuning servo holds the intensity I_o constant by continuously controlling the cavity length by means of a piezoelectric driver which moves one of the cavity mirrors. As the servo dwells at point X for example, the electronic counter measures the beat frequency produced between the two counter-rotating beams. At the end of the counter gate time, the counter produces an end-of-gate pulse which triggers logic elements in the tuning servo causing it to switch the cavity length to position Y. After switching, the counter is reset and measures the beat at the new position. The end-of-gate pulse then causes the cavity to return to position X and the cycle continues.

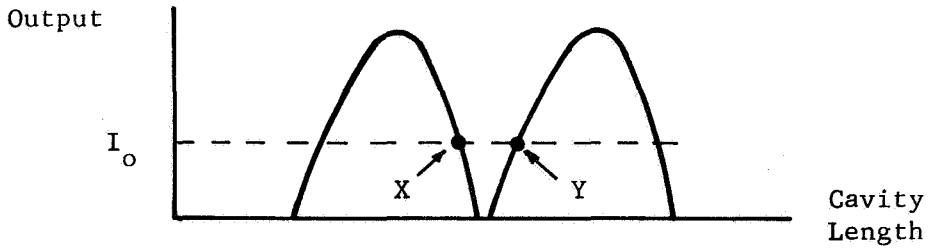


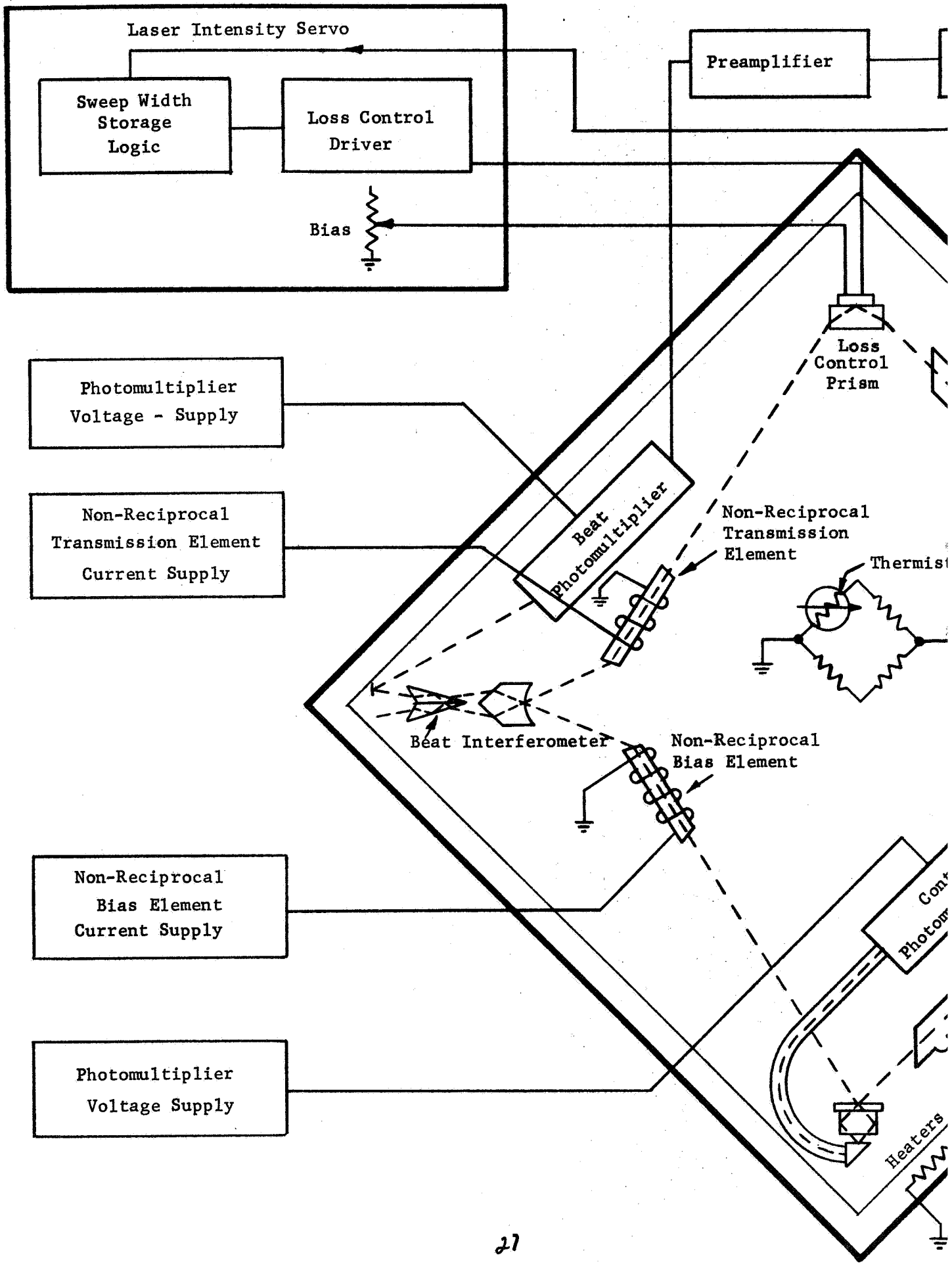
Figure 13.

A switch is provided in the servo so that the beat may be measured continuously at either position X or Y. The cavity position can be transferred from X and Y manually, or vice versa, by pressing a button.

B. LASER INTENSITY SERVO

Stable operation of the ring laser rotation sensor requires that the intensity of the laser remains constant during measurement. Since operation of the tuning servo utilizes intensity as a reference to adjust the cavity length, length is not an available parameter for control of the gain. For this purpose, a variable loss element is used in the intensity servo. The variable loss element is a frustrated total internal reflection prism placed at one corner of the optical circuit. To introduce loss into the cavity, a fused silica plate is moved piezoelectrically into close proximity to the total internal reflecting surface of the prism. As the gap approaches the dimensions of a wavelength of light, energy is coupled across it, and lost from the resonator.

Error signal for the intensity servo is the difference in voltage required to switch the mirror between points X and Y on the gain curve. As this voltage difference becomes larger, it represents a decrease in overall laser gain, and the servo drives the loss element so as to produce a smaller loss.


Laser Intensity Servo
Sweep Width Storage Logic
Loss Control Driver
Bias
Preamplifier
Photomultiplier Voltage - Supply
Non-Reciprocal Transmission Element Current Supply
Non-Reciprocal Bias Element Current Supply
Photomultiplier Voltage Supply
Loss Control Prism
Beat Photomultiplier
Non-Reciprocal Transmission Element
Thermist
Beat Interferometer
Non-Reciprocal Bias Element
Heaters

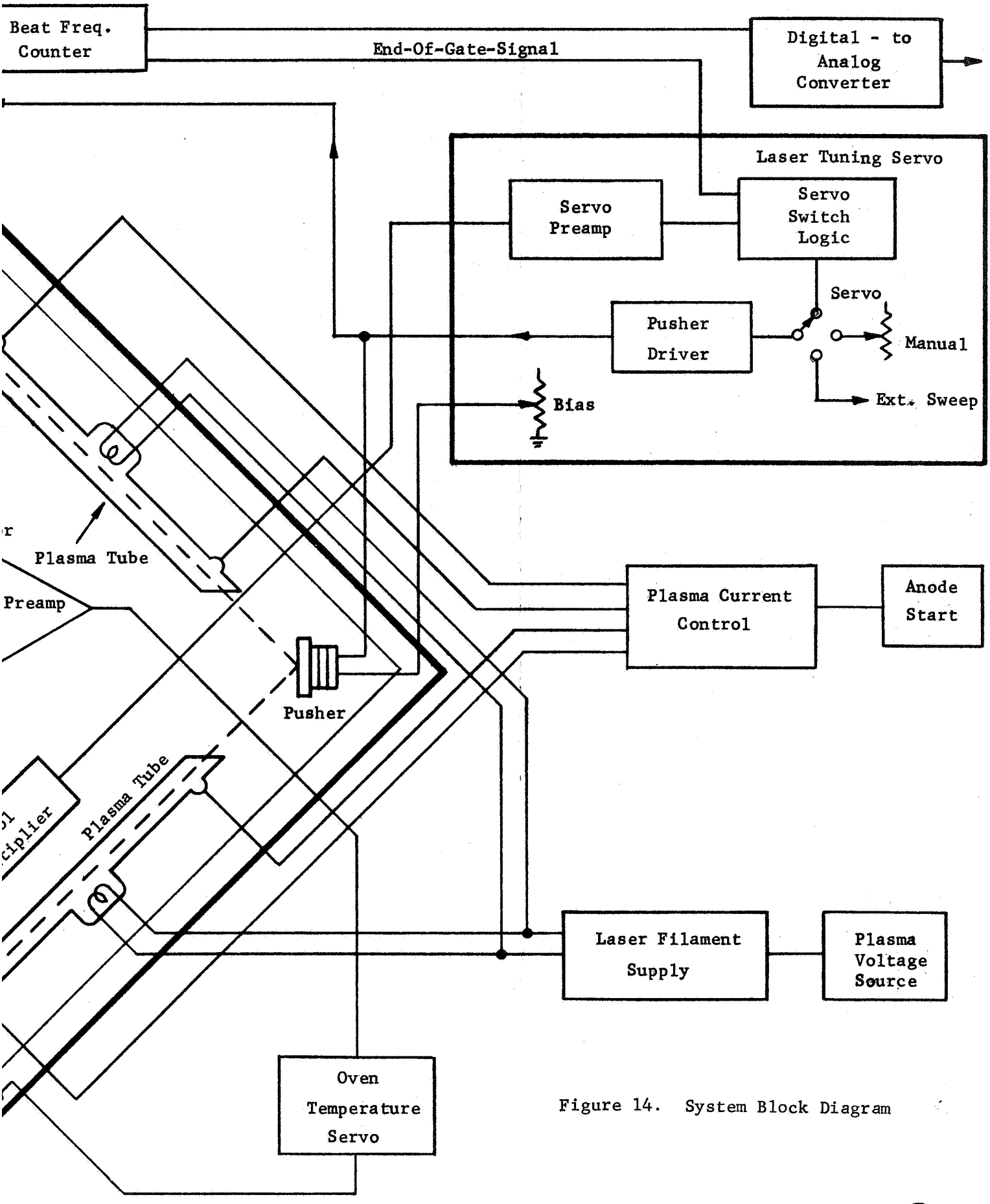


Figure 14. System Block Diagram

C. LASER FILAMENT SUPPLY AND PLASMA VOLTAGE SOURCE

Current for heating the plasma tube filaments is supplied from this unit, which is isolated from ground in an insulated enclosure. Voltage and current adjustments are made through insulated shafts. The entire filament supply is maintained at a negative voltage with respect to ground, to provide the necessary drop across the plasma, while allowing the anodes, and associated current controls, to operate near ground potential.

D. PLASMA CURRENT CONTROL

The anode current control chassis (XC-594-0040) contains controls and meters to vary and measure the total current in the two sections of each plasma tube (A + B) and (C + D), and the difference in current between the two sections of each tube (A - B) and (C - D).

The START circuit, also located on this chassis, provides a high voltage to the four anodes when the START button is pressed.

Two operational amplifiers, A_1 and A_2, are available on this chassis, and may be connected to modulate the plasma currents.

E. BEAT FREQUENCY OFFSET AND MEASUREMENT

Current for the nonreciprocal bias element is supplied from an unusually well-regulated precision power supply. The beat frequency formed by combining the two beams at the beat interferometer prism is sensed by a photomultiplier inside the laser housing. The signal is amplified and shaped by circuits in the servo control chassis, and supplied to a frequency counter. The digital output of the counter is indicated on the front panel. It is also connected to a built-in digital-to-analog converter. Any three decades of the

counter reading may be selected by a switch and the reading appears as a (negative) voltage at the converter output jack.

F. TEMPERATURE CONTROL SERVO

The temperature of the laser housing is maintained several degrees above ambient by a group of heaters distributed about the inside. The sense element is a thermistor, in thermal contact with the bottom of the housing. Bridge resistors, and a preamplifier are located inside the housing. The signal is further amplified on board "C" and applied to a driver power supply which feeds current to the heaters.

SECTION IV

RESULTS OBTAINED

A. EARTH'S ROTATION

The ring laser was evaluated in the laboratory with respect to stability and sensitivity. Facilities were not available for actually rotating the structure; however, a tilting stand was constructed which allowed alignment of the axis of the ring either parallel or perpendicular to the axis of rotation of the earth. This corresponds to a change in rotation rate from 15 arc-sec/sec to zero. ΔF measured for this change in position was 50 ± 5 cps. The theoretical value which should have been obtained by calculation from the equation

$$\Delta F = \frac{4\Omega A}{\lambda P}$$

(where A is the projected area of the optical circuit, P is the length of its perimeter, λ is the wavelength, and Ω is the rotation rate),

gives a figure of 25 cps for one earth rate rotation.

B. MAGNETIC FIELD SENSITIVITY

Subsequent measurements of the sensitivity of the apparatus to magnetic fields gave a maximum sensitivity of 170 Hz per oersted, a minimum figure of 34 Hz per Oe, depending on the orientation of the field, so that

the earth's field of approximately 0.2 Oe at this location, could fully account for the difference of the measured beat from the calculated value.

C. BEAT STABILITY

Several long-term runs were made to measure beat stability under servo control of intensity and position in the Doppler curve. The tuning servo was adjusted to hold the intensity during beat counting at approximately 25% of peak intensity, and the intensity servo assured that this intensity corresponded to a fixed relation to the line center. Under these conditions, the beat stability was ±3 Hz for periods of several hours. This degree of stability was readily obtained as long as the laser housing remained stationary. However, if the housing was tilted, as was done to measure earth's rotation, a gradual shift in the beat frequency was observed, and an hour or more was required to re-establish the original beat frequency. This effect is probably due to changes in internal temperature gradients causing local temperature changes in the Faraday bias element.

D. BEAT PUSHING

Measurements were made of the beat-pushing effects as the resonant frequency of the ring laser cavity was tuned across the Doppler curve. As discussed in Reference 2, the change in beat frequency is dependent on the relative intensities of the two beams in the resonator. Intensities for these measurements were set as nearly equal as possible with the nonreciprocal transmission control by observing the behavior of the sum intensity of the two beams. When this remained constant as the frequency was scanned over the line center, the intensities were judged equal.

Variations in the beat of more than 100 Hz at the line center were observed when the sum intensities were unequal. With careful balance of the sum intensities, the variation in beat at line center was less than 30 Hz, and at points away from the line center was less than 5 Hz. Recorder traces of the beat frequency and sum intensity versus resonator tuning are shown in Figures 15 and 16 for conditions where the sum intensity increases, remains constant, or decreases.

E. BIAS CURRENT CALIBRATION

Figure 17 shows a calibration of beat frequency versus current in the nonreciprocal bias element coil. Slope of the line is 57.3 Hz per milliampere. Departures of measured points from the line are attributed to changes in the Verdet constant of the element with temperature, as power input to the coil varied from 200 milliwatts for large bias values, to 7.5 milliwatts for the lowest point. For operation as a biased rotation sensor, the power input to the coil would normally be constant during the entire measuring time.

F. PLASMA CURRENT BALANCE

Measurements were made of the change in beat frequency as a result of changing the balance of the plasma currents in the laser tubes. For a total unbalance between cw and ccw currents of 2.5 mA, the difference in the beat frequency was 162 Hz, or a sensitivity of 65 Hz per milliampere of unbalance. In normal operation, tube currents were always balanced to better than 0.01 mA.

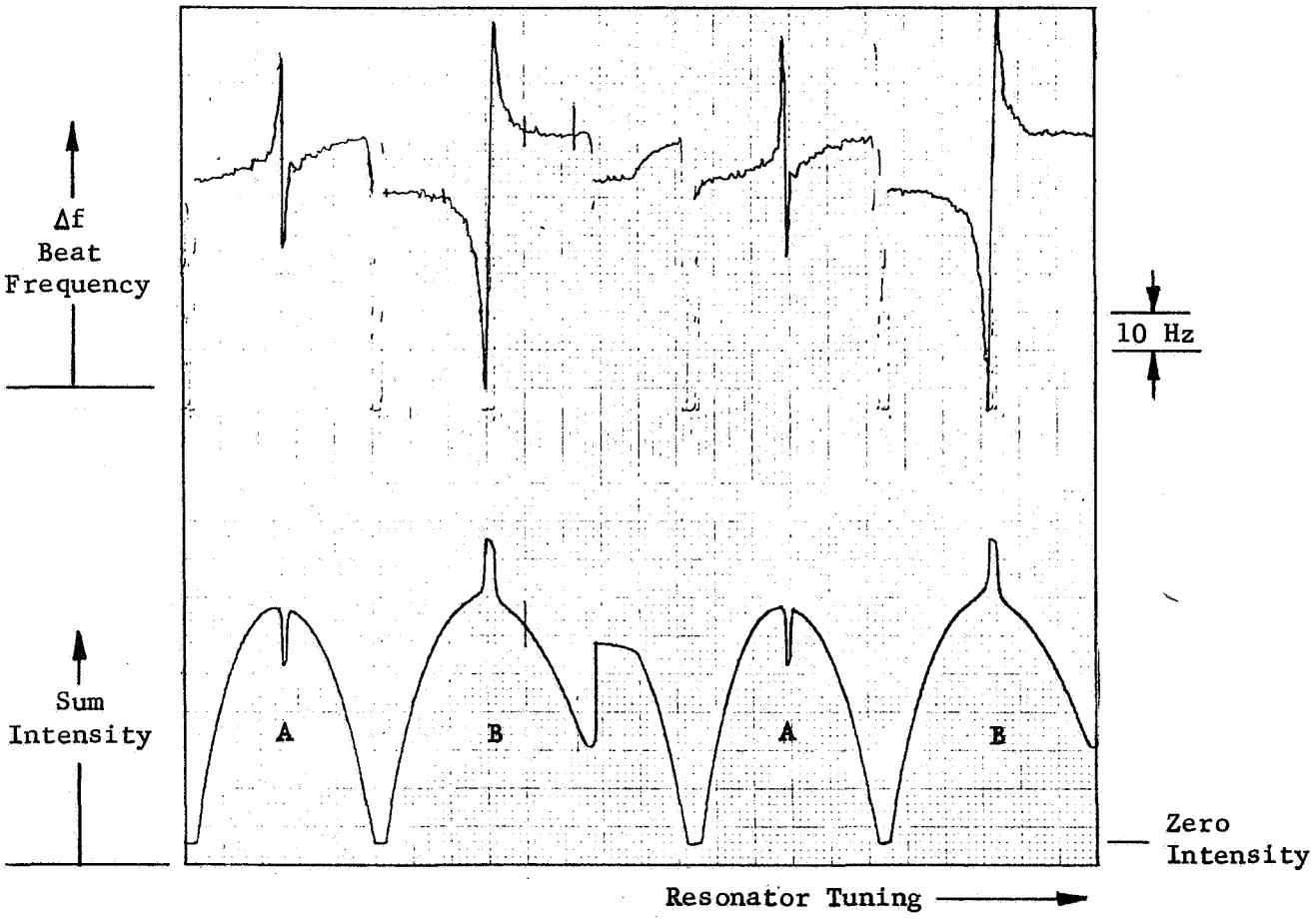


Figure 15. Representative Scans of Length Versus Analog Conversion of Beat Frequency Output, Nonreciprocal Gain Set so Sum Intensity in Order A Goes Negative, in Order B Goes Positive.

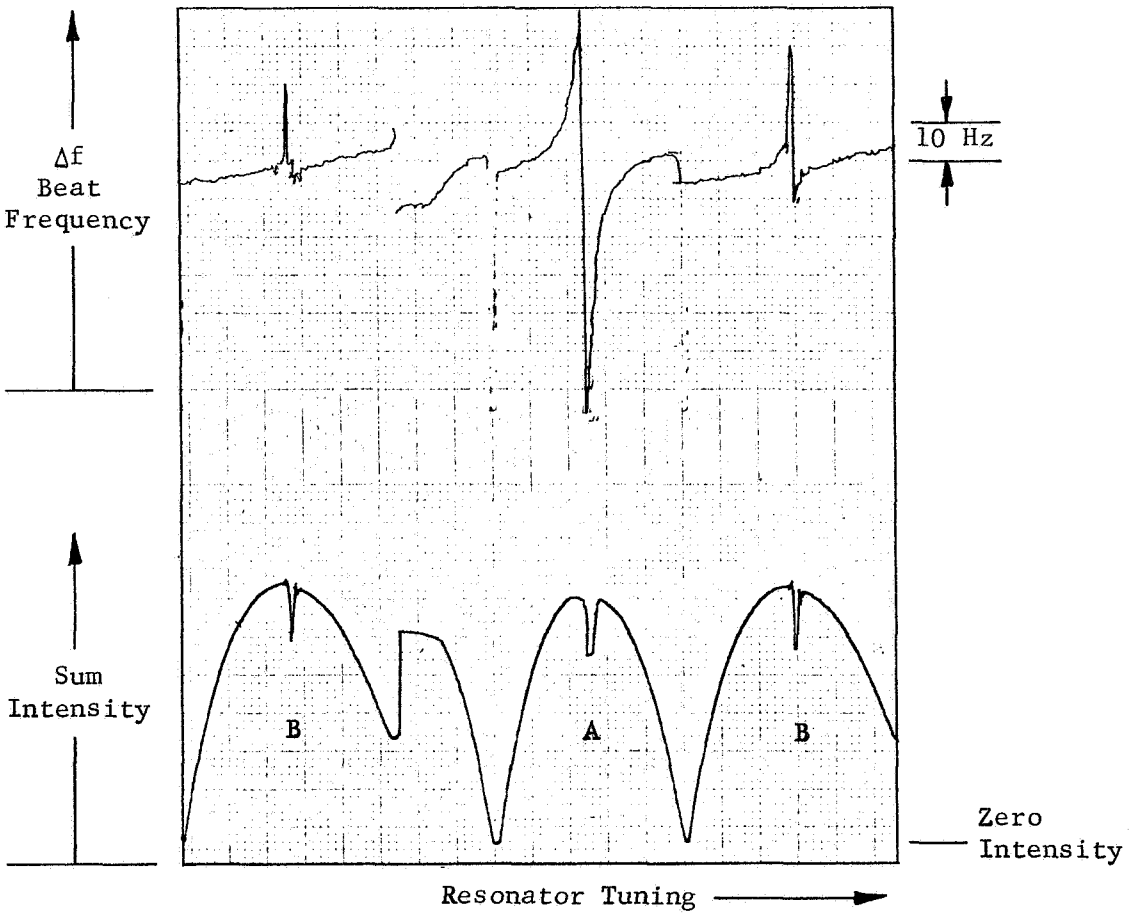


Figure 16. Representative Scans of Length Versus Analog Conversion of Beat Frequency Output, Nonreciprocal Gain Set so Sum Intensity in Order A Goes Negative, in Order B Goes Nearly Constant

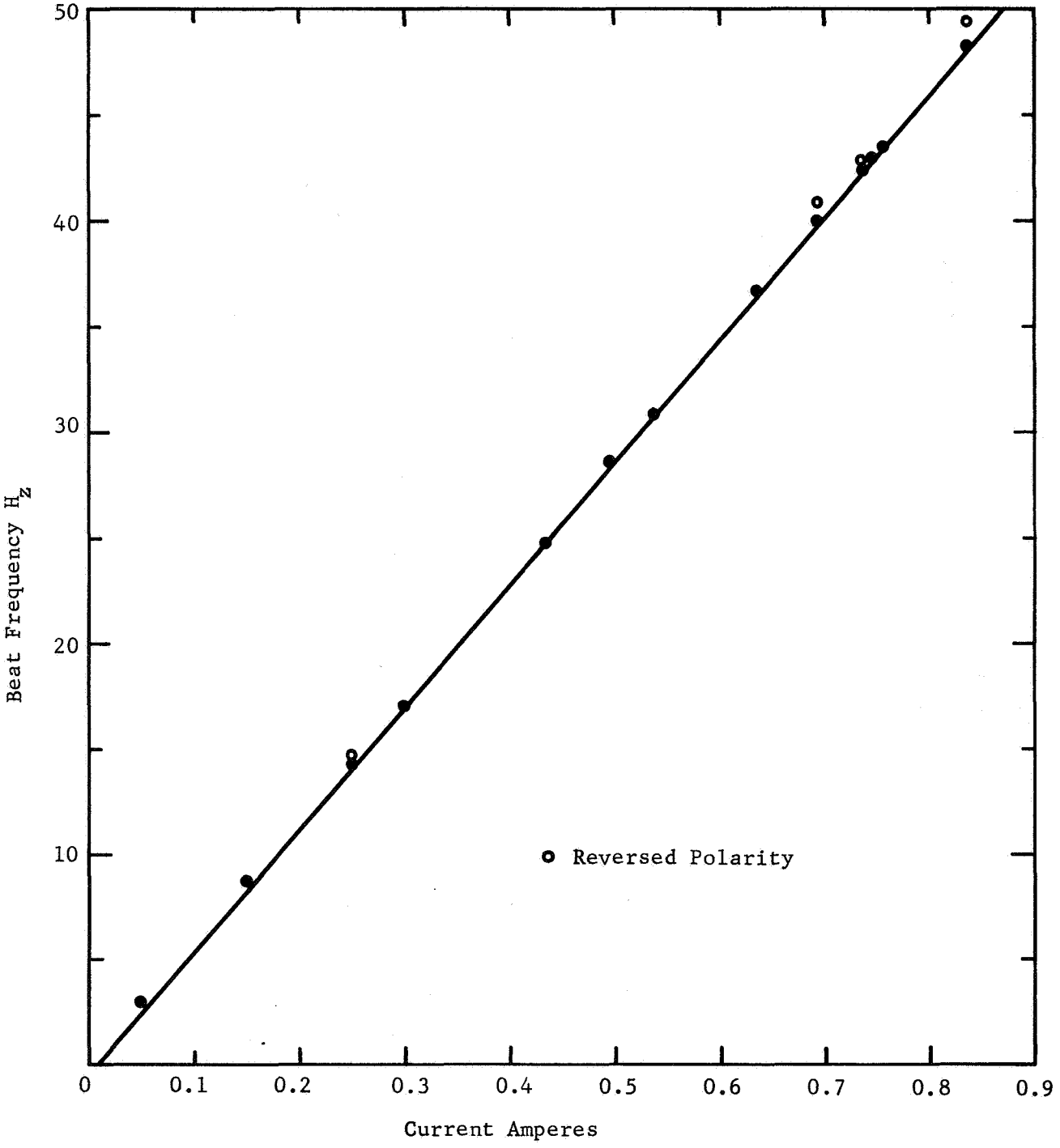


Figure 17 . Beat Frequency vs. Nonreciprocal Bias Element Current

SECTION V

CONCLUSIONS AND RECOMMENDATIONS

It was clear at the beginning of this research program that many of the factors affecting the stability of ring laser rotation sensors had not yet been measured and it was suspected that some were still unknown. In designing and building a new ring laser we tried, therefore, to build an instrument in which we could control as many potentially important parameters as practical within the contract scope. This approach was based in part on the desire to make the instrument itself a successful rotation sensor; and in part with the hope of discovering or measuring effects important for advancing the art.

The performance of the instrument has now been described in some detail, and it is expected that more measurements will be made at Marshall Space Flight Center.

Some measurements have been made with this laser and reported above which may be of value in future rotation sensor design.

Conclusions drawn from these measurements are briefly reviewed here:

1. DC plasma tube excitation under controlled conditions is thoroughly adequate for accurate rotation sensors. This is fortunate because, used in combination with hot cathodes, this form of excitation yields long tube life and freedom from radio interference.

2. Pumping level variation is a suitable output power control mechanism if heat input changes are properly compensated.

3. Faraday bias elements can be built with the stability needed for ring lasers having this considerable accuracy.

4. The following general control parameters remain important:

   a. Frequency control must be maintained with respect to the atomic line center. This implies open loop mechanical stability, low temperature coefficient materials, thermal isolation and barometric pressure control - in addition to adequate sensing schemes for servo frequency control.

   b. The difference in nonreciprocal transmission ΔT must be constant and very small. Ring laser designs would become most practical if this condition could be imposed simply by building a very clean ring resonator with a minimum number of nearly perfect reflecting or refracting surfaces. We are aware that this "open loop" approach is the one being taken by most of the other workers in this field. The important question is whether adequate control of nonreciprocal transmission can be achieved by open loop methods. At the conclusion of this program, it is now our opinion that the nonreciprocal transmission will have to be measured and controlled during operation of sensitive and stable laser rotation sensors.

5. It is possible to measure and control the nonreciprocal transmission in a ring laser without significantly disturbing either the bias or other important operating constants.

6. It is important to reduce nonreciprocal scattering from the beam because through a variety of mechanisms this scattering makes the beat frequency a less reliable measure of rotation. Ring lasers based on any design philosophy will be improved by the elimination of dust, and by the use of mirrors with a minimum of scatter.

7. We found beat frequency errors resulted from changes in the ambient magnetic field which could be eliminated in any future magnetically shielded instrument.

8. We note that the Verdet constant which describes the magnitude of the Faraday effect for various materials, has a substantial temperature coefficient. Future laser designs using this effect should provide better local temperature control of Faraday effect elements.

9. Better internal baffling is needed to reduce convection currents in the air around the laser. In the absence of these, our laser beat frequency responded (after a noticable delay) to tipping and to other acceleration changes.

At the end of this contract, we can reach these conclusions:

First, we have built a laser rotation sensor which is unusually sensitive by present standards. That laser embodies a complex optical resonator having a number of controlled variable parameters. We think, by using improved components and control techniques, that future instruments based on this design philosophy, can be made substantially better.

Second, we feel that considerably more theoretical and experimental work will have to be done to increase our understanding of ring laser

phenomena before sensitive, stable and practical instruments will be conceived. Then more experience with construction and control techniques will be needed before they can be built. Work done under this contract has made several contributions toward increasing understanding of ring laser phenomena, and of some techniques adequate to control them.

APPENDIX I

OPERATION MANUAL, ELECTRONIC CIRCUITS, AND PARTS LIST

APPENDIX I

TABLE OF CONTENTS

Operation Manual	I-1
System Block Diagram XD-594-0043	I-21
Cabling Diagram - Rear Of Rack	I-23
Ring Laser Anode Circuit XC-594-0040	I-25
System Cabling Diagram	I-27
Photograph of Laser Anode Circuit Board	I-28
Photograph of Anode Panel - Front	I-29
Photograph of Anode Panel - Rear	I-30
Servo Chassis Panel Interconnections With Circuit Boards XB-594-0045	I-31
Photograph Of Front of Servo Panel	I-33
Pusher and Loss Control Meter and Bias Panel Schematic	I-34
Photograph Of Rear of Servo Panel	I-35
Rotation Sensor Interconnections For Circuit Boards	I-37
Schematic of Board 1 XB-594-0046	I-39
Photograph of Board 1	I-40
Schematic of Board 2 XB-594-0047	I-41
Photograph of Board 2	I-42
Schematic of Board 7 XB-594-0048	I-43
Photograph of Board 7 - Front	I-44
Photograph of Board 7 - Rear	I-45
Schematic of Board 8 XB-594-0049	I-46
Photograph of Board 8	I-47
Schematic of Board 9 XB-594-0050	I-48
Photograph of Board 9	I-49

TABLE OF CONTENTS (Continued)

Schematic of Board 10 XB-594-0051	I-50
Photograph of Board 10	I-51
Schematic of Board 11 XB-594-0052	I-52
Photograph of Board 11	I-53
Schematic of Board 12 XB-594-0053	I-54
Photograph of Board 12 - Front	I-55
Photograph of Board 12 - Rear	I-56
Schematic of Boards 14, 15 XB-594-0054	I-57
Photograph of Boards 14, 15	I-58
Schematic of Board 16 XB-594-0055	I-59
Photograph of Board 16 - Front	I-61
Photograph of Board 17 - Rear	I-62
Schematic of Board A XB-594-0041	I-63
Photograph of Board A	I-64
Schematic of Board B XB-594-0042	I-65
Photograph of Board B	I-66
Schematic of Board C XB-594-0056	I-67
Photograph of Board C - Front	I-69
Photograph of Board C - Rear	I-70
Photograph of Front of Analog-Intensity-Temperature Panel	I-71
Photograph of Rear of Analog-Intensity-Temperature Panel	I-72
Digital-Analog Converter-Interconnection With CMC	I-73
Parts List	I-75

THE PERKIN-ELMER CORPORATION

OPTICAL GROUP - - - RESEARCH

OPERATION MANUAL

RING LASER ROTATION SENSOR

27 September 1966

TABLE OF CONTENTS

Title	Page
GENERAL	I-3
ELECTRONIC SYSTEM OPERATION	I-3
1. Laser Tuning Servo	I-3
2. Laser Intensity Servo	I-5
OPTICAL UNIT	I-5
ELECTRONIC CONSOLE	I-5
A. Photomultiplier Hv	I-5
B. Photomultiplier Hv	I-5
C. Low Voltage Power Supply	I-5
D. Low Voltage Power Supply	I-5
E. Electronic Counter	I-5
F. Servo Control Chassis	I-10
G. Counter Analog - Intensity Servo - Oven Amplifier Panel	I-12
H. Driver Power Supply	I-13
I. Oven Heater Driver	I-13
J. Plasma Current Control and Start Circuit	I-13
K. Transmission Element Current Control and Bias Control Panel	I-14
L. Plasma Voltage Source	I-15
M. Plasma Tube Filament Current Supply	I-15
N. Non-Reciprocal Bias Element Current Supply	I-15
O. Bias Polarity Reversing Switch	I-15
RING LASER SENSOR - START UP PROCEDURE	I-15
ADJUSTMENT OF TUNING CONTROL SERVO	I-16
ADJUSTMENT OF INTENSITY (LOSS) CONTROL SERVO	I-19
ADJUSTMENT OF TEMPERATURE CONTROL SERVO	I-19

Consists of two consoles and interconnecting cables. Unit one, an aluminum container 19" x 19" x 8" deep, contains the optical portion and photoelectric pickups. Unit two, a 6' rack panel, contains power supplies, electronic servo controls and readout devices. A Tectronix 585 oscilloscope or equivalent is required for setup and monitoring of the servos.

ELECTRONIC SYSTEM OPERATION

Reference is made to the system block diagram, XD-594-0043, on page I-21.

1. Laser Tuning Servo

The purpose of the Laser Tuning Servo is to switch the cavity length of the laser between positions giving equal laser intensity on opposite sides of the Doppler-broadened gain curve. Adjacent orders of the cavity are used to avoid competition effects at the line center.

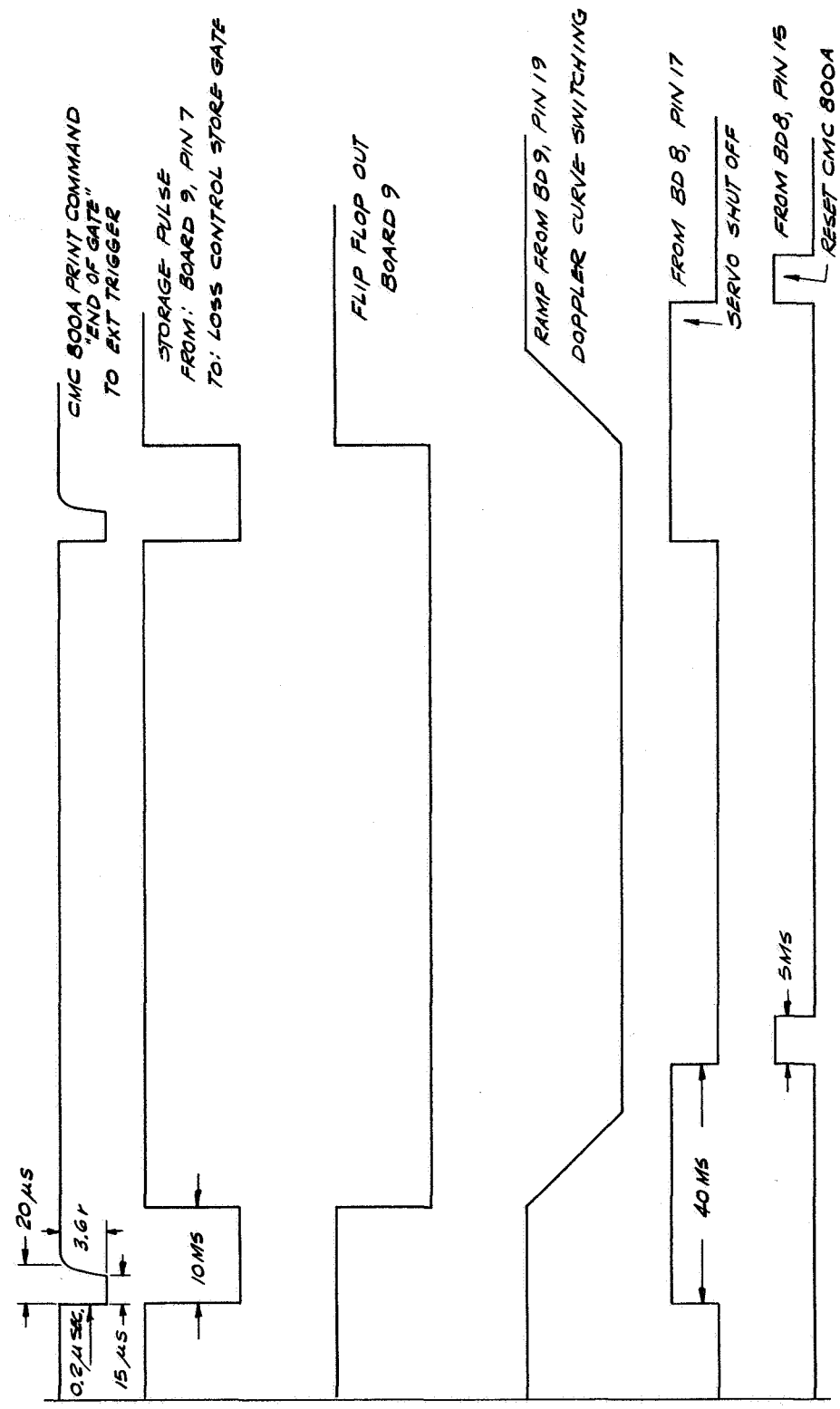
The intensity of the combined beams of the laser is measured by a photomultiplier, amplified on boards 7, 10, 11, and 12, and applied to the pusher with the proper polarity to maintain the intensity constant. While the intensity is thus being regulated, the beat-frequency counter registers the beat frequency. Input for the counter is the beat frequency formed by the interferometer and sensed by another photomultiplier in the laser housing. The beat-frequency signal is amplified and shaped on circuit boards 1 & 2.

At the end of the counter gate time, the counter produces an "end-of-gate" pulse (Drawing XB-594-0065). This pulse is applied both to board 8 and board 9. From the one-shot multivibrator on board 8, a 40-millisecond pulse is produced which disconnects the servo loop. At the same time, a one-shot multivibrator on board 9 produces a 10-millisecond pulse. This 10-millisecond pulse is applied to a flip-flop circuit which reverses the polarity of the intensity servo loop. It also initiates a ramp signal which moves the pusher to the opposite side of the Doppler-gain curve.

The 10-millisecond pulse, as well as the polarity information from the flip-flop on board 9, is also used in the intensity servo, to be described later.

At the end of the 40-millisecond pulse, a 5-millisecond counter reset pulse is produced from board 8, and the servo loop is reconnected.

When the switch at the input to board 8 is in "External Trigger" position, the tuning servo is cycled by the counter, and the gate time may be selected using the counter controls. For this mode of operation, the counter display time should be set to "∞". When the input switch is turned to "Single Pulse" the tuning servo is cycled manually by pressing the pushbutton. In order to operate the counter in "Single Pulse" mode, the display time selector must be moved away from "∞", otherwise the previous counter reading will be displayed indefinitely.



Drawing XB-594-0065. Rotation Sensor Logic Waveforms

2. Laser Intensity Servo

The tuning servo, described in the foregoing, uses intensity as a reference to control the length tuning of the laser cavity. The intensity servo uses as its reference the voltage difference between the two pusher positions controlled by the tuning servo. For this reason, the intensity servo can only be adjusted and operated after the tuning servo is operating properly.

The voltage at the output of board 11, representing one pusher position, is stored in a capacitor on board 14 or 15. The voltage representing the opposite pusher position is subsequently stored on the alternate capacitor. The difference of these two voltages is applied through a variable attenuator to a differential amplifier, on board 16. The output of the differential amplifier is further amplified and then used to control a variable loss element in the ring laser cavity. As the difference voltage, representing the two pusher positions, becomes larger indicating lower overall laser intensity, the servo drives the loss element to give less loss and maintain the intensity constant.

OPTICAL UNIT

An aluminum container 19" x 19" square by 8" high encloses the optical elements of the system. Input power is supplied through two 10-pin hermetic connectors, "A" and "B" in photo 1 and outputs and plasma anode voltages are through 4 type BNC coaxial connectors, W, X, Y, and Z, and 4 MHV coaxial connectors, A , B, C and D in photo 2. Also, housed in this unit are the thermistor temperature sensor, bridge resistors, preamplifier and heater resistors for the temperature control system. The temperature set-point adjustment is located on the preamplifier card (R_x on board 5). (Photo 3).

ELECTRONIC CONSOLE

The electronic circuitry and power supplies for the ring laser are mounted on this rack. Referring to photograph 4 their functions are:

A. Photomultiplier Hv: supplies high voltage to the control photomultiplier which senses power output of the laser. Normal setting 1.5 Kv.

B. Photomultiplier Hv: supplies high voltage to the beat photomultiplier, which senses beat frequency output of the laser. Normal setting 1.5 Kv.

C.D. Low-voltage Power Supplies. Supply positive and negative DC to various amplifiers and control circuits. Normal settings 15V.

E. Electronic Counter. Measures beat frequency output of ring laser. Also provides reset pulse for gating control circuits. Input A normally connected to BEAT OUT jack of Panel F.

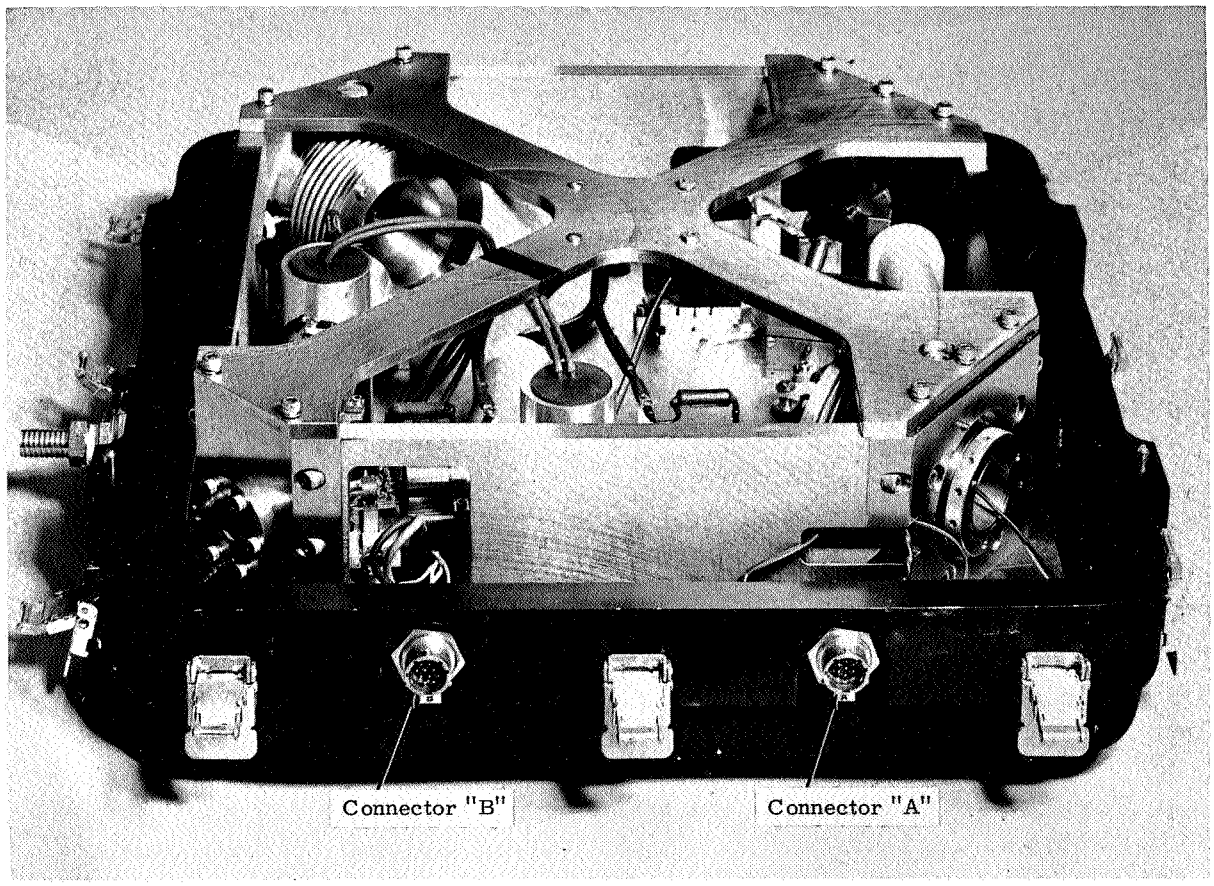


Photo 1. Optical Unit

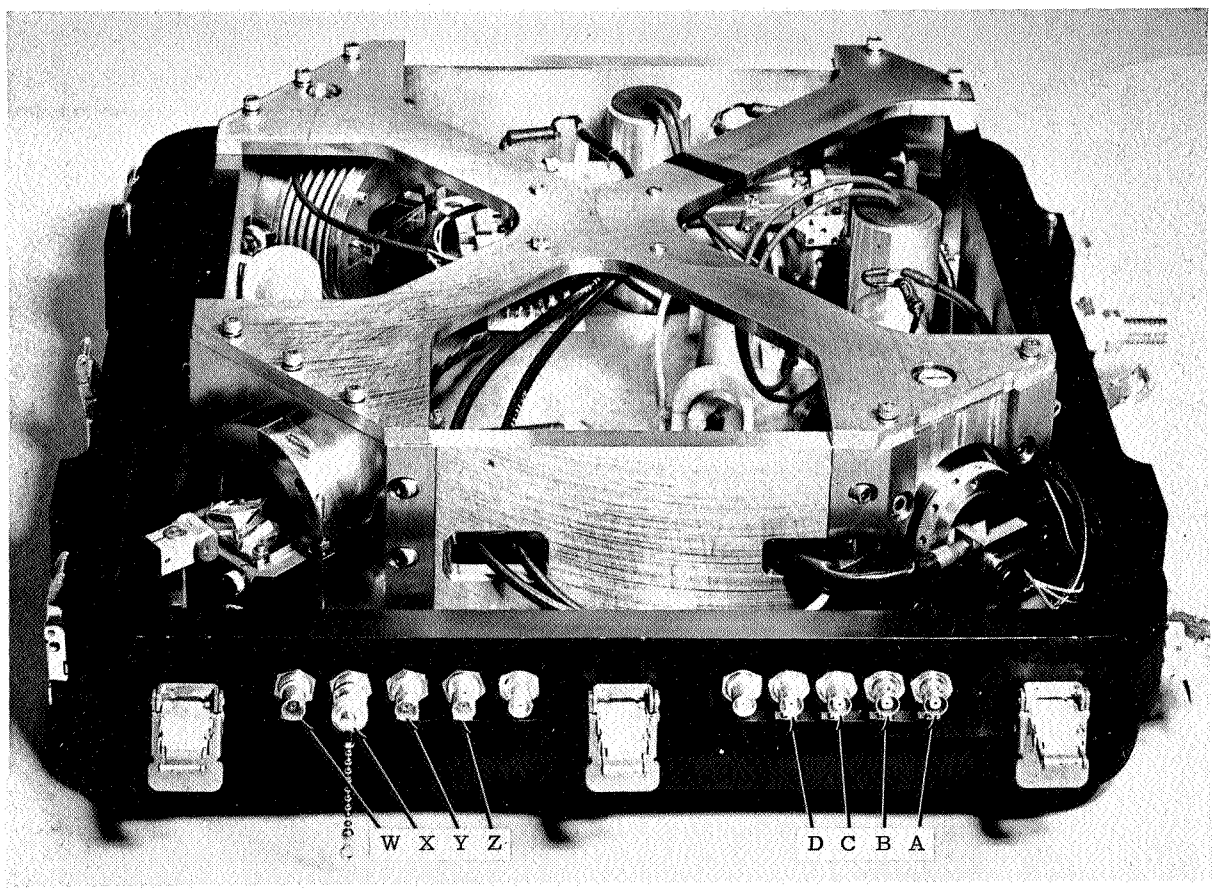


Photo 2. Optical Unit

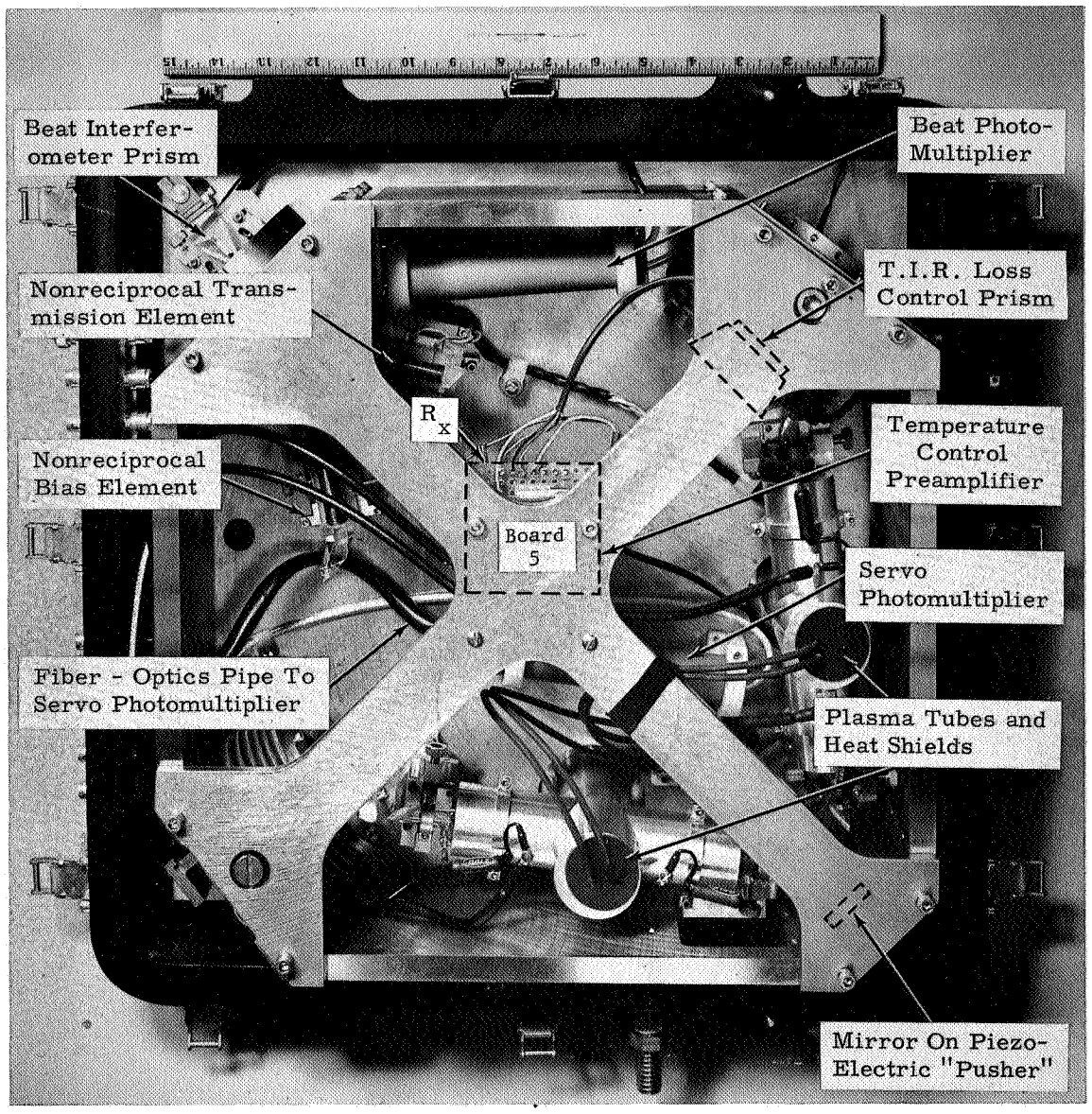


Photo 3. Optical Unit, Adjustment Point

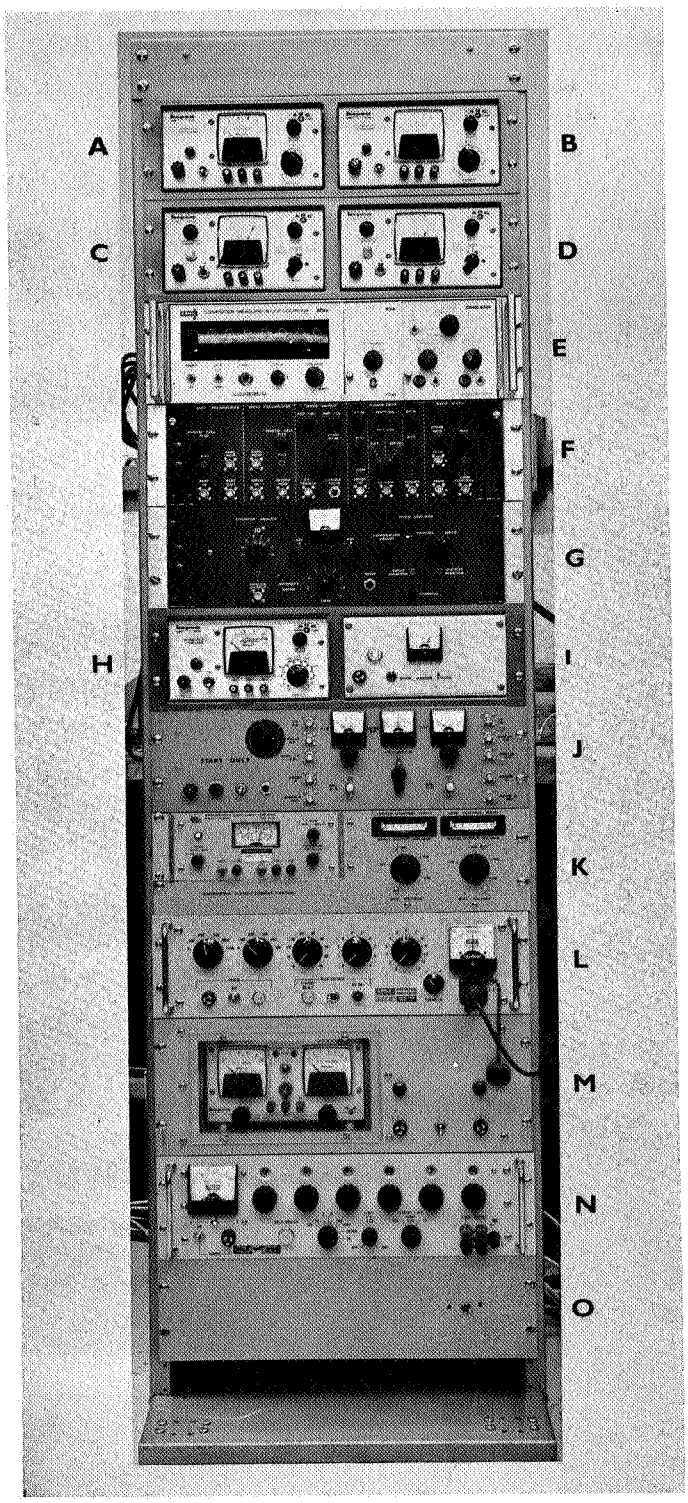


Photo 4. Electronic Console

F. Servo Control Chassis. Contains circuits and controls for operating tuning servo, and output driver for intensity servo. Controls and connections are as follows:

Beat Preamplifier Section

PHOTOCELL BIAS. Controls bias on amplifier for beat photocell. Monitored at BIAS jack.

AMPL. MON. jack allows output of amplifier to be displayed on oscilloscope.

BEAT IN (W) connected to output of beat photocell in laser housing (W).

BEAT OUT connected after squaring amplifier, operates counter (E).

Servo Preamplifier Section

PHOTOCELL BIAS. Controls bias on amplifier for tuning control photocell, monitored at BIAS jack.

AMPL. MON. jack allows output of amplifier to be displayed on oscilloscope.

SERVO IN (Z) connected to output of control photomultiplier in laser housing (Z).

SWITCH MON. allows monitoring output of servo switch.

Servo Switch Section

POS. ADJ. sets positive level of ramp voltage which tunes pusher.

NEG. ADJ. sets negative level of ramp voltage which tunes pusher.

SWEEP GAIN. adjusts magnitude of ramp voltage which tunes pusher.

EXT. TRIGGER:SINGLE PULSE switch. In EXT. TRIGGER connects servo to counter reset pulse for automatic cycling. In SINGLE PULSE position connects servo to push button for manual switching of servo position.

EXT. TRIGGER jack. Allows trigger to be extracted to synchronize oscilloscope.

Single pulse push button. Switches logic to opposite state.

Pusher Drive Section

EXTERNAL-MANUAL-SERVO selector switch - selects input to pusher drive amplifier.

EXT position: pusher drive amplifier receives input from SWEEP IN jack: 120v p-p sawtooth required for full drive of amplifier.

BIAS--adjusts operating point of pusher amplifier
GAIN--adjusts amplitude of pusher amplifier output

MANUAL position: pusher drive amplifier receives input from adjustment knob labeled POSITION, located directly above switch.

SERVO position: pusher drive amplifier receives input from intensity photocell and amplifiers.

IN MON jack. Connected to input of pusher driver amplifier.

PUSHER jack. Connects output to pusher (Y).

The red tip jack above PUSHER jack is also connected to the output.

The black tip jack labeled COMMON is the common power supply return for the servo circuits.

Sweep Width Section

Contains the adjustments for the driver stage of the laser intensity control servo.

STORE RATE control. Controls the amount of difference voltage applied to the intensity control servo.

BIAS. Controls the operating point of the loss control amplifier.

MON. A jack. Connects to + input of difference amplifier.
MON. B jack. Connects to - input of difference amplifier.

LOSS CONTROL jack. Connects output of amplifier to loss control (X). The red tip jack directly above also connects to the amplifier output.

G. Counter Analog - Intensity Servo - Oven amplifier panel

Analog Section

Connected behind the panel to the frequency counter. The 10^X switch selects any 3 adjacent decades of the counter display and provides an analog voltage at the ANALOG OUTPUT jack proportional to the displayed number. The voltage is inverted, in that a full scale voltage of 10v is produced for zero displayed count, decreasing to zero as the count increases to 999.

Intensity Servo Section

The zero center microammeter reads the output of the intensity servo differential amplifier for all positions of the selector switch directly below it.

ADJ A position and knob sets positive input bias level of amplifier.

ADJ B position and knob sets negative input bias level of amplifier.

RUN position connects both inputs for servo operation.

GAIN control adjusts gain of differential amplifier. Position 1 is off.

RESET push button discharges condensers in feedback circuit, to facilitate setup.

Oven Amplifier Section

MANUAL-SERVO switch, in MANUAL position connects oven heater driver input to a fixed, manually adjustable

voltage, adjusted with TEMPERATURE ADJUST potentiometer at left of switch. In SERVO position input is the error signal from the thermistor bridge located in the laser housing.

INPUT MONITOR connects to the input line to the amplifier. OUTPUT MONITOR connects to the output line from the amplifier.

COMMON jack is the common power supply line for the circuits.

H. Driver power supply - supplies positive 500v to pusher driver and loss control driver. Normal setting 500v.

I. Oven heater driver - supplies output current to housing heater resistors. The meter reads the resistor current in amperes. Normal reading - about 2 amp, depending on ambient. ON-OFF switch turns off only the driver circuits.

J. Plasma current control and start circuit.

START ONLY section is required when starting the plasma tube discharges. It applies a high voltage pulse to each anode to break down the plasma. The plasma cathode voltage must be applied to maintain the discharge (Power Supply L).

START LEVEL adjustment - adjusts the magnitude of the starting pulse. Normal setting 70.

Push button - applies pulse to anodes.

ON-OFF switch, pilot light, and fuse at left of panel refer only to START controls.

JACK: TP A,B monitors input to A-B current control.
JACK: MOD IN A, B allows connecting a signal input to current control of A,B
JACK: AMP IN A, B not functional
JACK: ANODE A connects to Anode A in laser housing
JACK: ANODE B connects to Anode B in laser housing
METER: A+B Reads total current through sections A and B of one plasma tube
POTENTIOMETER: A+B - adjusts sum of currents of A and B sections

POTENTIOMETER: A-B - balances currents in sections A and B.
METER: ANODE BAL - reads difference in currents between A and B or C and D, depending on position of switch located directly below. In START position of switch the meter is disconnected and the START circuitry is enabled.
METER: C+B - reads total current through sections C and D of one plasma tube.
POTENTIOMETER: C+D - adjusts sum of currents of C and D sections.
POTENTIOMETER: C-D - balances currents in sections C and D.
JACK: TP C,D - monitors input to C-D current control.
JACK: MOD IN C, D - allows connecting a signal input to current control of C-D.
JACK: AMP IN C-D - not functional.
JACK: ANODE C - connects to anode C in laser housing.
JACK: ANODE D - connects to anode D in laser housing.

K. Transmission Element Current Control Section

Supplies regulated current to the non-reciprocal transmission element in the laser.

SWITCH OFF-VOLTS-AMPS: normally set to AMPS, the panel meter then reads coil current. Normal reading about .2 amp.

MODE SWITCH - normally set to SUPPLY.

VOLTS-GAIN switch-functions as a current adjustment. Coarse and fine adjustments are available.

Front panel input and output terminals are not used.

Meter and Bias Section

PUSHER CONTROL SERVO section. The meter reads output voltage of the pusher driver amplifier. BIAS VOLTAGE potentiometer adjusts voltage on pusher element return lead. Range is zero to 400 volts. This voltage is added to the voltage indicated on the meter above the knob.

LOSS CONTROL SERVO section. The meter reads output voltage of the loss control driver amplifier.

BIAS VOLTAGE potentiometer adjusts voltage on loss control element return lead. Range is zero to 400 volts. This voltage is added to the voltage indicated on the meter directly above the knob, up to a total of 700v. At that voltage, a zener regulator limits the total value to prevent damage to the element.

L. **Plasma Voltage Source,** supplies a negative voltage to the cathodes of the plasma tubes.

M. Plasma Tube Filament Current supply provides current for the hot cathodes of the plasma tubes. An isolation transformer and standoff insulators are provided inside the housing to allow operation of the entire supply at elevated potential.

N. Non-reciprocal Bias Element Current Supply. Supplies current to the Faraday bias cell. Normal setting: about .7 amp for 40 Kc bias.

O. Bias Polarity Reversing Switch, reverses polarity of current to non-reciprocal bias element.

RING LASER SENSOR - START-UP PROCEDURE

Assume all individual unit power switches are OFF.

1. Connect anode cables A, B, C, D to the respective labeled jacks on laser housing, and on panel J.

2. Connect Input and Output coaxial cables W, X, Y, and Z to the respective labeled jacks on laser housing and on panel F.

3. Connect BEAT OUT jack, panel F to input A of CMC counter, panel E.

4. Connect AMPL MON jack of Servo Preamplifier section panel F to vertical input of oscilloscope; sensitivity 1v/cm.

5. Connect sawtooth output of scope to SWEEP IN jack of Pusher Drive section of panel F.

6. Connect PUSHER output pin jack to horizontal input of scope (range 0 to 500v).

7. Connect power cables A and B to respective labeled jacks on laser housing.

8. Plug in main power cord to a source of 115v-60 cps AC.

9. Turn on Power supplies C, D and set to 15v.

10. Turn on power supply M and set voltage control for current of 2.8 amp. This occurs at a voltage of 5.6v. Set current limit (right hand knob) to be slightly above 2.8 amp.

11. Turn on power supply L. High voltage switch must be in STANDBY position. This unit is energized from unit M and will not operate when M is off. Set voltage to 1100v, Polarity Switch to negative. When STANDBY light comes on, turn switch to Hv-ON.

12. On panel J set BAL A-B and BAL C-D to mid-range. Set ADJ A+B and ADJ C+D knobs to mid-range. Set switch S_3 to START. Set START LEVEL potentiometer to 70. Turn on switch and press START button momentarily. Meters A+B and C+D should now read total currents of about 6mA. Check balance of sections by turning selector switch to A-B. Adjust center meter to zero by rotating A-B control. Repeat for C-D. Set A+B and C+D to 5 mA. If currents cannot be balanced it indicates one section of the tube did not fire. To restart, turn off High Voltage momentarily, and repeat above steps, increasing START LEVEL potentiometer setting if necessary.

13. Turn on photomultiplier supplies A, B, and set to 1500v.

14. Turn on power supply H and set to 500v.

15. Turn on Oven Heater Driver I. Set switch on Oven Amplifier control panel G to MANUAL and adjust meter on panel I to 2 amp using TEMPERATURE ADJ on panel G.

16. Turn on Transmission Element Current Control (panel K).
    Set METER switch to AMPS.
    MODE switch to SUPPLY.
    VOLTS-GAIN knobs to give about .2 amps current.

17. Turn on power supply (panel N) and set to .7 amps.

ADJUSTMENT OF TUNING CONTROL SERVO

Operation of the tuning control servo requires that the laser be running in a single mode at an intensity low enough to be out or nearly out near the ends of the Doppler-broadened gain curve. Sufficient warm-up time should be allowed so that this condition can be maintained during adjustment of the servo.

The intensity servo should be turned off during adjustment of the tuning servo. Set GAIN switch on panel G to position 1.

1. Connect oscilloscope sawtooth output to SWEEP IN jack on panel F.

2. Set selector switch on panel F, Pusher Drive Section to EXT position.

3. Set oscilloscope sweep rate to 20 millisec per cm (5 cps).

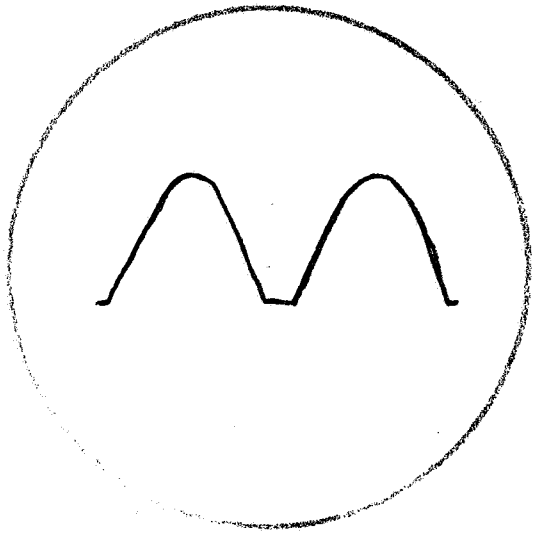
4. Connect oscilloscope vertical input to AMPL MON jack, Servo Pre-Amplifier section of panel F. Vertical sens 1v/cm.

5. Set Photo cell Bias Servo Pre-amplifier section to give a voltage of 2v at BIAS jack.

   Set Photo cell BIAS in BEAT PREAMPLIFIER section to give a voltage of 2v at BIAS jack.

6. Set Loss Control BIAS (Sweep Width Section of panel F) to give 250v out of Loss Control Driver. This voltage may be read on the meter at the right side of panel K.

7. Increase BIAS VOLTAGE knob setting on loss control (panel K, right hand knob) until the laser is going out between orders, as indicated by the oscilloscope pattern, sketched below:



8. Set Counter (panel E) DISPLAY to ∞ (fully CW). Connect BEAT OUT jack to Input jack A on counter.

9. Set Counter Time Base to give .1 sec gate.

10. Set Counter A attenuator to X1 position.

11. Set Counter function switch to FREQ A.

12. Turn PUSHER DRIVE selector switch (panel F) to SERVO position.

13. Set GAIN control for SERVO side of selector switch to about 70% of fully CW position.

14. Place a grounding cap on IN MON jack just below switch, and adjust BIAS potentiometer on **panel** F to give 250v at output of Pusher driver. This voltage may be read on the center meter on panel K. Remove grounding **c**ap after making adjustment.

15. Set selector switch in SERVO SWITCH section of panel F to EXT TRIGGER position.

16. Press RESET button on counter, to initiate servo timing circuits.

17. Connect horizontal input of oscilloscope to pusher output tip jack (panel F).

18. Adjust POS ADJ and NEG ADJ (SERVO SWITCH section of panel F) to give minimum over-and undershoot on oscilloscope pattern.

19. Adjust width of scan pattern by adjusting Loss Control Servo BIAS VOLTAGE (right hand knob on panel K) to give a scan width of about 1/4 of an order. Reset POS ADJ and NEG ADJ if necessary to correct overshoot.

The positions on the Doppler curve between which the servo tunes may now be adjusted by changing the servo Pre-Amplifier PHOTO CELL BIAS setting. Increasing the photocell bias tunes to a pair of positions at a higher intensity level; decreasing bias tunes to positions nearer zero intensity.

The tuning positions relative to the Doppler curve may also be changed by changing the laser intensity, either with the Loss Control BIAS VOLTAGE control, or by changing plasma currents (ADJ A+B or ADJ C+D on panel J).

ADJUSTMENT OF INTENSITY (LOSS) CONTROL SERVO

Adjustment of this servo will be facilitated if counter is set for 0.1 second gate.

1. Set GAIN control (in center of panel G) to position 2.

2. Set ADJ A - RUN - ADJ B selector switch to position ADJ A.

3. Set knob A so that the meter remains at zero. Recovery from large unbalances may be speeded up by pushing RESET button on panel G.

4. Set selector switch to position ADJ B.

5. Set knob B so that meter remains at zero. Use RESET button if necessary.

6. Set selector switch to RUN and increase GAIN switch setting. Maximum setting is about 8 for 0.1 second counter gate time, 5 for 1 second gate time.

7. Make final adjustment of scan width by adjusting knob B with switch in RUN position, to bring meter to zero reading.

ADJUSTMENT OF TEMPERATURE CONTROL SERVO

1. Set Oven Amplifier selector switch to MANUAL position (panel G).

2. Set TEMPERATURE ADJUST knob to give a reading of 2 amperes on Oven Heater Driver meter. (Panel I).

3. Allow several hours for oven to reach a steady state condition.

4. Connect a DC voltmeter 0-10v range between Tip Jack INPUT MONITOR and COMMON on Oven Amplifier chassis.

5. Remove cover from laser housing (NOTE: Unplug heater cable to cover before lifting cover more than a few inches).

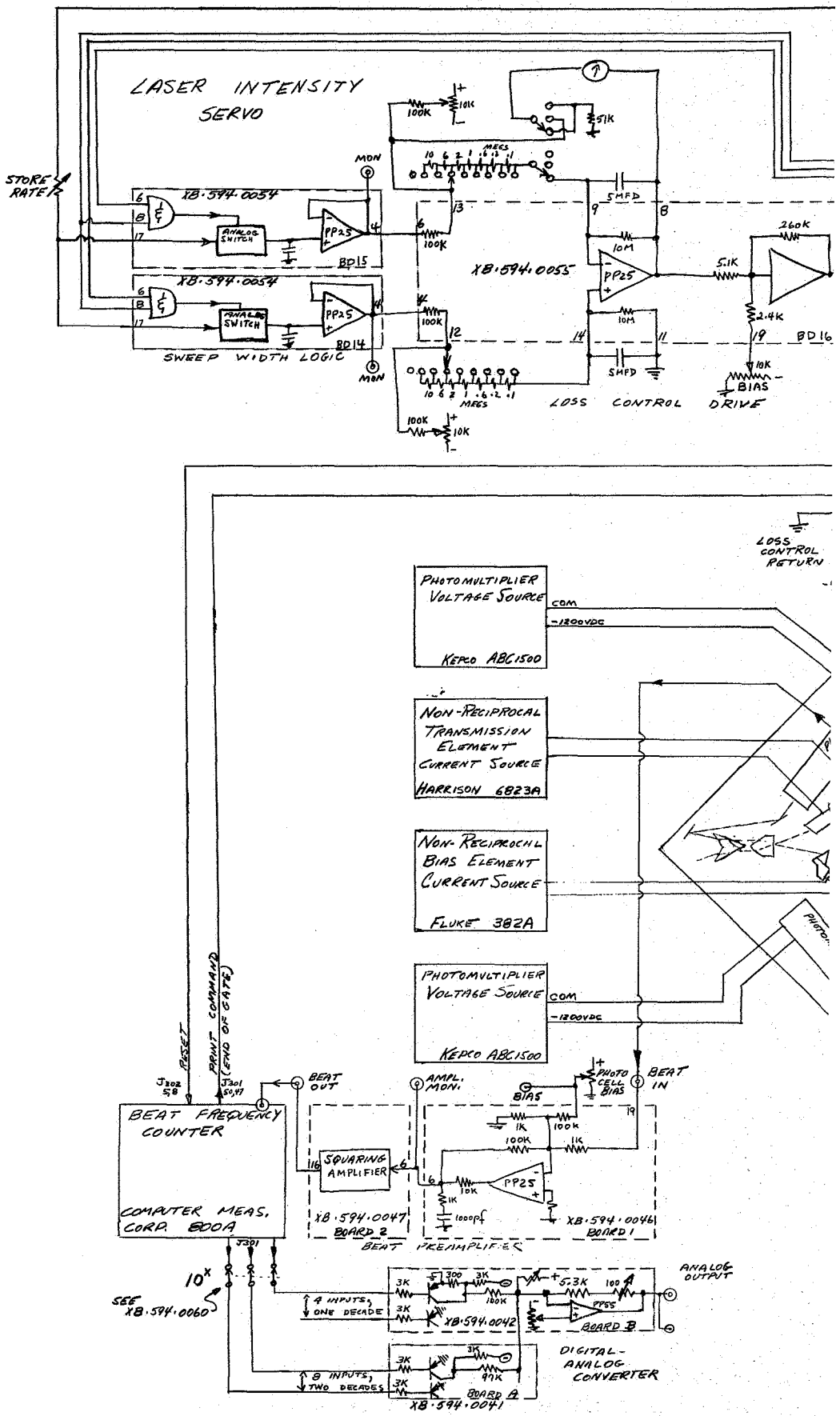
6. Quickly, before inside temperature changes, adjust resistor

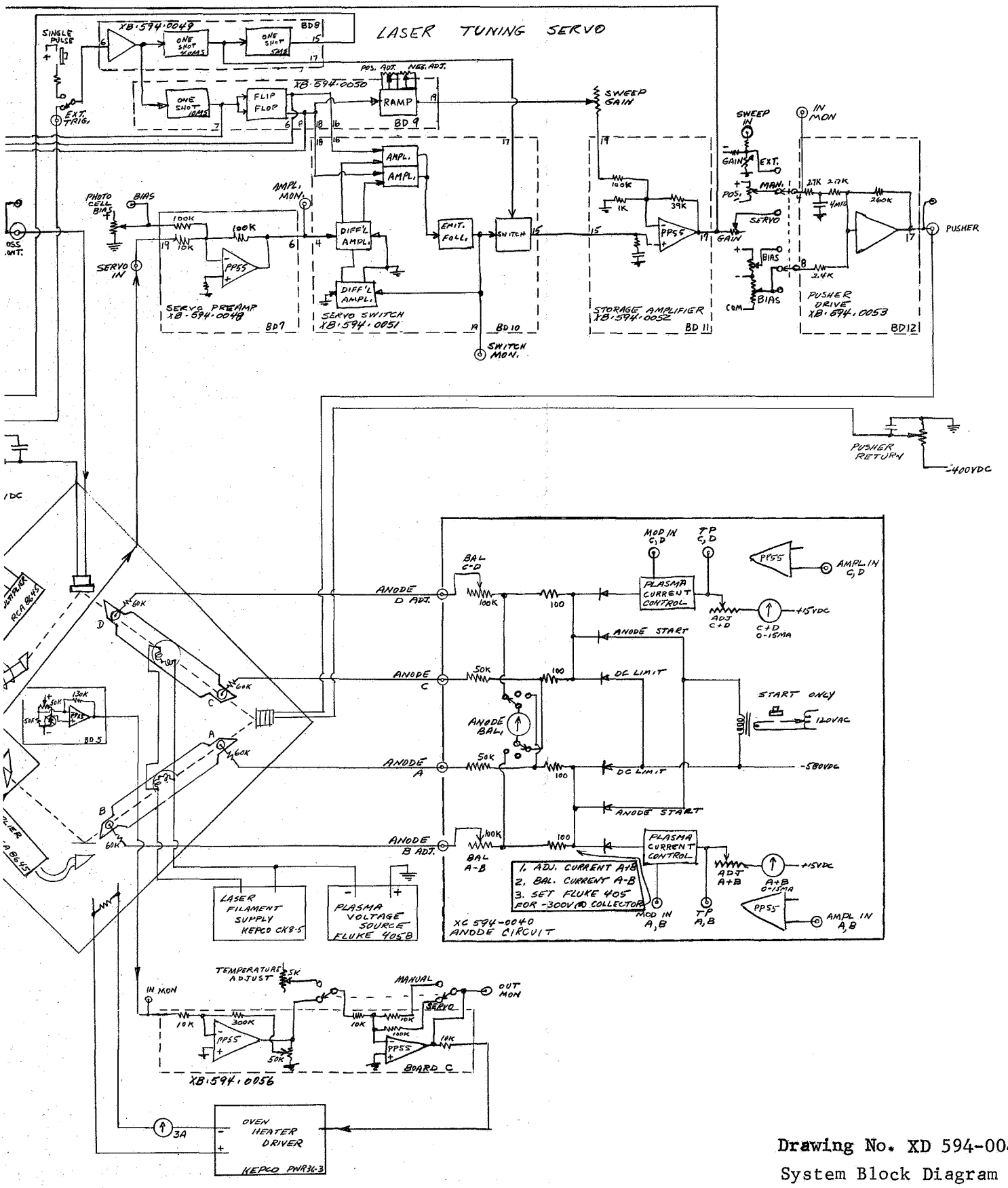
R_X on Temperature Control Preamplifier to bring voltmeter reading to zero. The Preamplifier card is attached to the center of the "X" brace of the laser invar frame. The location of resistor R_X is indicated on photograph 4. A short screwdriver having a 1/16" wide blade is required for the adjustment.

7. Replace cover, replugging cover heater cable at the same time.

8. Turn Oven Amplifier selector switch to SERVO.

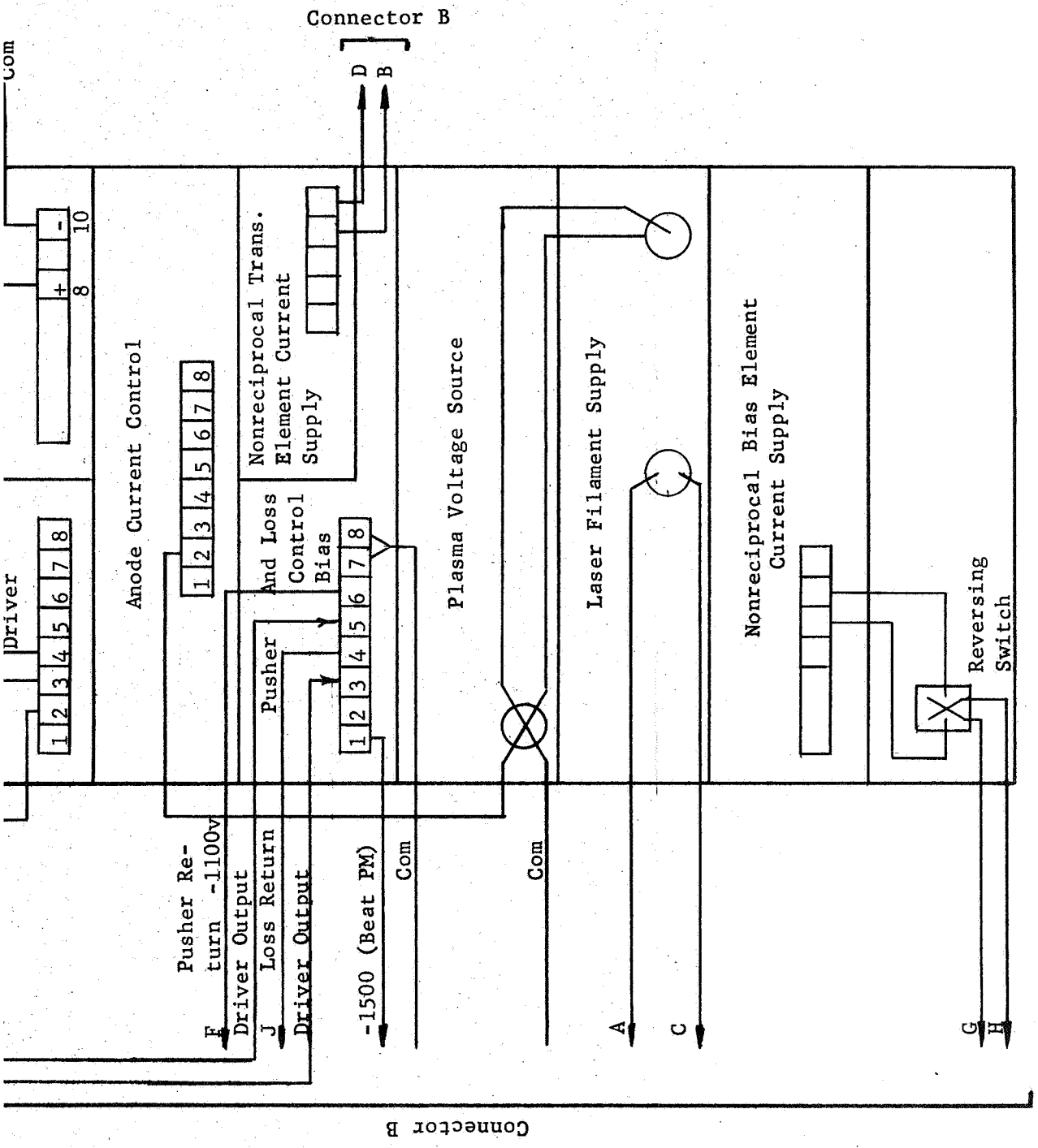
Heater current should stabilize near the initial value of 2 amperes. If not, it is necessary to repeat the above steps.


LASER INTENSITY SERVO
STORE RATE
XB·594·0054
ANALOG SWITCH
PP25
BD15
XB·594·0054
ANALOG SWITCH
PP25
BD14
SWEEP WIDTH LOGIC
MON
MON
100K
101K
51K
MEGS
10 6 2 1 .6 .2 .1
5MFD
XB·594·0055
10M
PP25
260K
5.1K
2.4K
BD16
100K
10K
BIAS
DRIVE
LOSS CONTROL
LOSS CONTROL RETURN
PHOTOMULTIPLIER VOLTAGE SOURCE
COM
-1200VDC
KEPCO ABC1500
NON-RECIPROCAL TRANSMISSION ELEMENT CURRENT SOURCE
HARRISON 6823A
NON-RECIPROCAL BIAS ELEMENT CURRENT SOURCE
FLUKE 382A
PHOTOMULTIPLIER VOLTAGE SOURCE
COM
-1200VDC
KEPCO ABC1500
PHOTOT...
RESET
PRINT COMMAND (END OF GATE)
J302 5,8
J301 50,47
BEAT FREQUENCY COUNTER
COMPUTER MEAS. CORP. 8004
BEAT OUT
AMPL. MONI.
BIAS
PHOTO CELL BIAS
BEAT IN
SQUARING AMPLIFIER
XB·594·0047
BOARD 2
BEAT PREAMPLIFIER
PP25
1000pf
XB·594·0046
BOARD 1
J301
10^X
SEE XB·594·0060
9 INPUTS, ONE DECADE
9 INPUTS, TWO DECADES
XB·594·0042
BOARD B
XB·594·0041
BOARD A
DIGITAL-ANALOG CONVERTER
ANALOG OUTPUT
5.3K
100
PP55

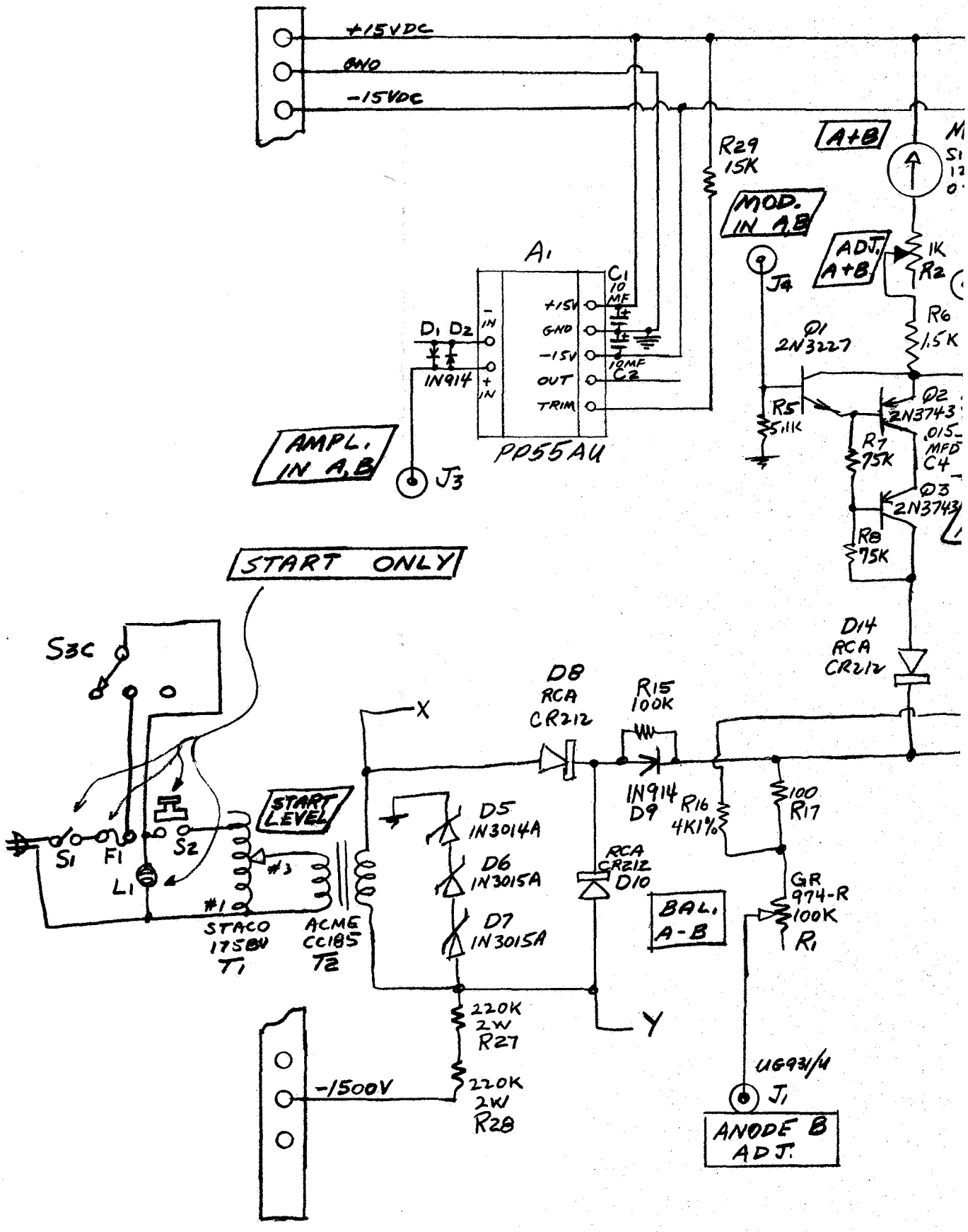


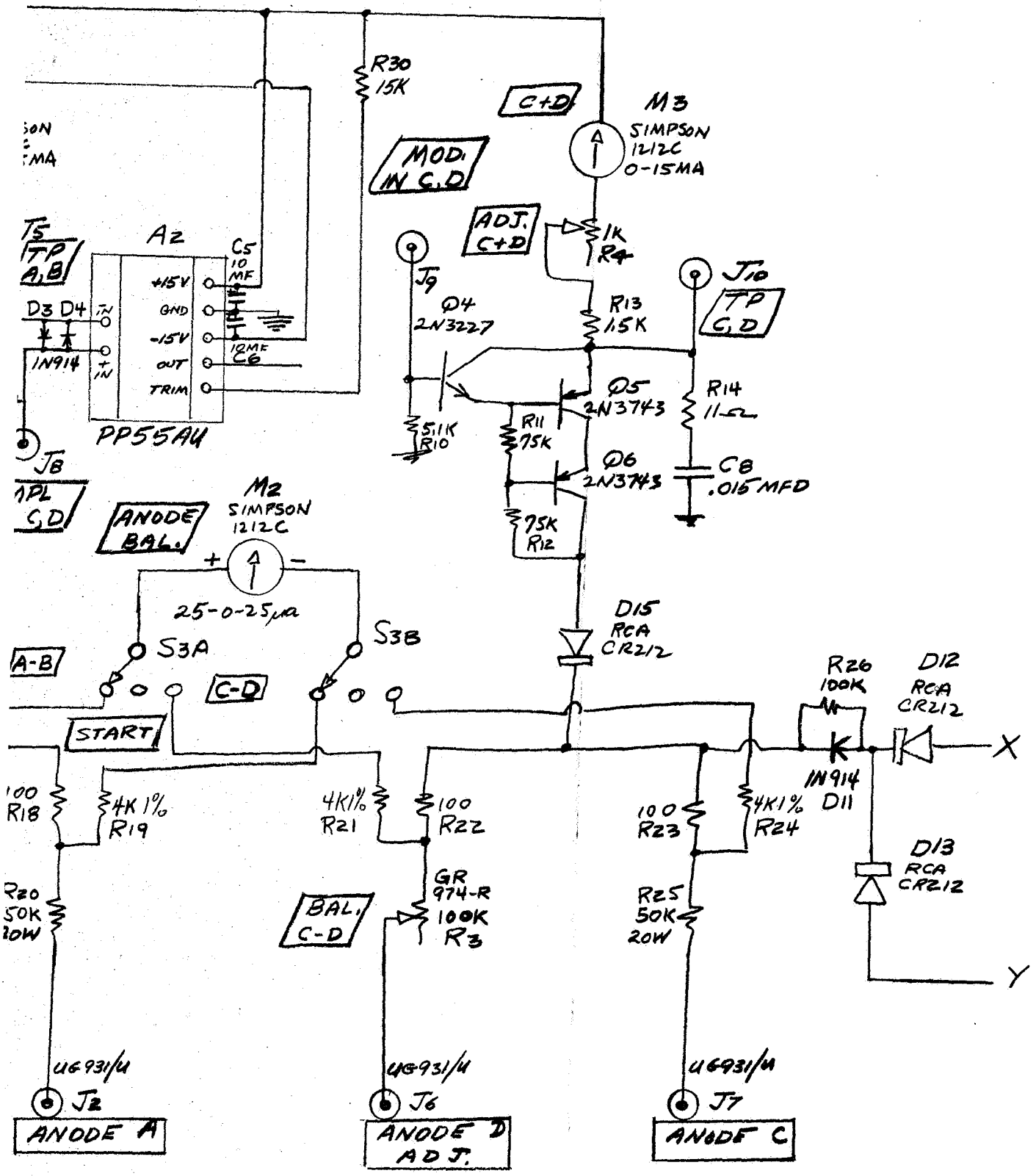
Drawing No. XD 594-0043
System Block Diagram

Connector A
(+1500 Servo PM)
C
(-1500)
(Servo P.M.)
D
Com
Servo P.M
Voltage Supply
8
10
+15 v. Supply
4
6
Beat P.M
Voltage Supply
8
10
-15 v. Supply
4
6
Counter
J301
J302
Servo Chassis
+500 v.
Digital-To-Analog Converter
Intensity Servo
Tempera-ture Control
+15v
Com
-15v
A (-1500)
Com
B (+1500 Beat PM)
F (+15)
H Com
G (-15v)
Com
E
J
Connector A

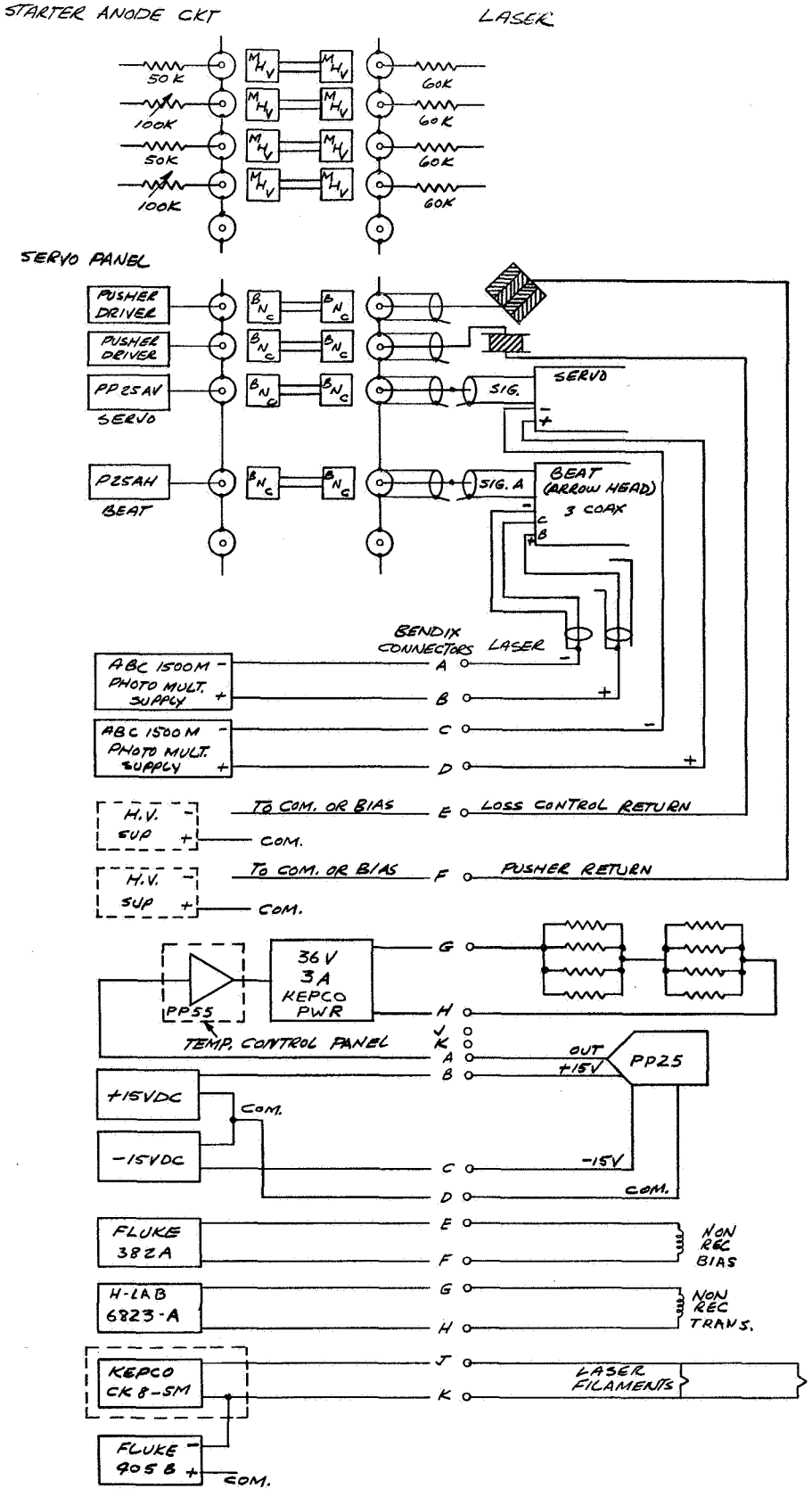


Cabling Diagram - Rear Of Rack

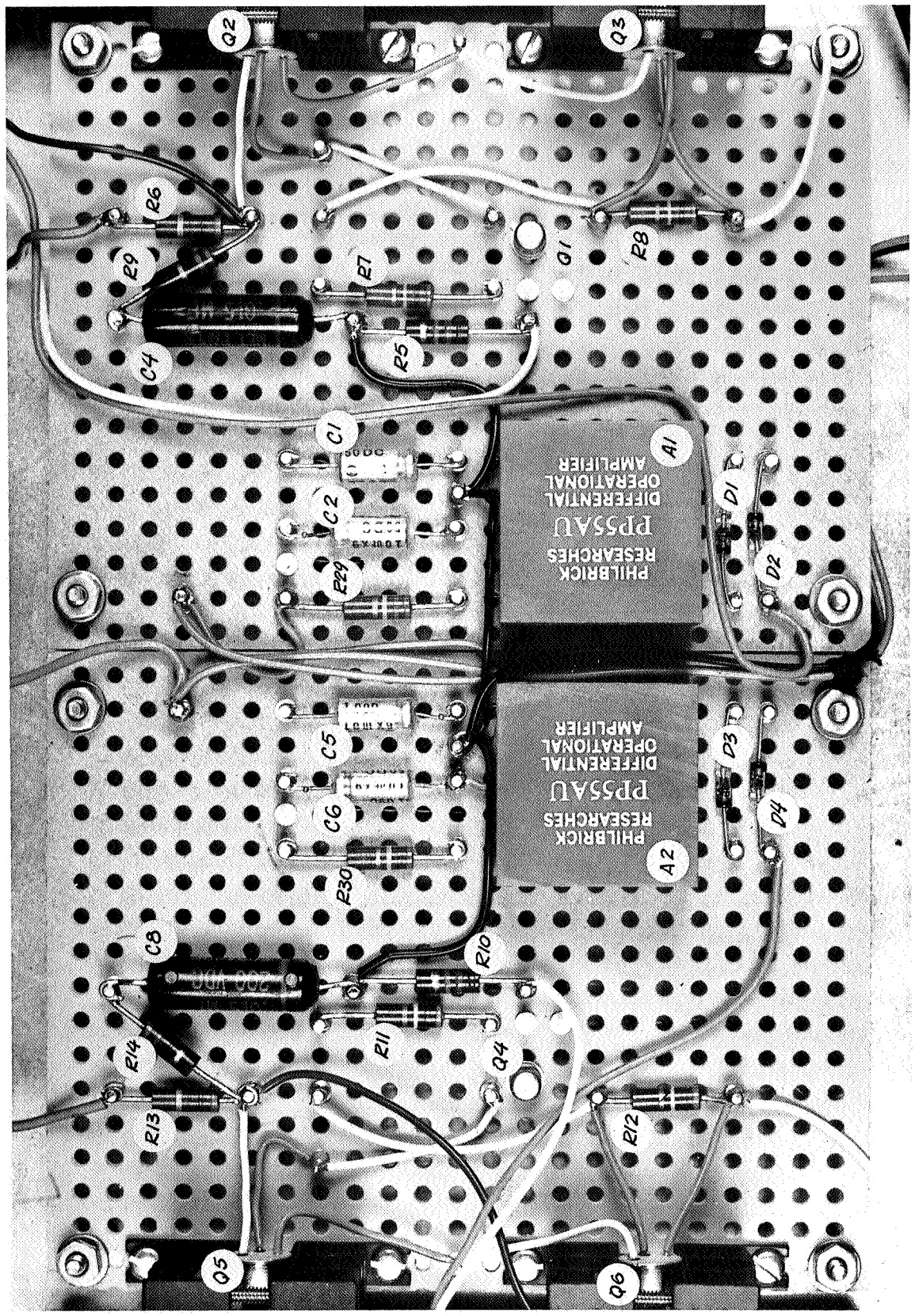

+15VDC
GND
-15VDC
R29
15K
A+B
MOD.
IN A,B
ADJ.
A+B
1K
R2
R6
1.5K
A1
C1
10
MF
D1 D2
IN914
-IN
+IN
+15V
GND
-15V
OUT
TRIM
12MF
C2
PP55AU
J4
Q1
2N3227
R5
5.11K
Q2
2N3743
.015
MFD
C4
R7
75K
Q3
2N3743
R8
75K
AMPL.
IN A,B
J3
START ONLY
D14
RCA
CR212
S3C
D8
RCA
CR212
R15
100K
X
START
LEVEL
S1
F1
S2
L1
#3
#1
STACO
175BV
T1
ACME
CC185
T2
D5
IN3014A
D6
IN3015A
D7
IN3015A
IN914
D9
R16
4K1%
100
R17
RCA
CR212
D10
BAL.
A-B
GR
974-R
100K
R1
220K
2W
R27
220K
2W
R28
-1500V
Y
UG931/U
J1
ANODE B
ADJ.



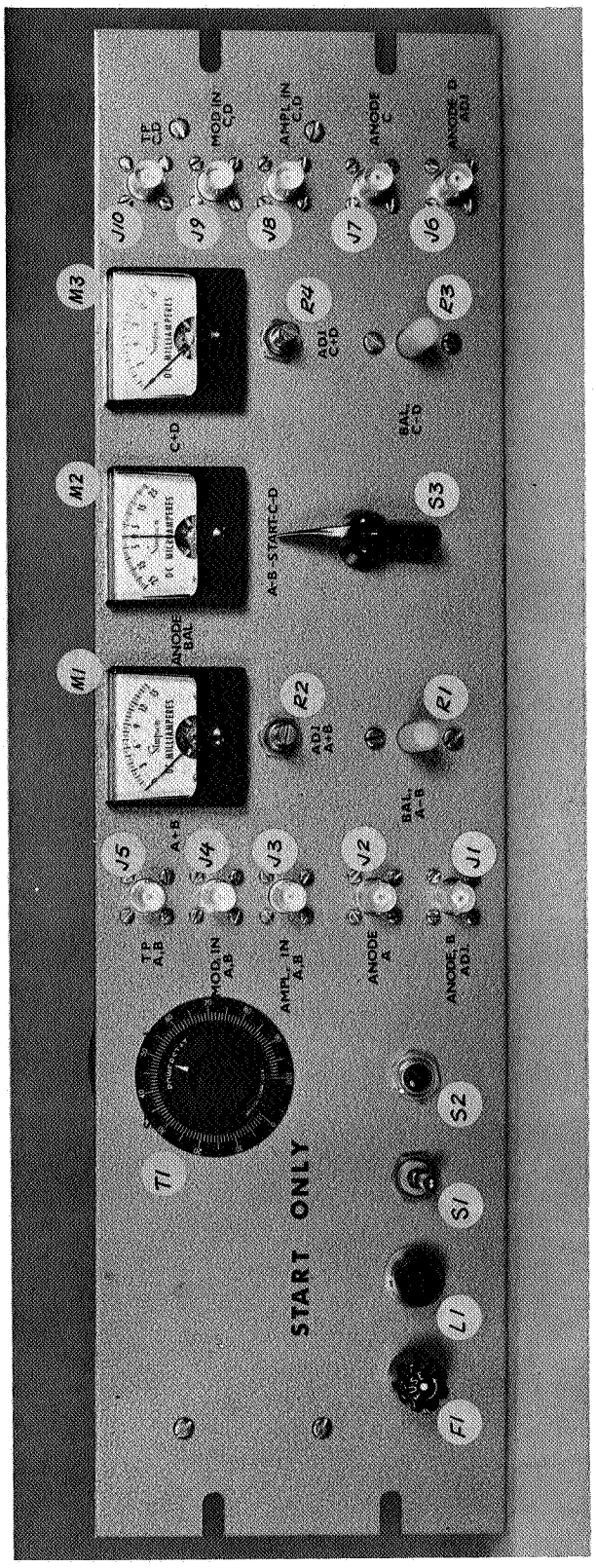
Ring Laser Anode Circuit



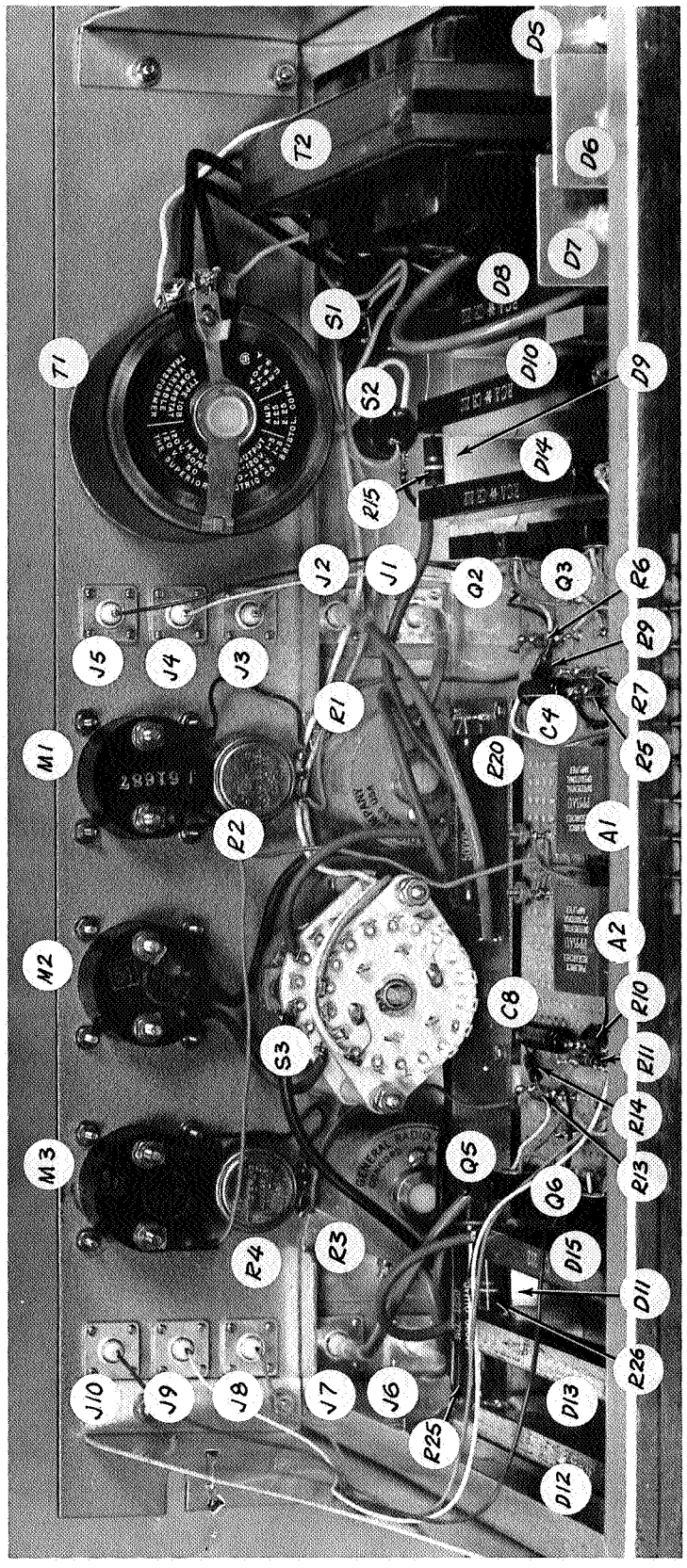
System Cabling Diagram



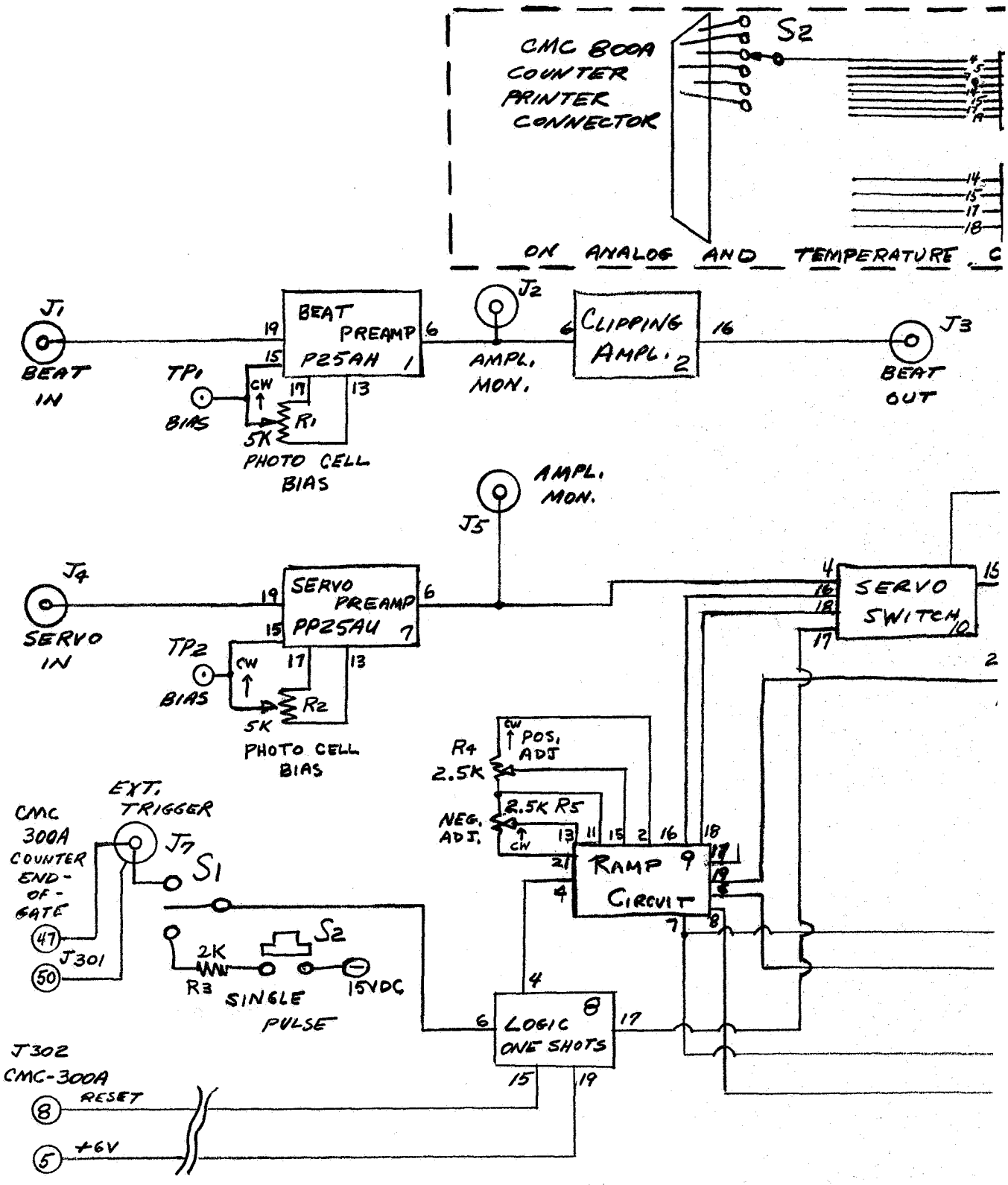
Photograph of Laser Anode Circuit Board

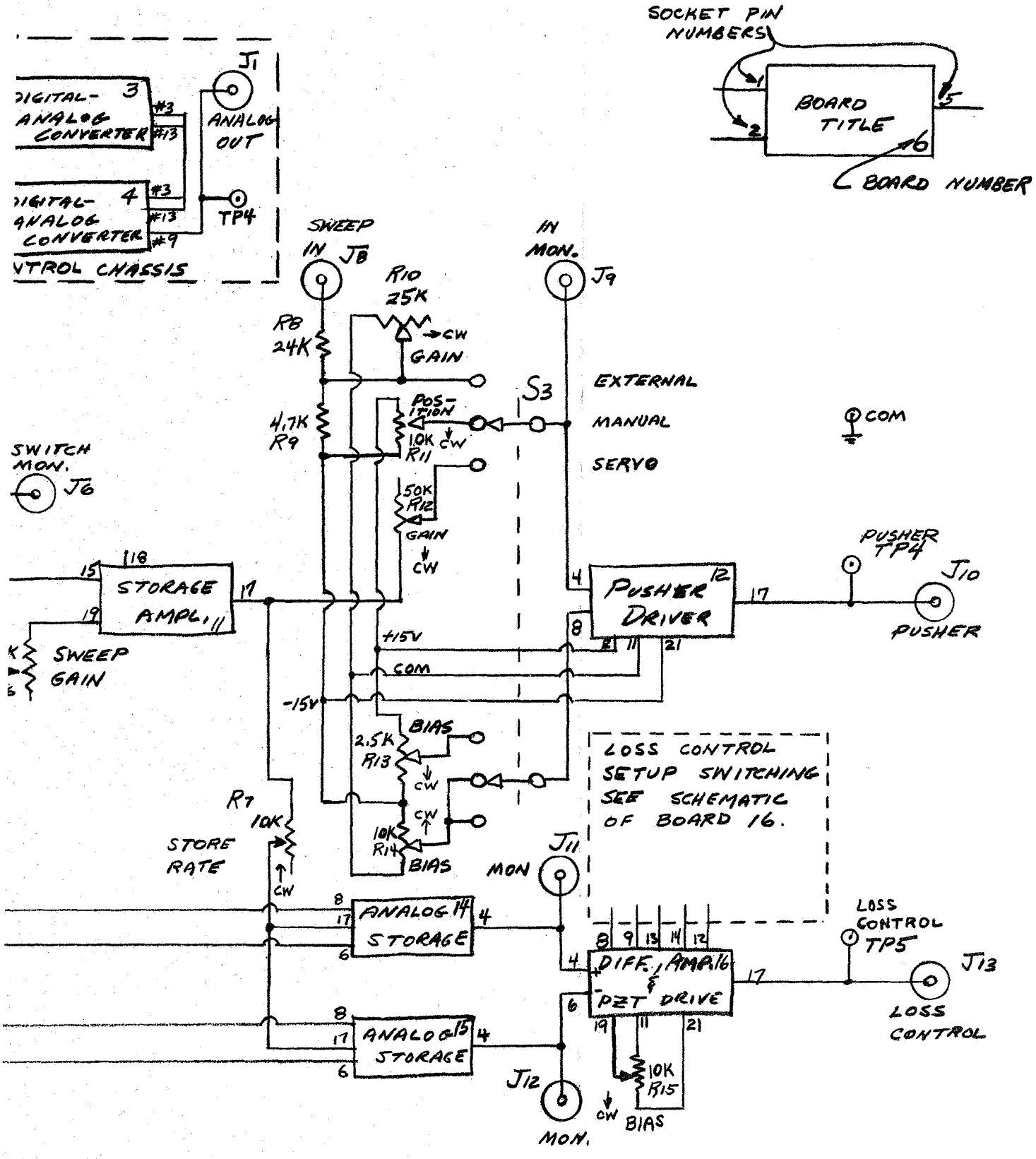


Photograph of Anode Panel - Front

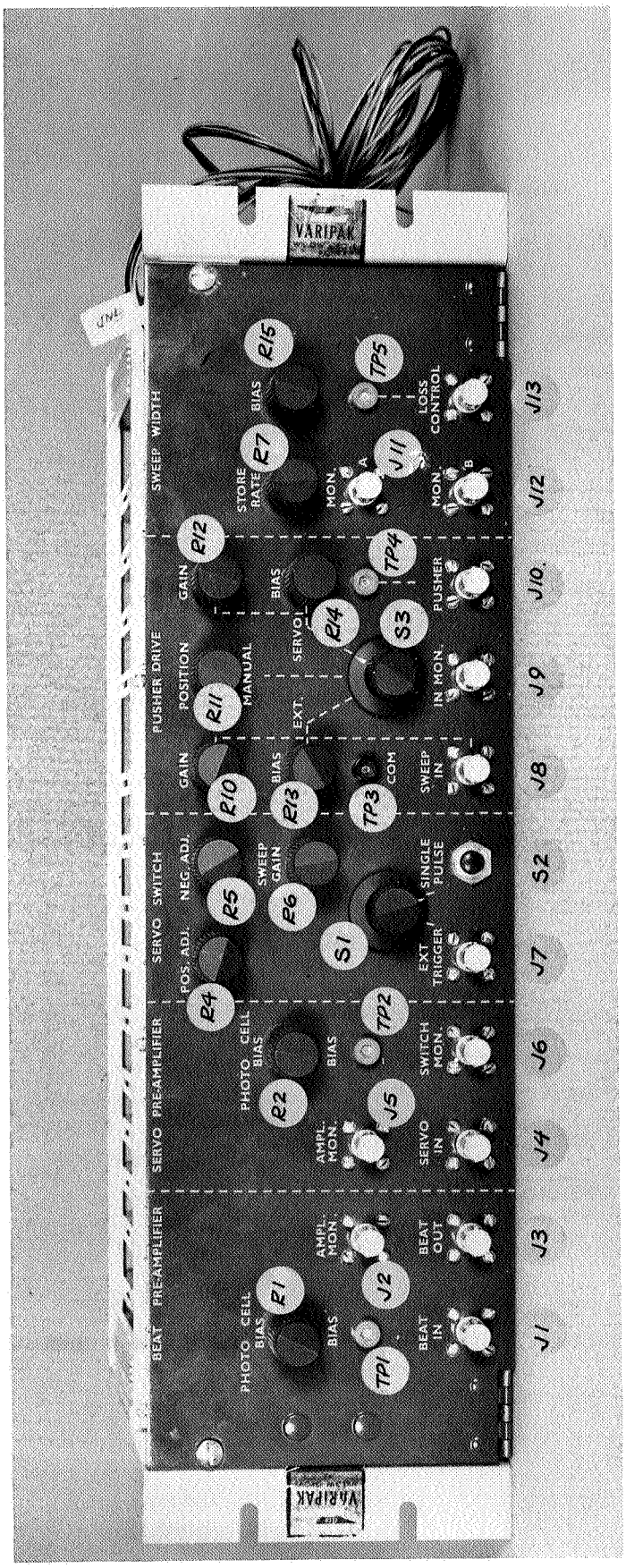


Photograph of Anode Panel - Rear

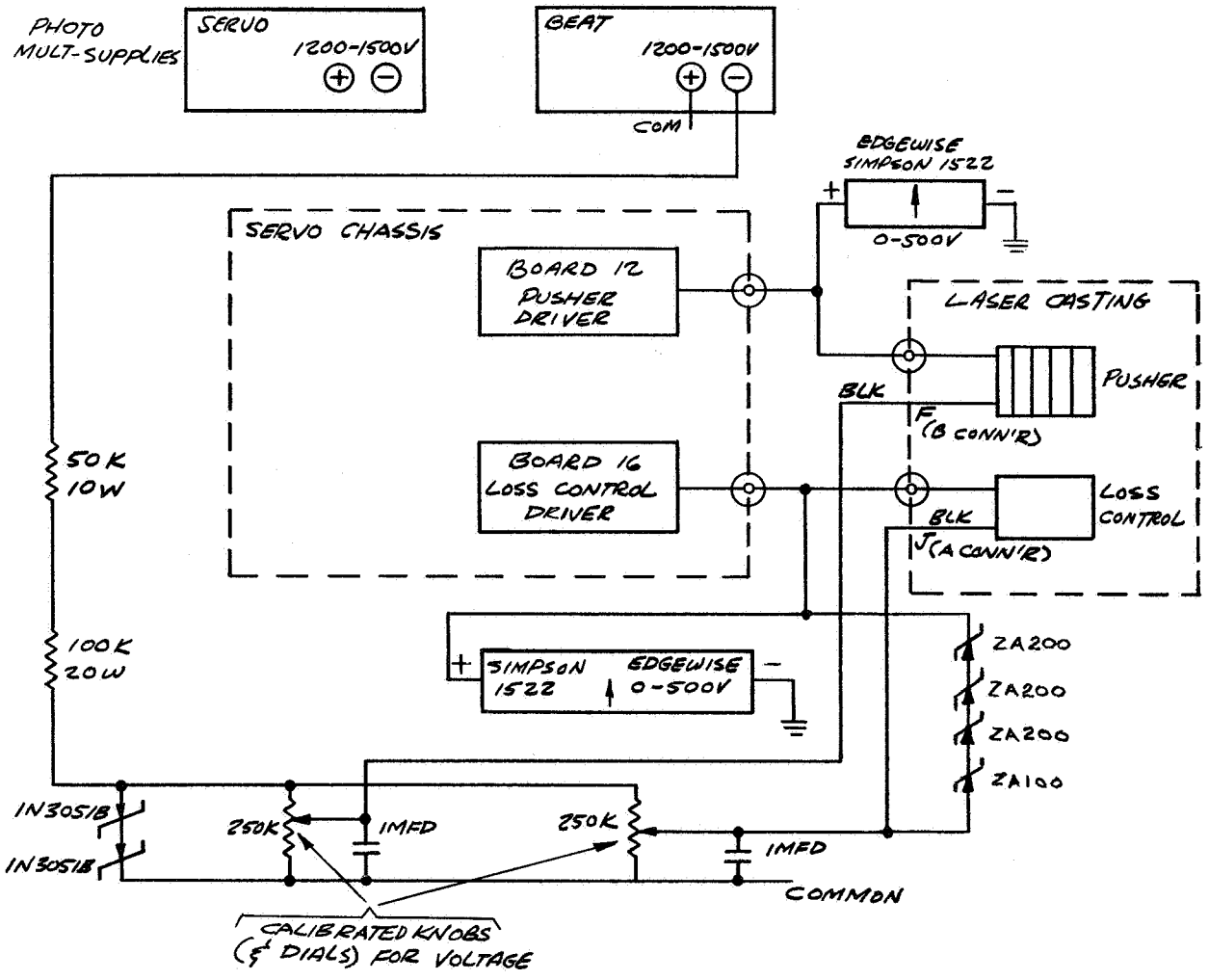

CMC 800A
COUNTER
PRINTER
CONNECTOR
S2
ON ANALOG AND TEMPERATURE
J1
BEAT IN
BEAT PREAMP P25AH 1
TP1
BIAS
CW
R1
5K
PHOTO CELL BIAS
J2
AMPL. MON.
CLIPPING AMPL. 2
J3
BEAT OUT
J5
AMPL. MON.
J4
SERVO IN
SERVO PREAMP PP25AU 7
TP2
BIAS
R2
5K
PHOTO CELL BIAS
SERVO SWITCH 10
R4
2.5K
CW POS. ADJ
2.5K R5
NEG. ADJ.
RAMP 9 CIRCUIT
CMC 300A COUNTER END-OF-GATE
EXT. TRIGGER
J7
S1
J301
47
50
S2
2K
R3
SINGLE PULSE
15VDC
LOGIC ONE SHOTS 8
J302
CMC-300A
8
RESET
5
+6V



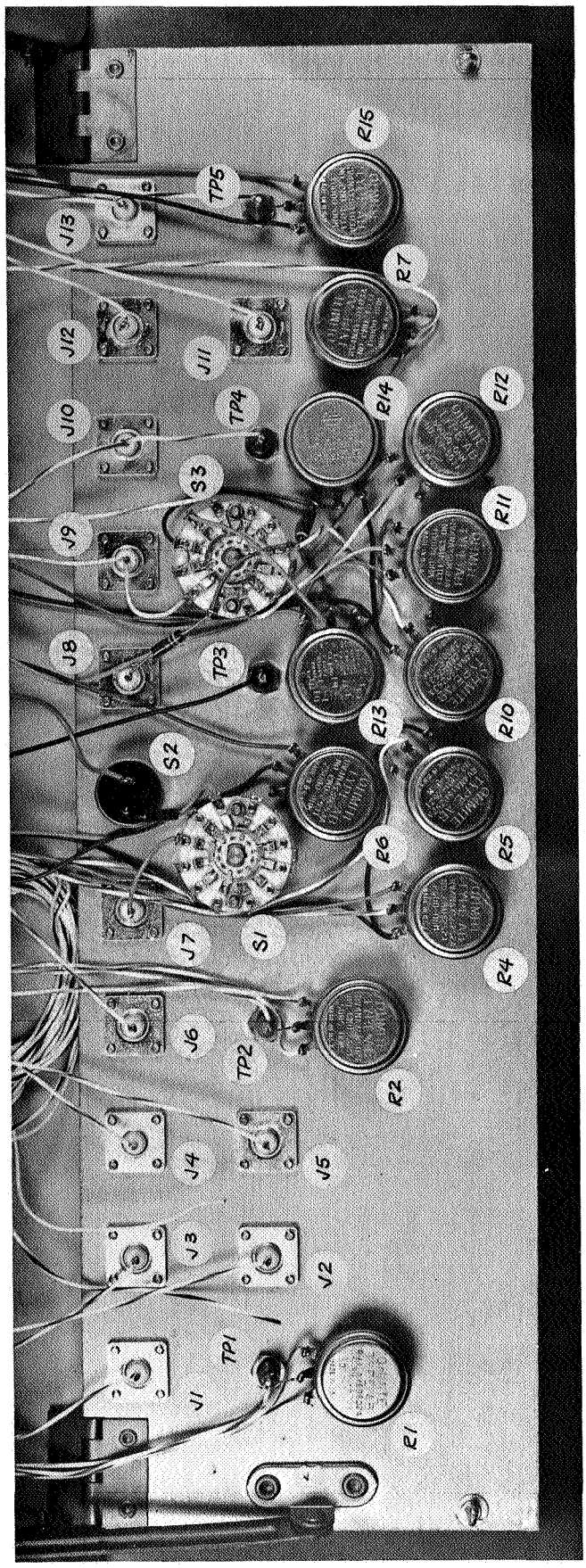
Servo Chassis Panel Interconnections
With Circuit Boards



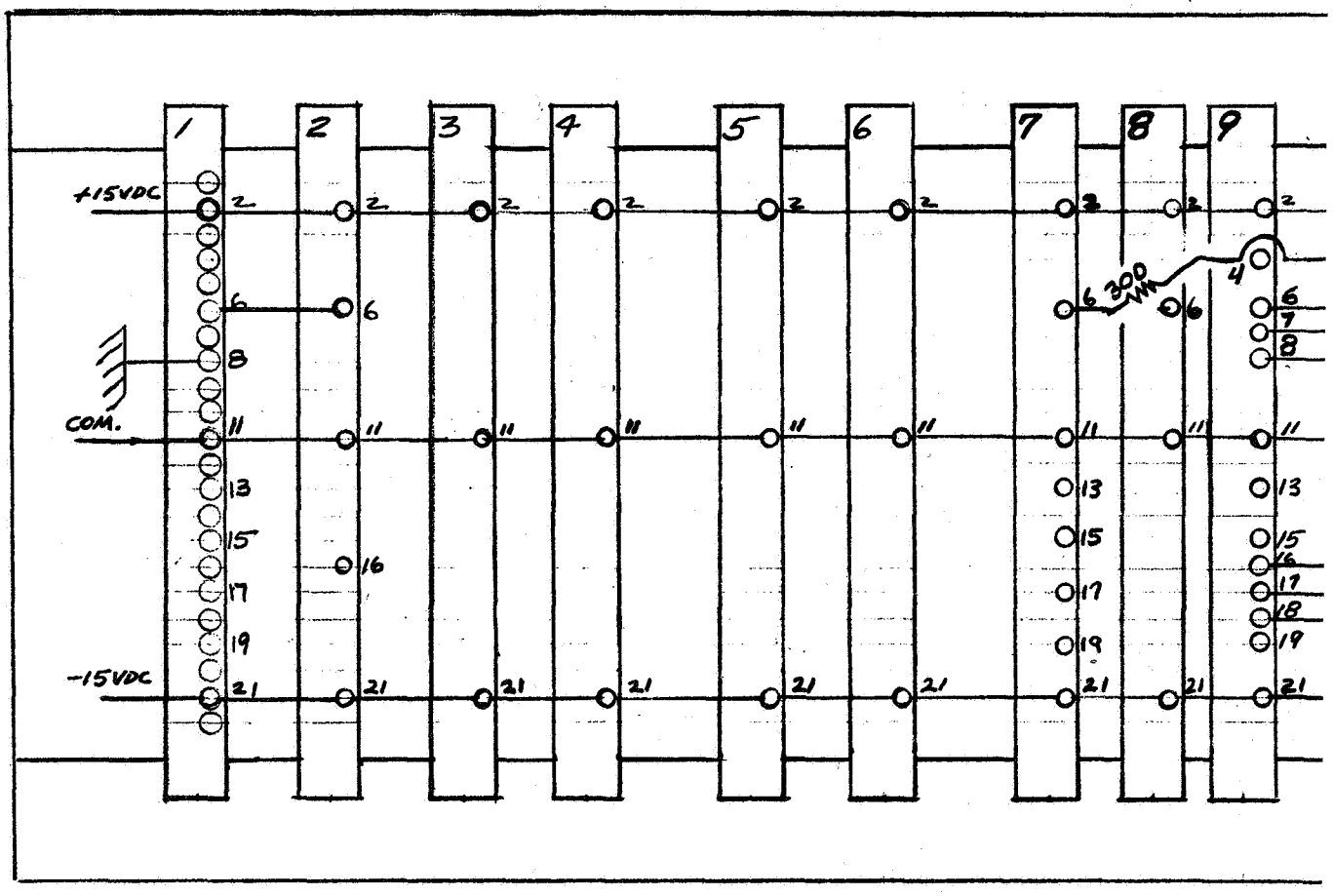
Photograph Of Front Of Servo Panel

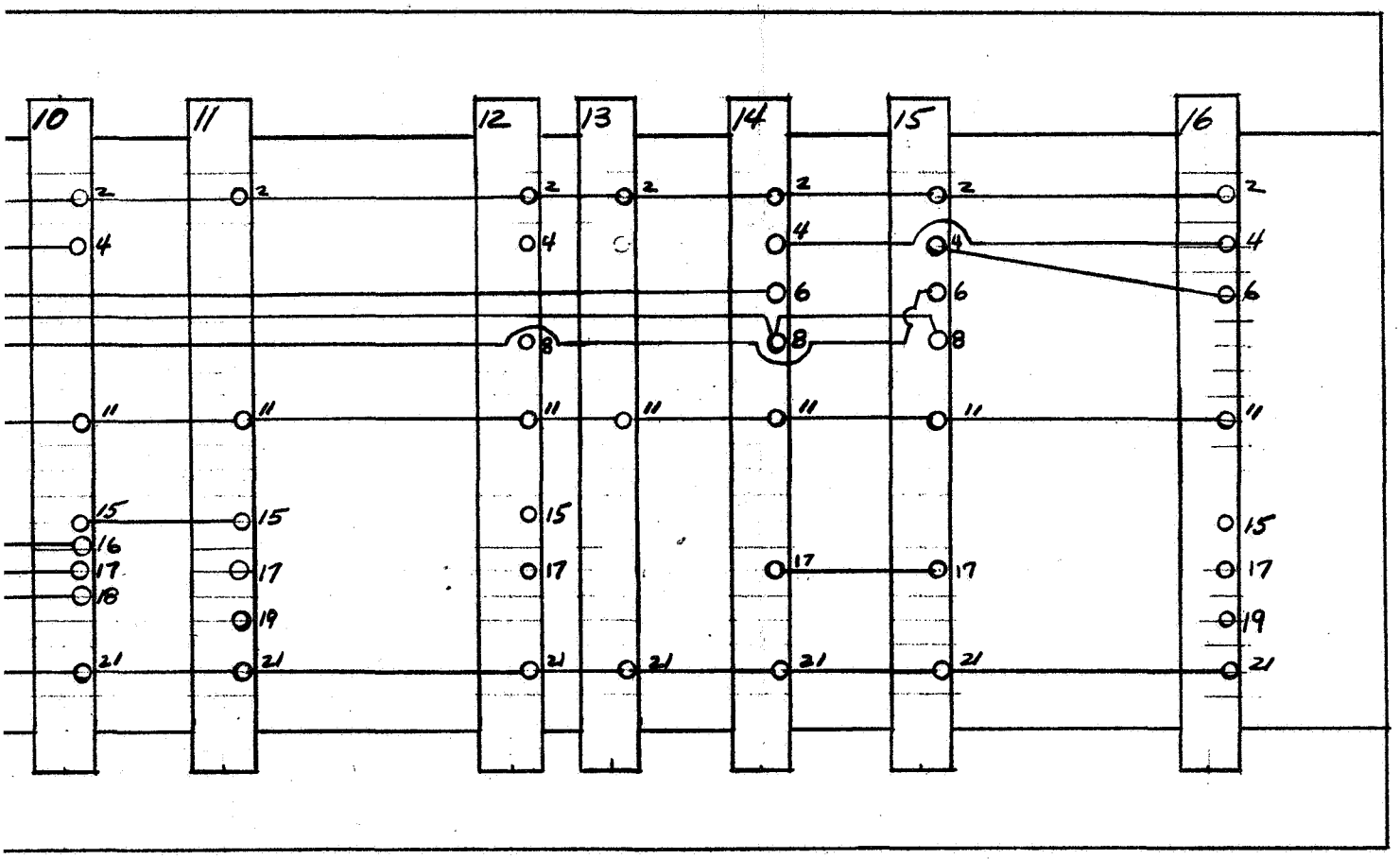


Pusher and Loss Control Meter and Bias Panel Schematic

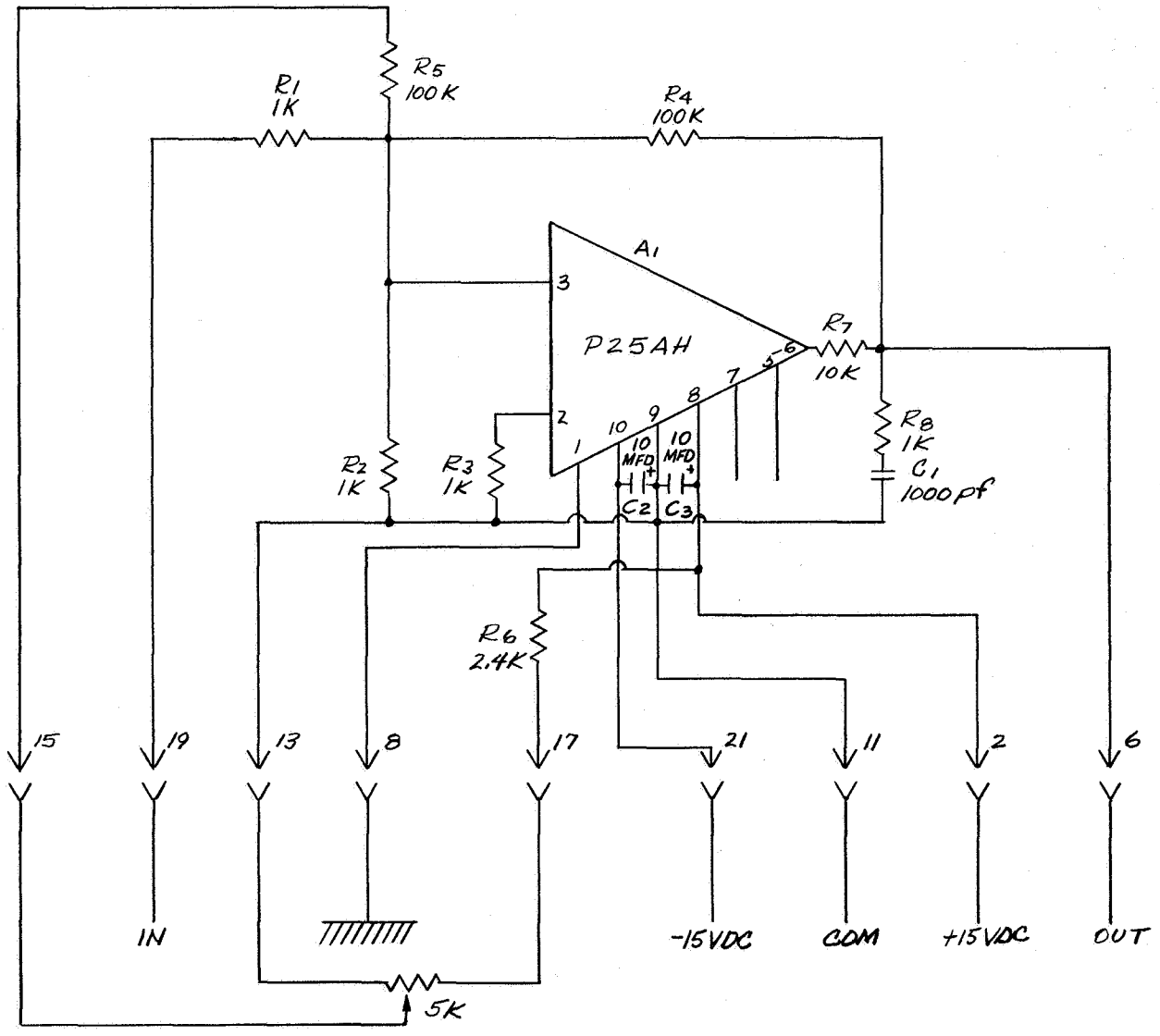


Photograph Of Rear Of Servo Panel

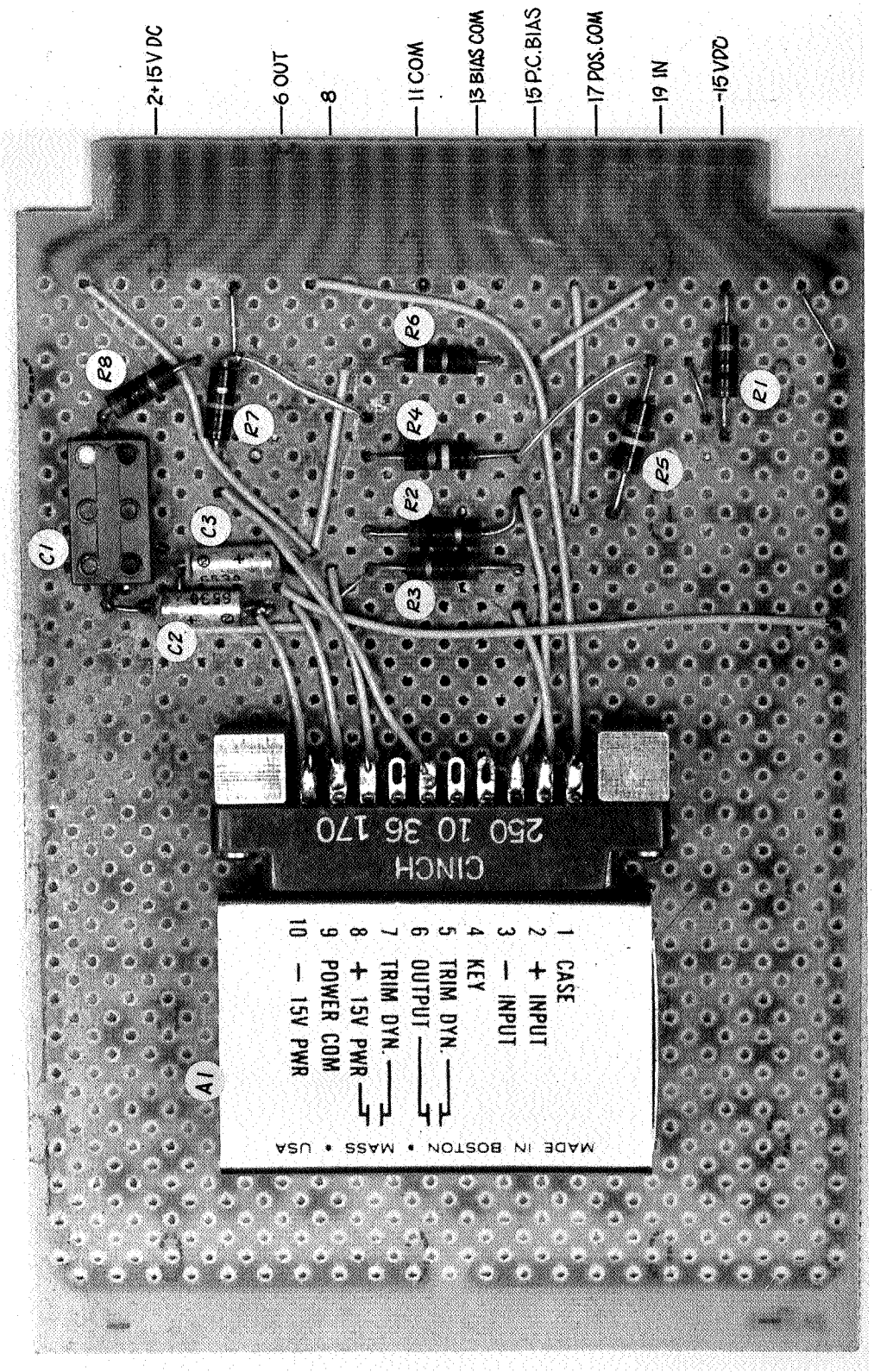

1
2
3
4
5
6
7
8
9
+15VDC
COM.
-15VDC
300 Ω



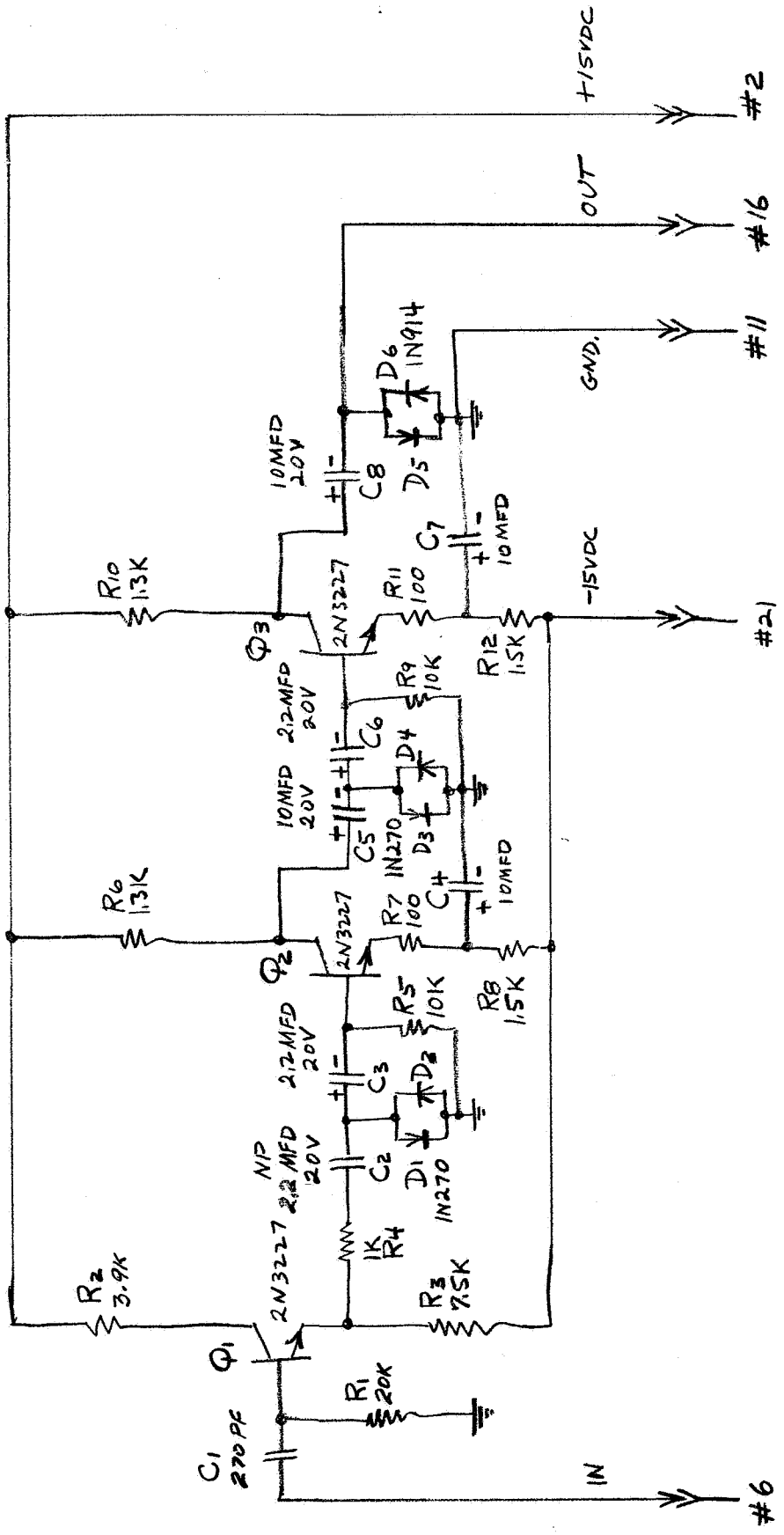
Rotation Sensor Interconnections
For Circuit Boards.



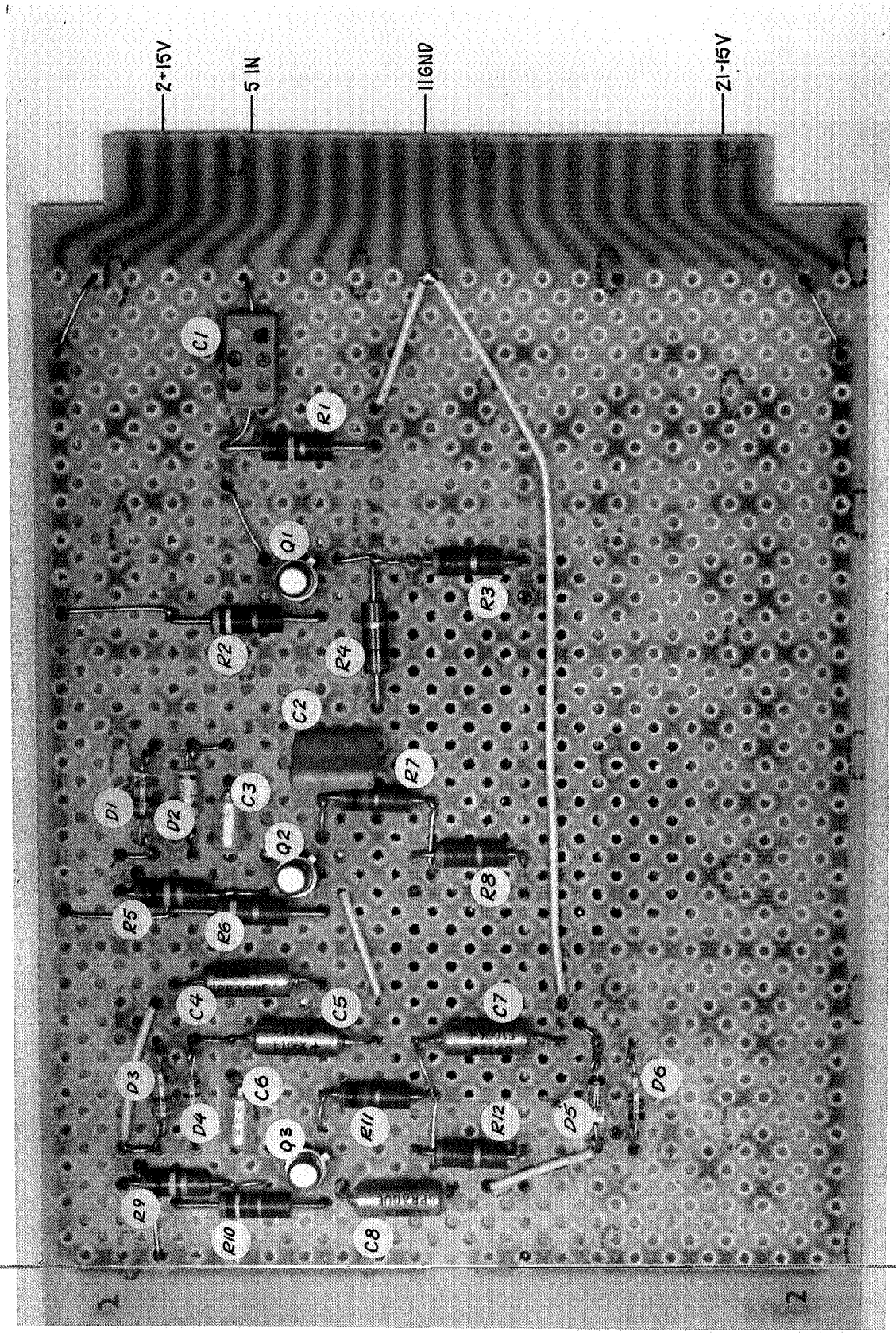
Schematic Of Board 1



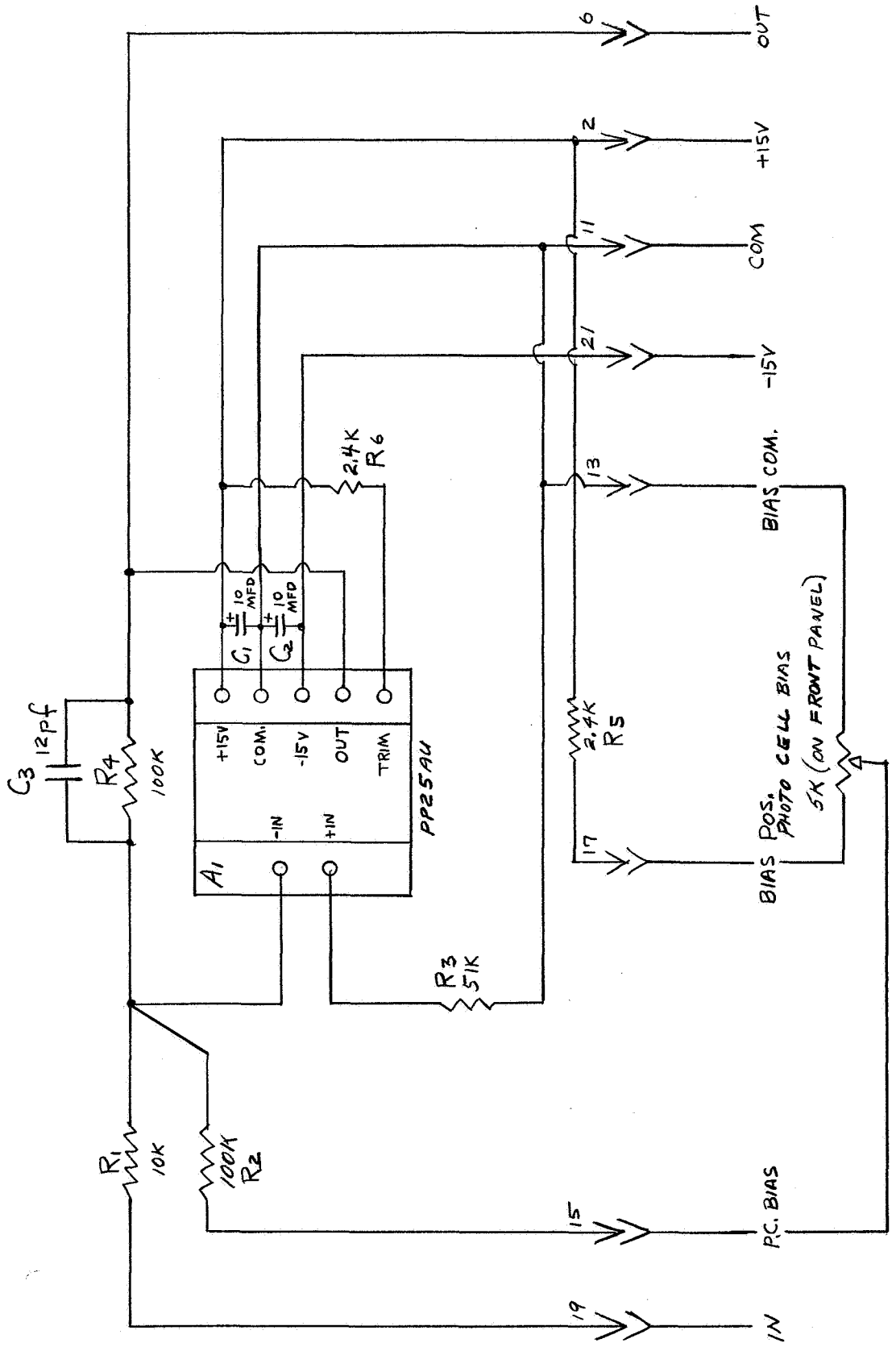
Photograph Of Board 1



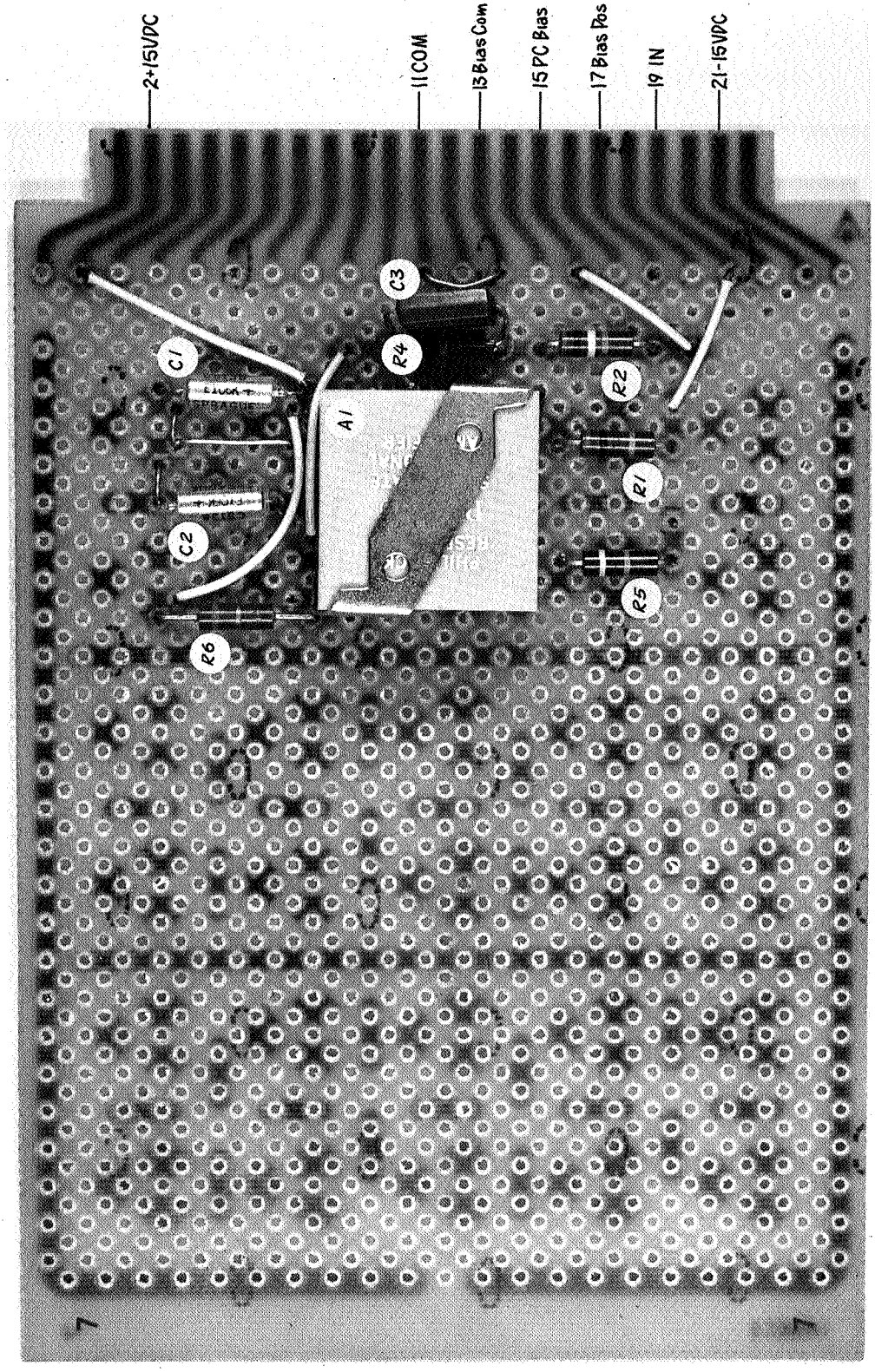
Schematic of Board 2



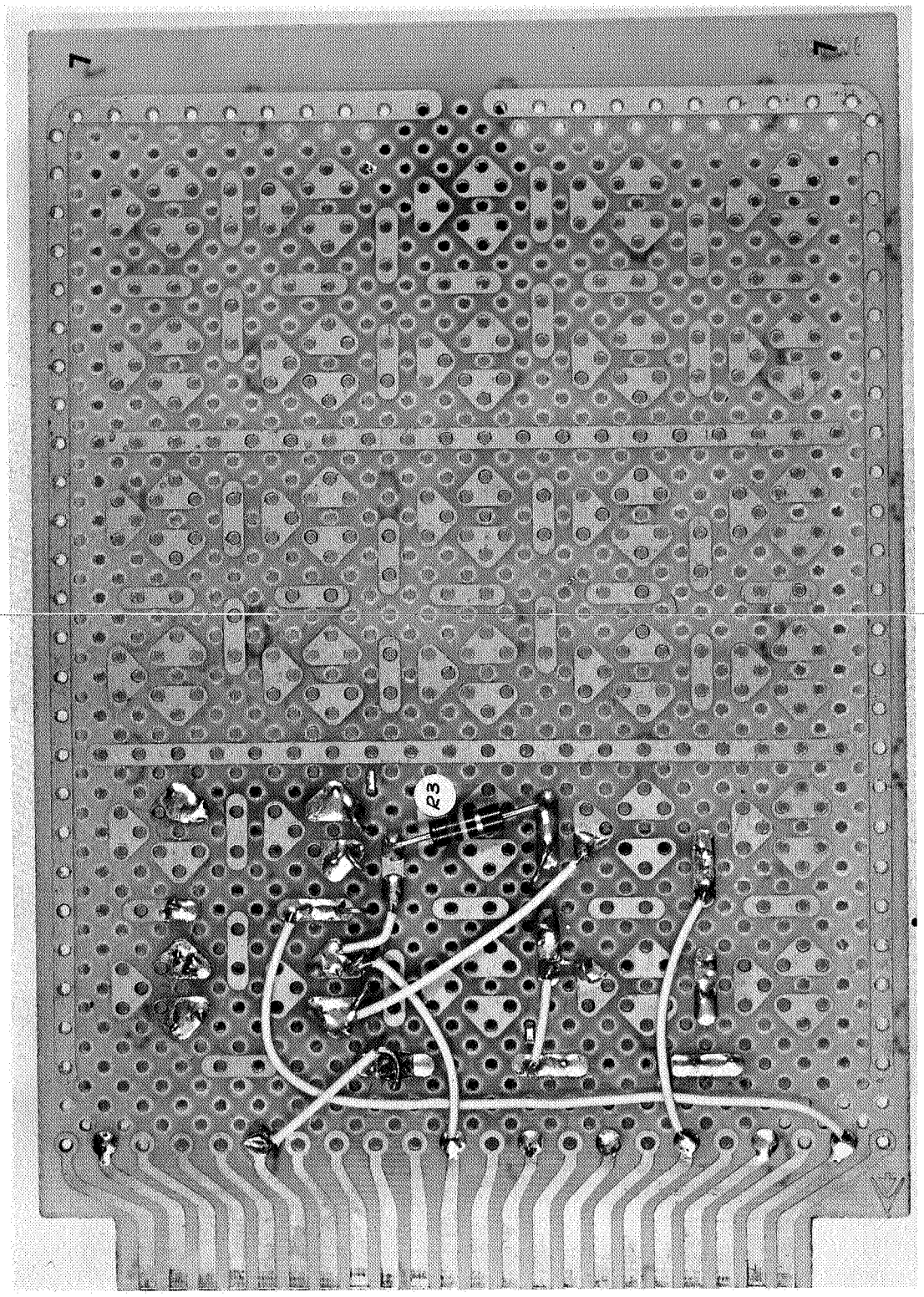
Photograph Of Board 2



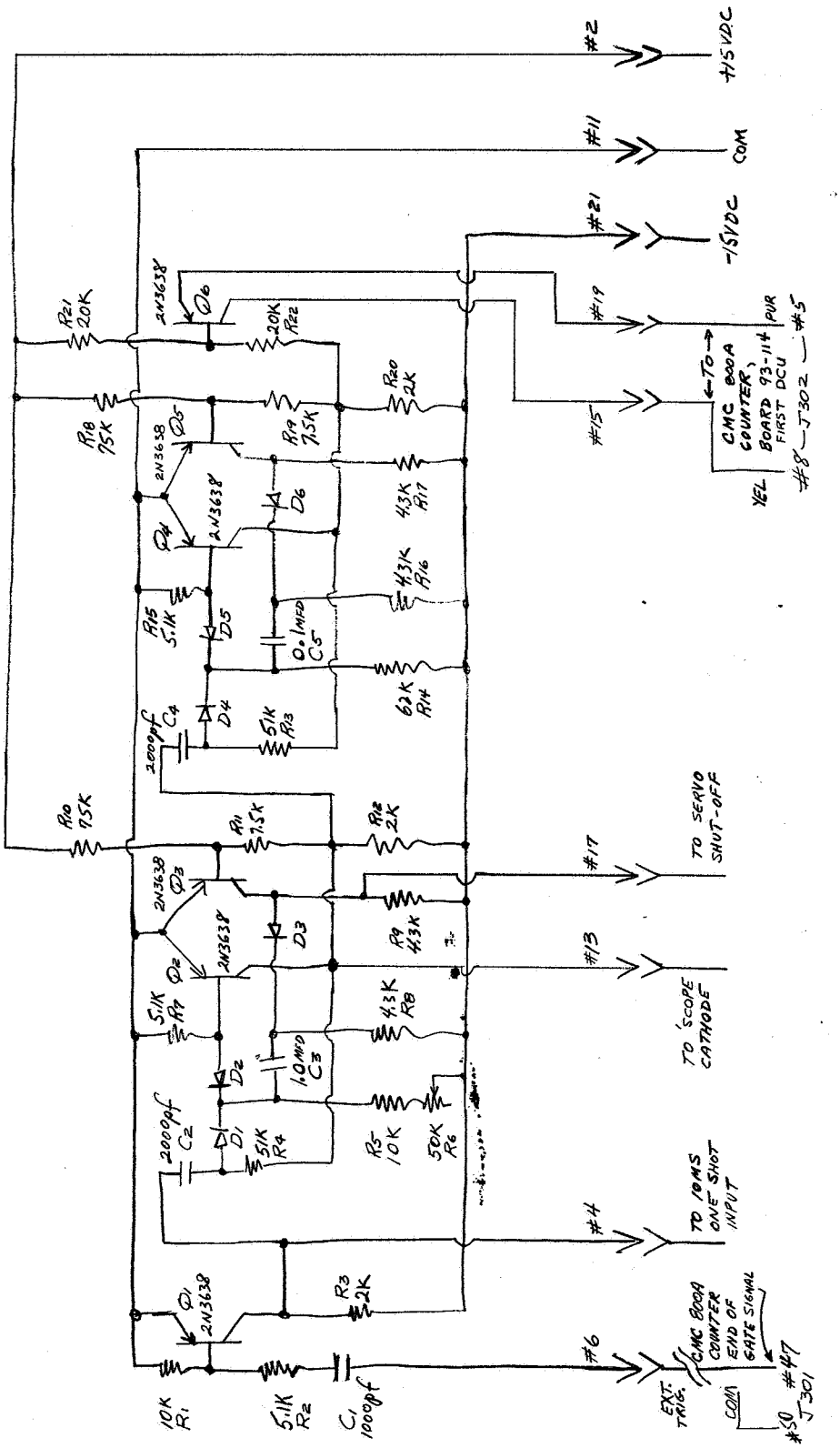
Schematic of Board 7



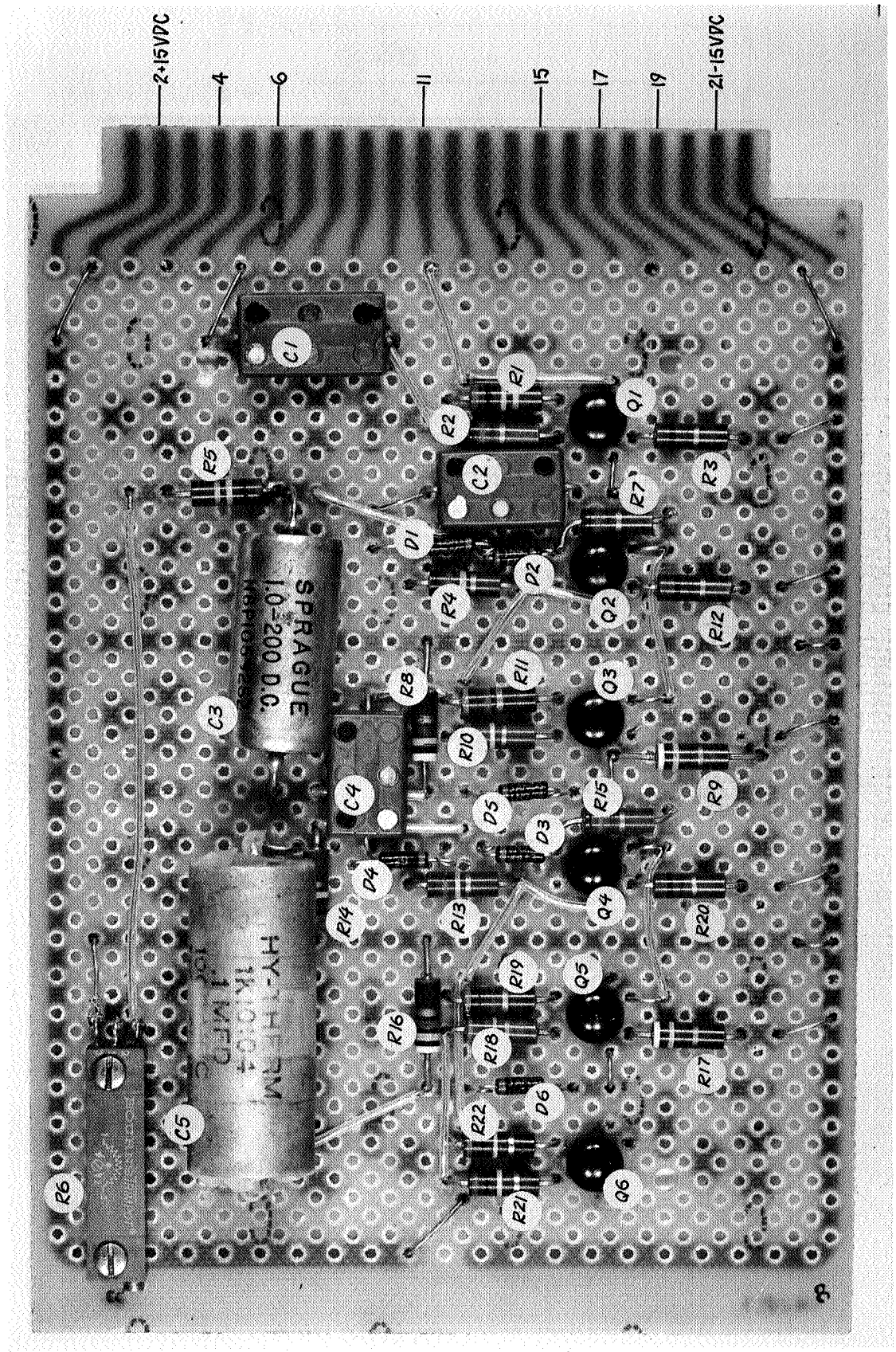
Photograph Of Board 7 - Front View



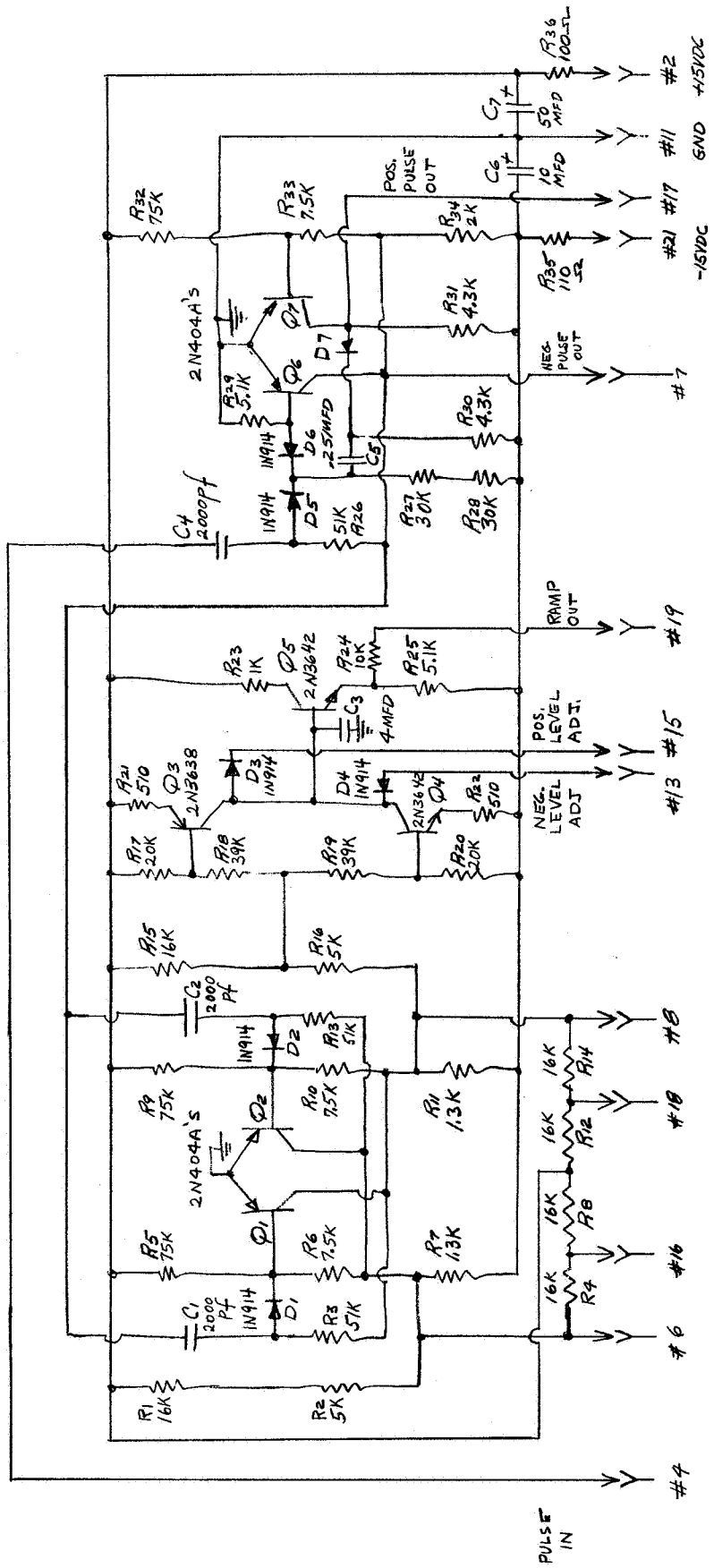
Photograph Of Board 7 - Rear View



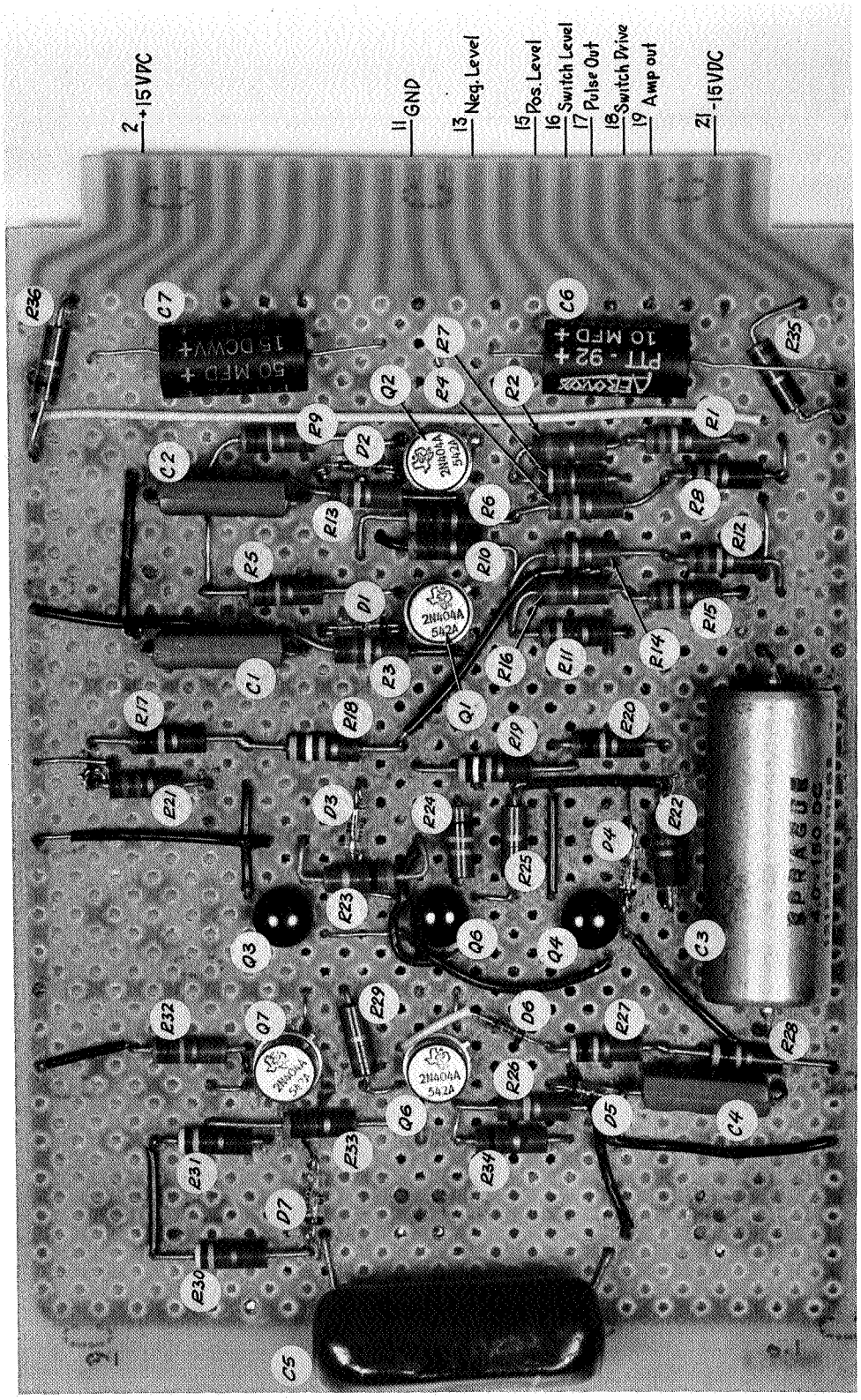
Schematic Of Board 8



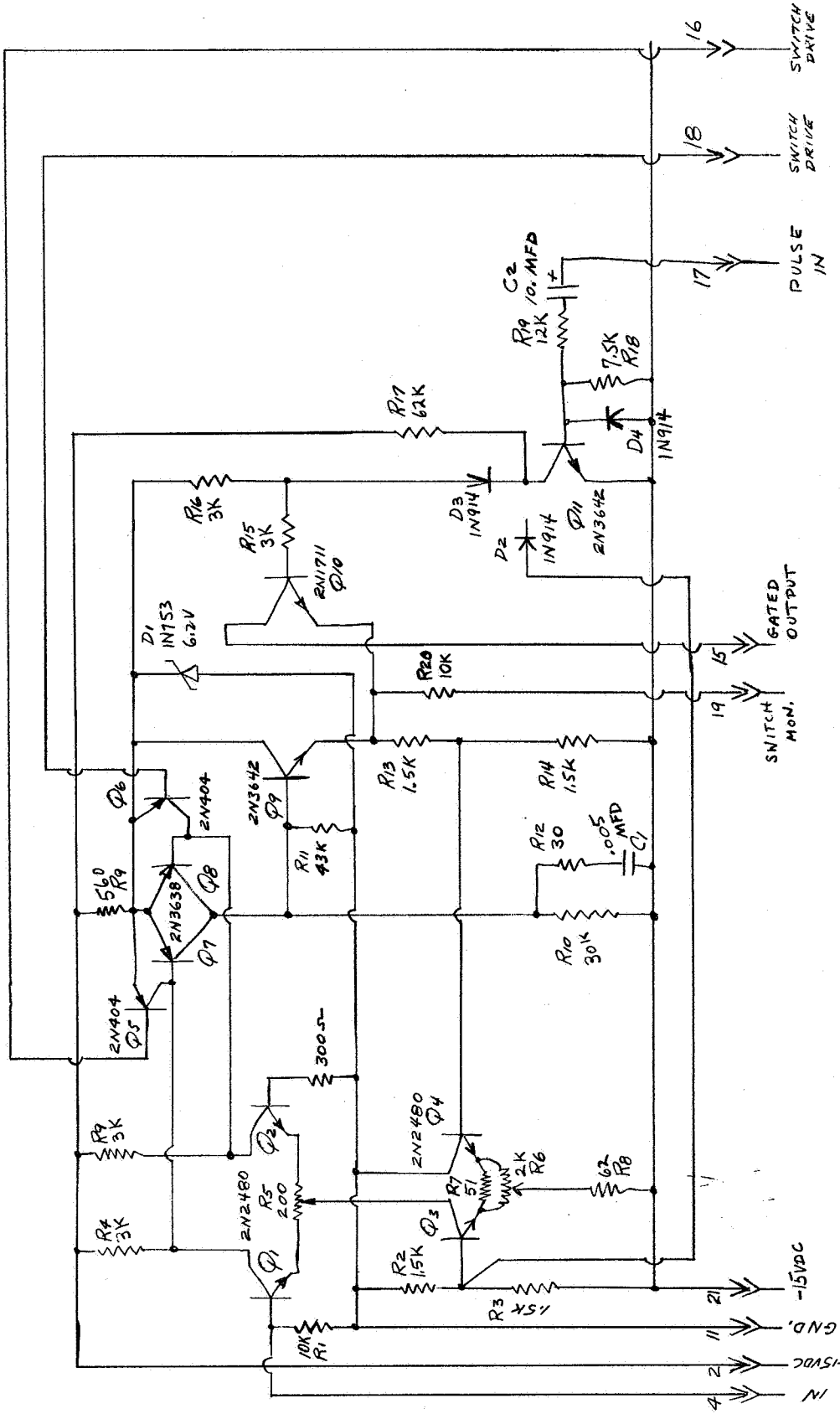
Photograph Of Board 8



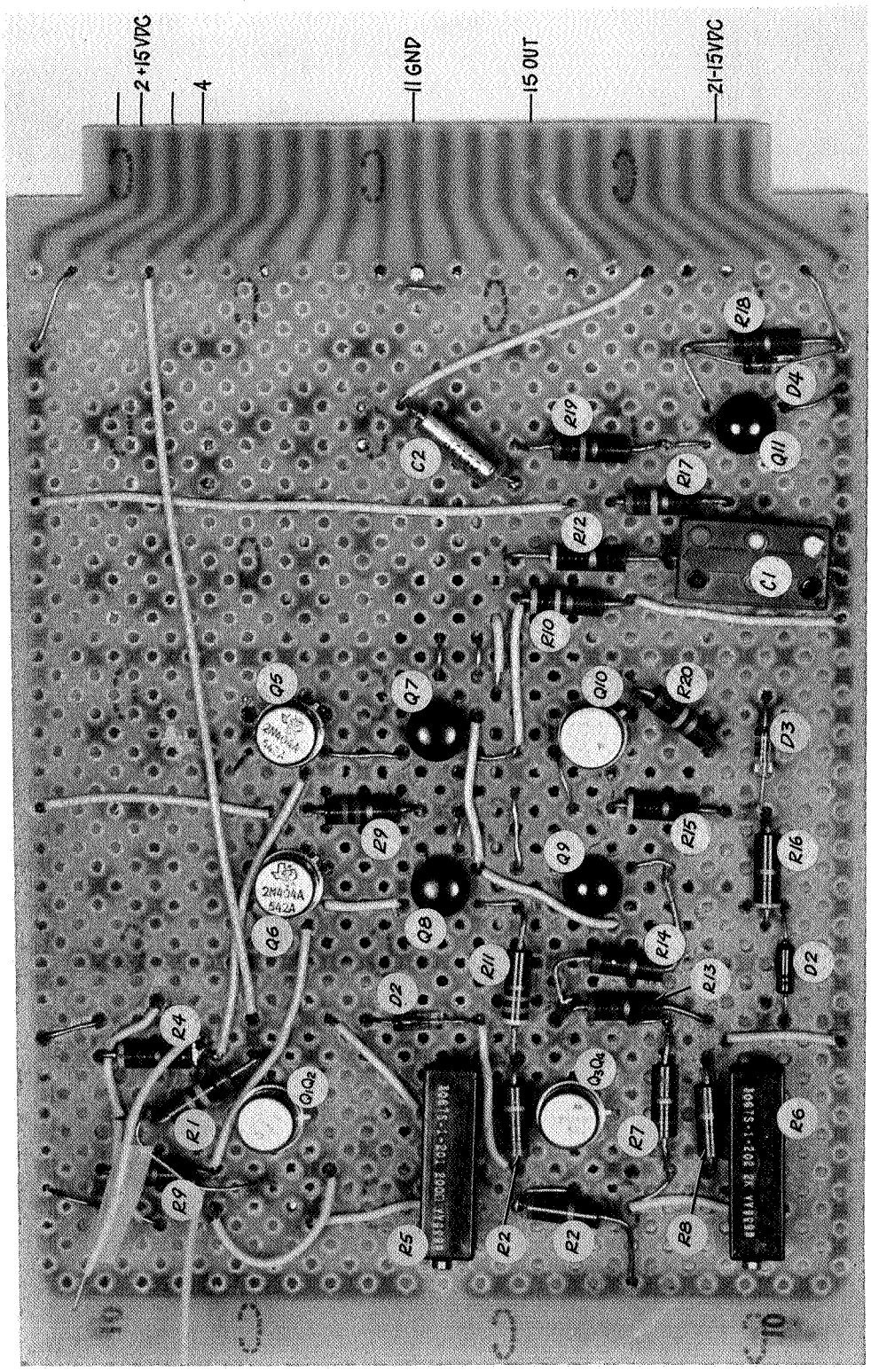
Schematic Of Board 9



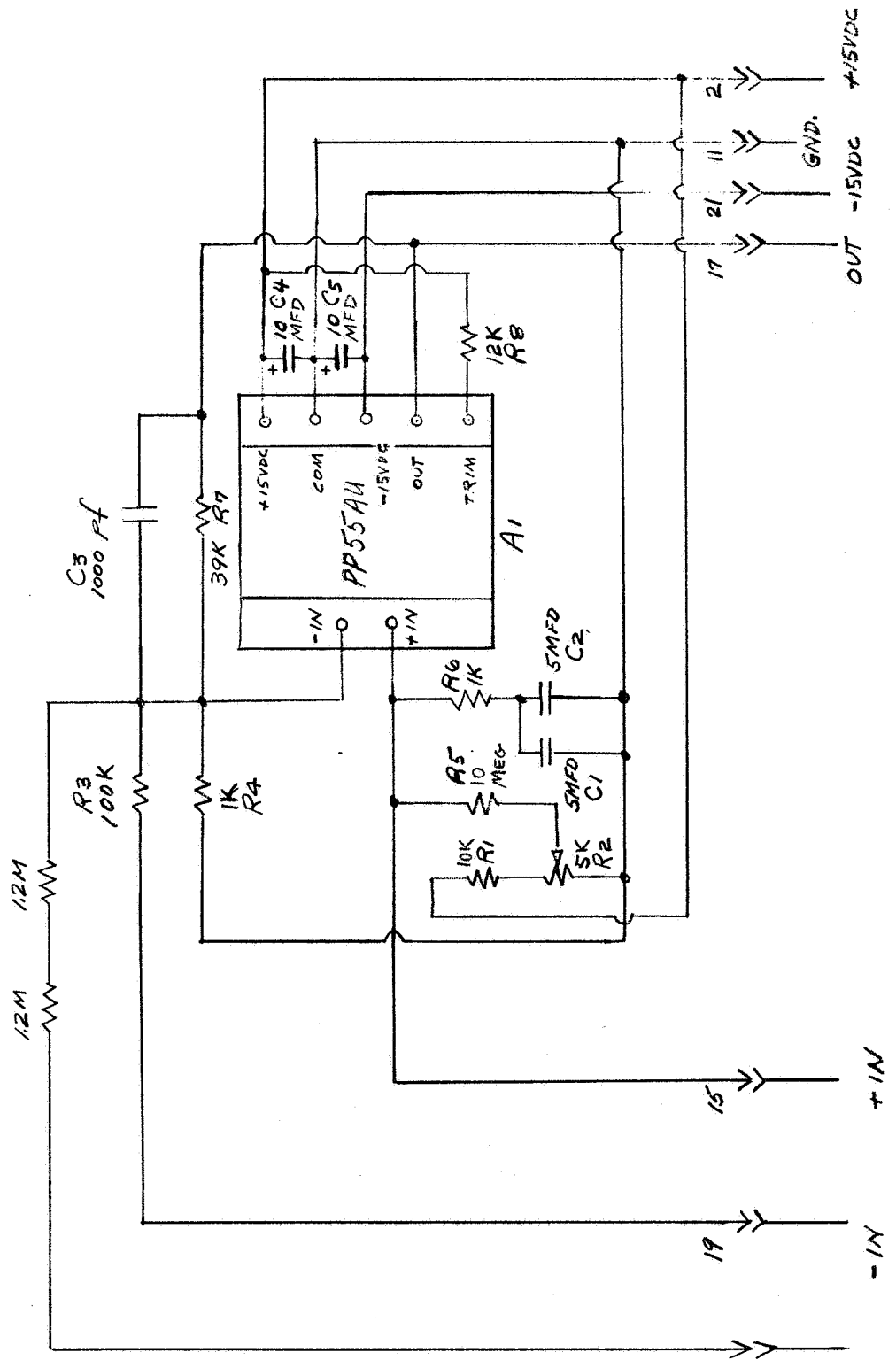
Photograph Of Board 9



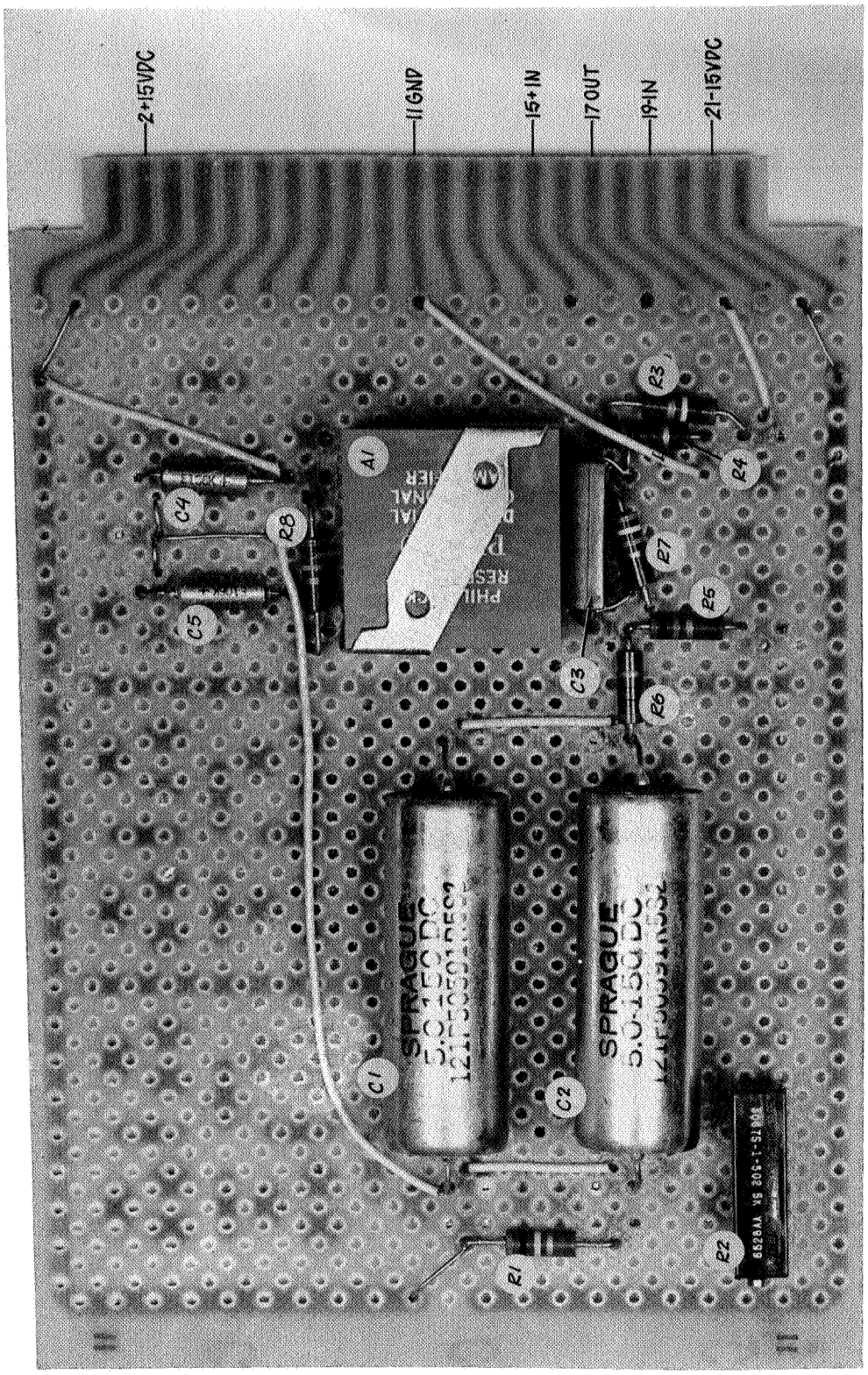
Schematic Of Board 10



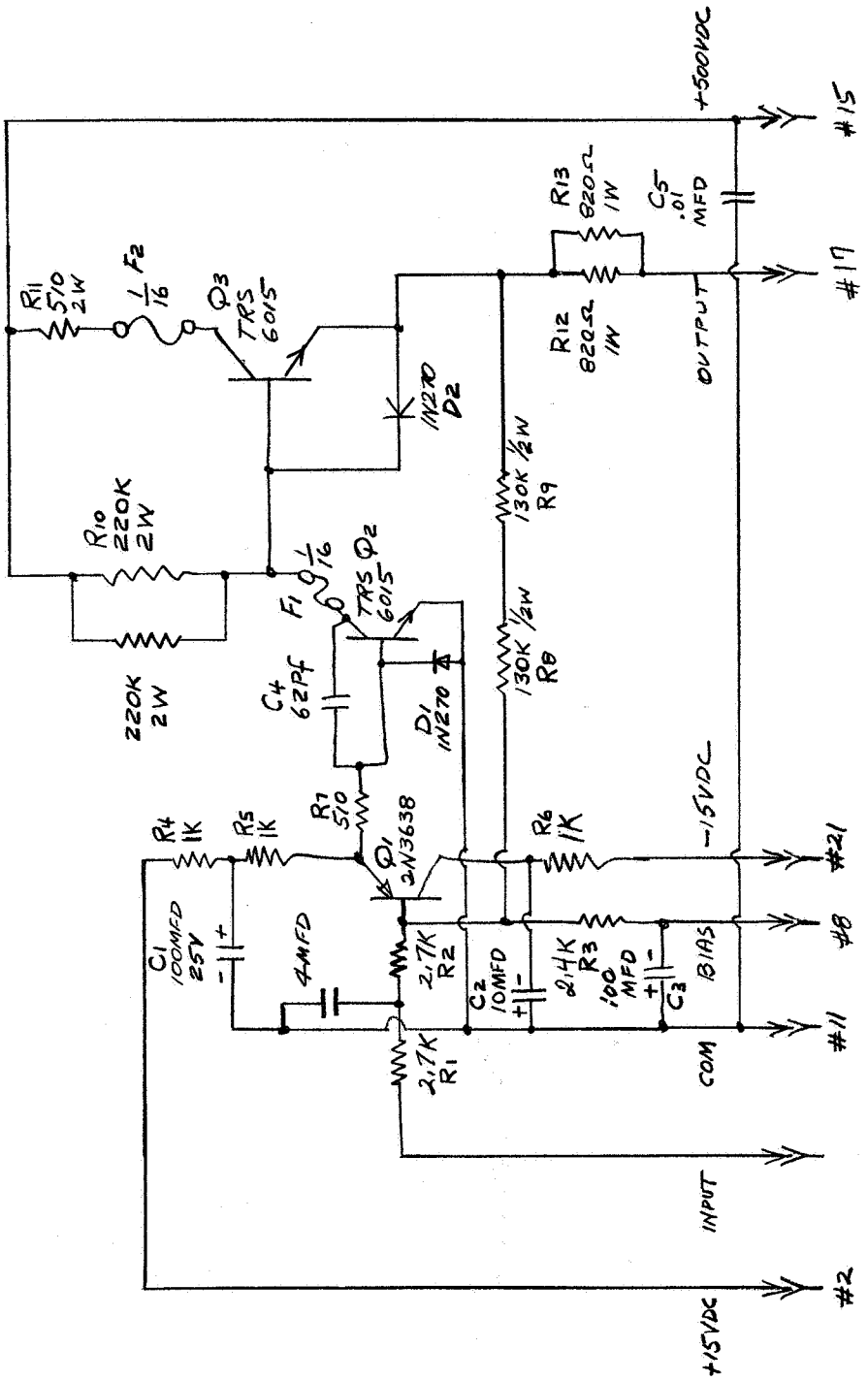
Photograph Of Board 10



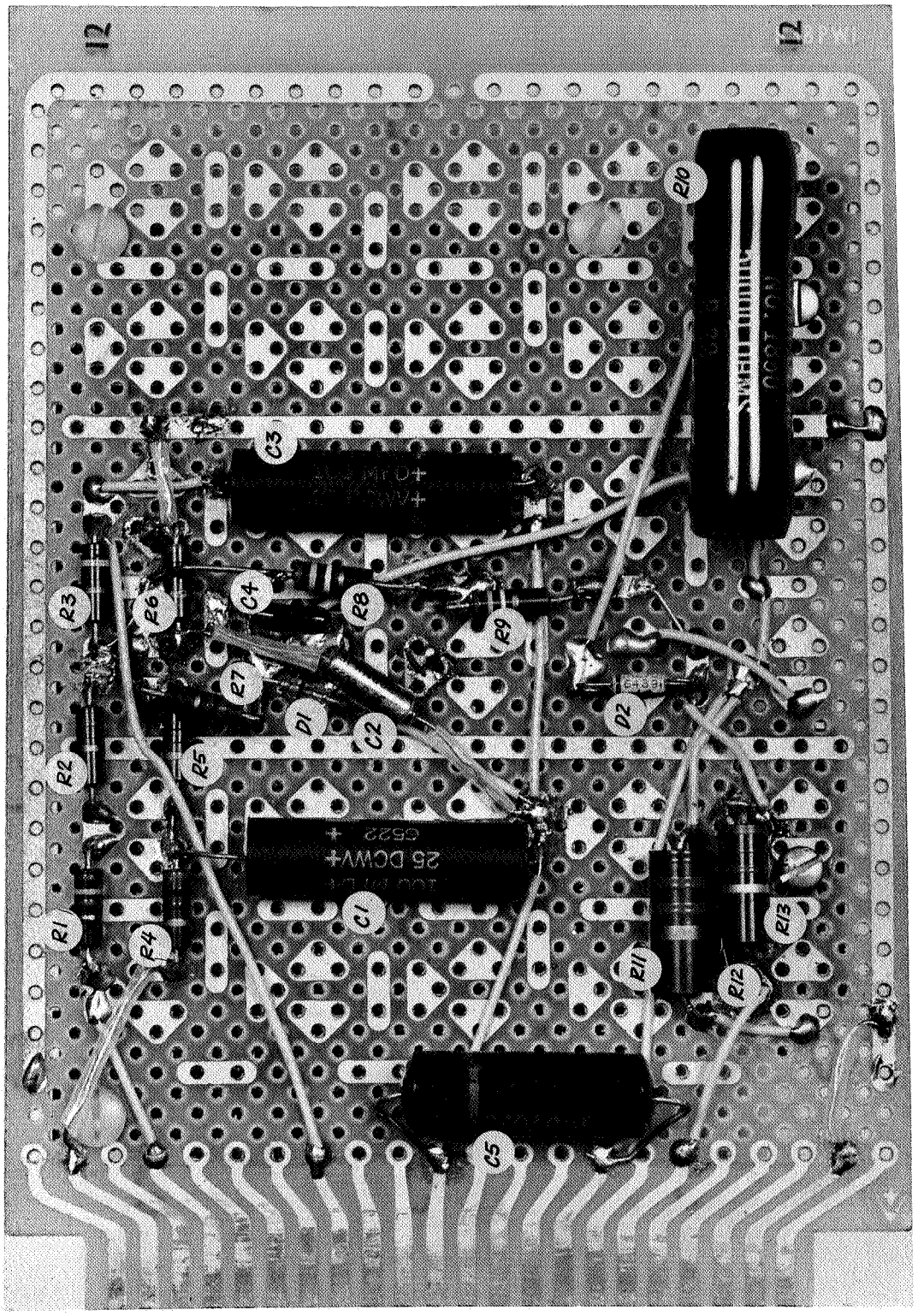
Schematic Of Board 11



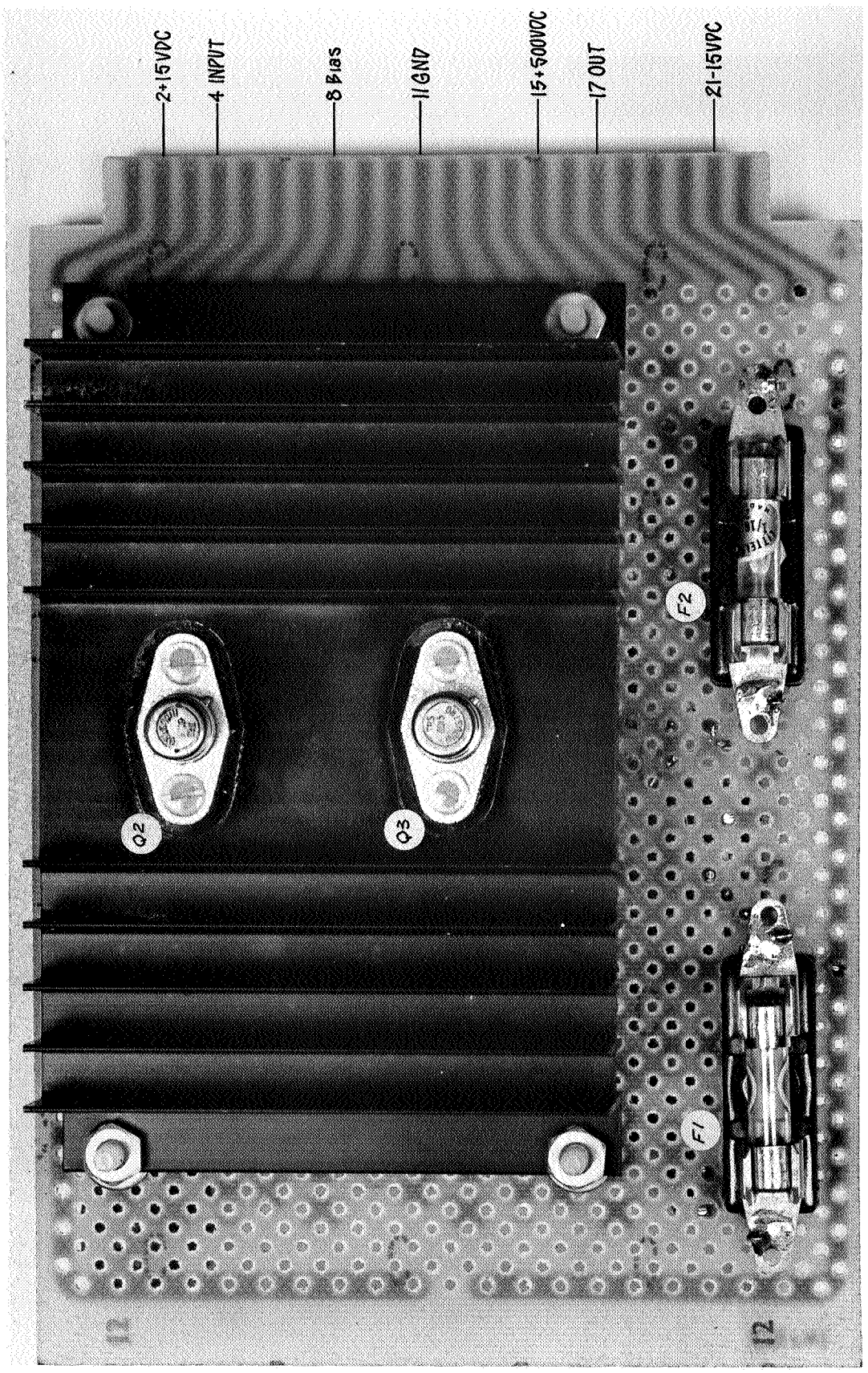
Photograph Of Board 11



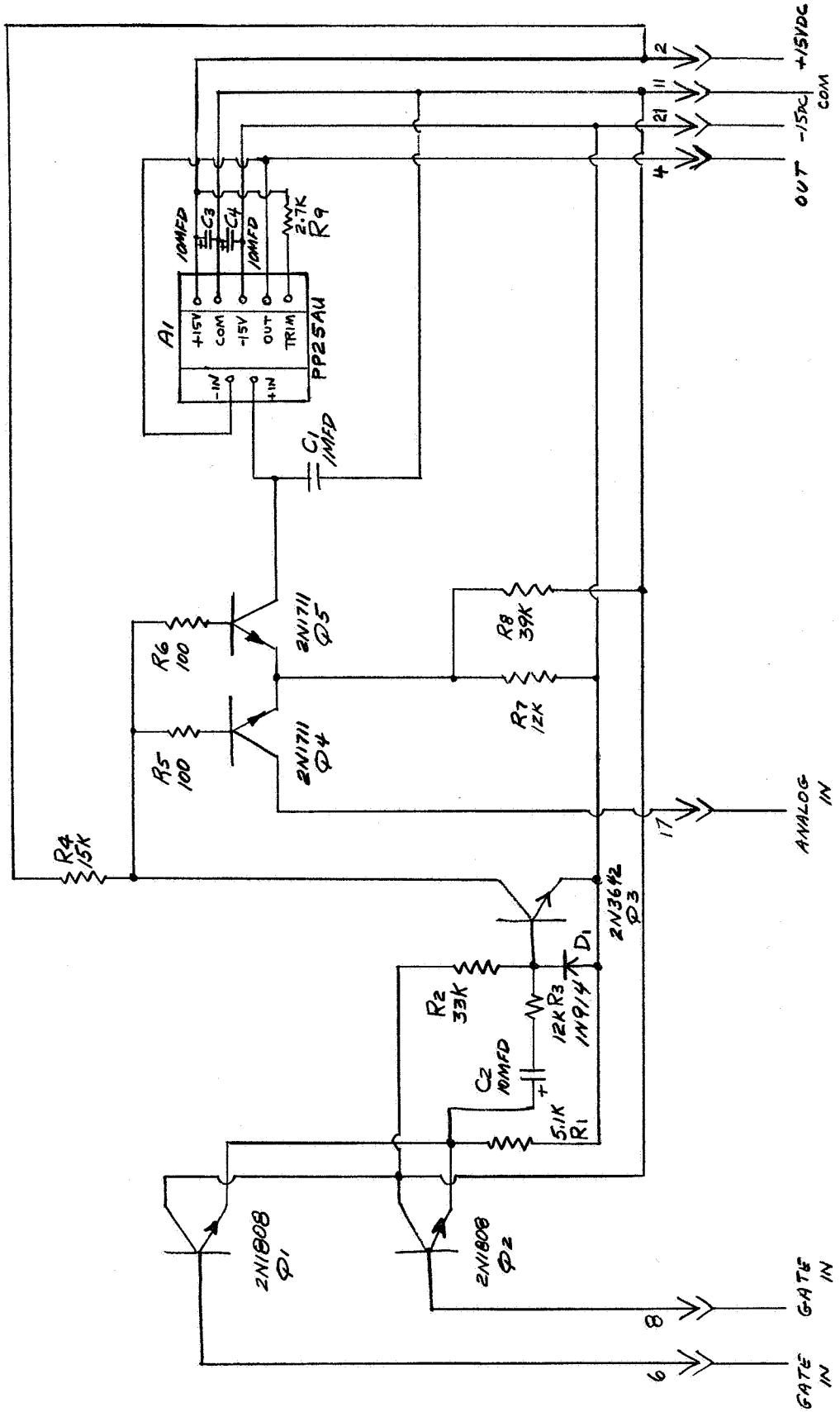
Schematic Of Board 12



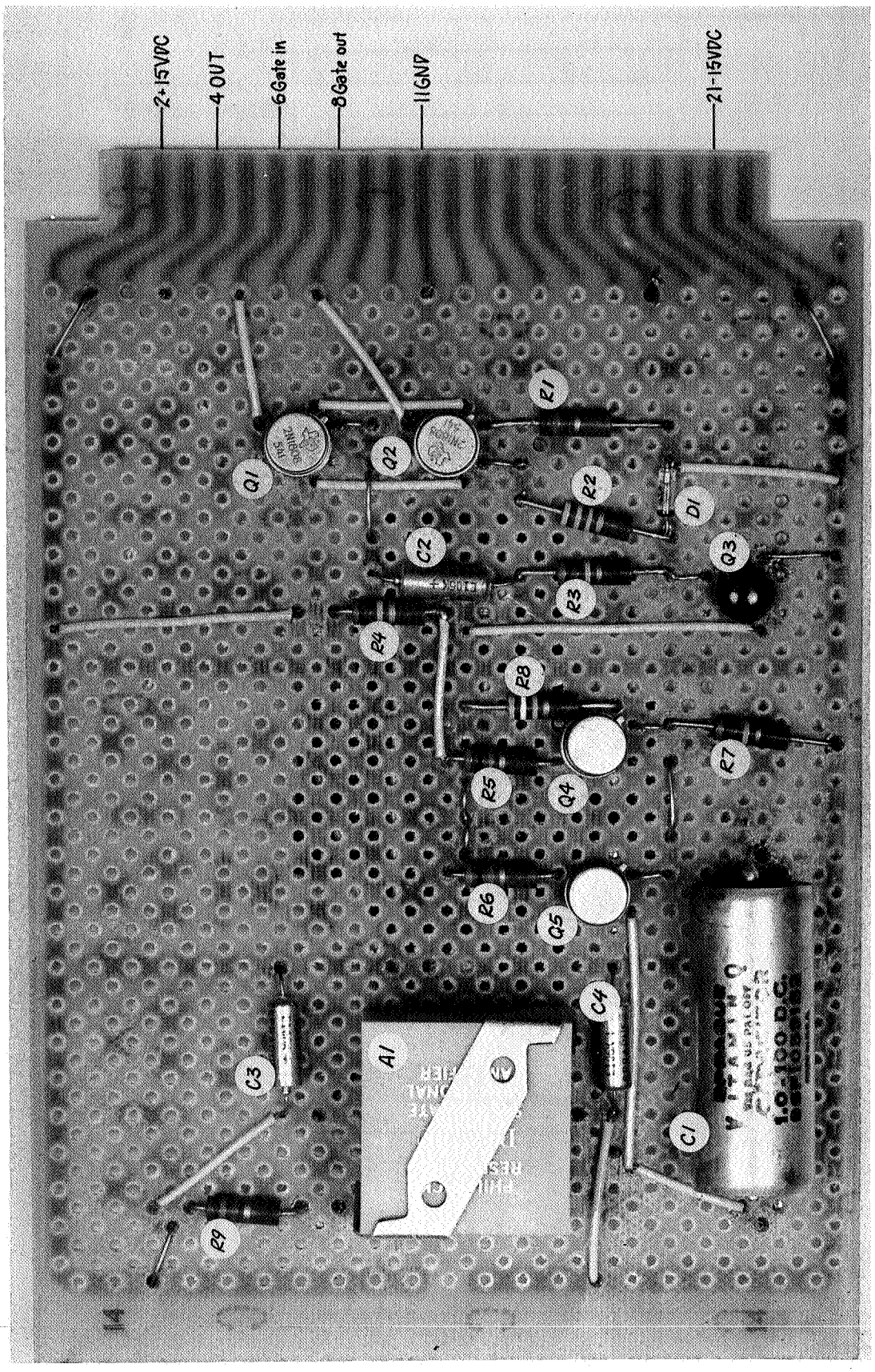
Photograph Of Board 12 - Front



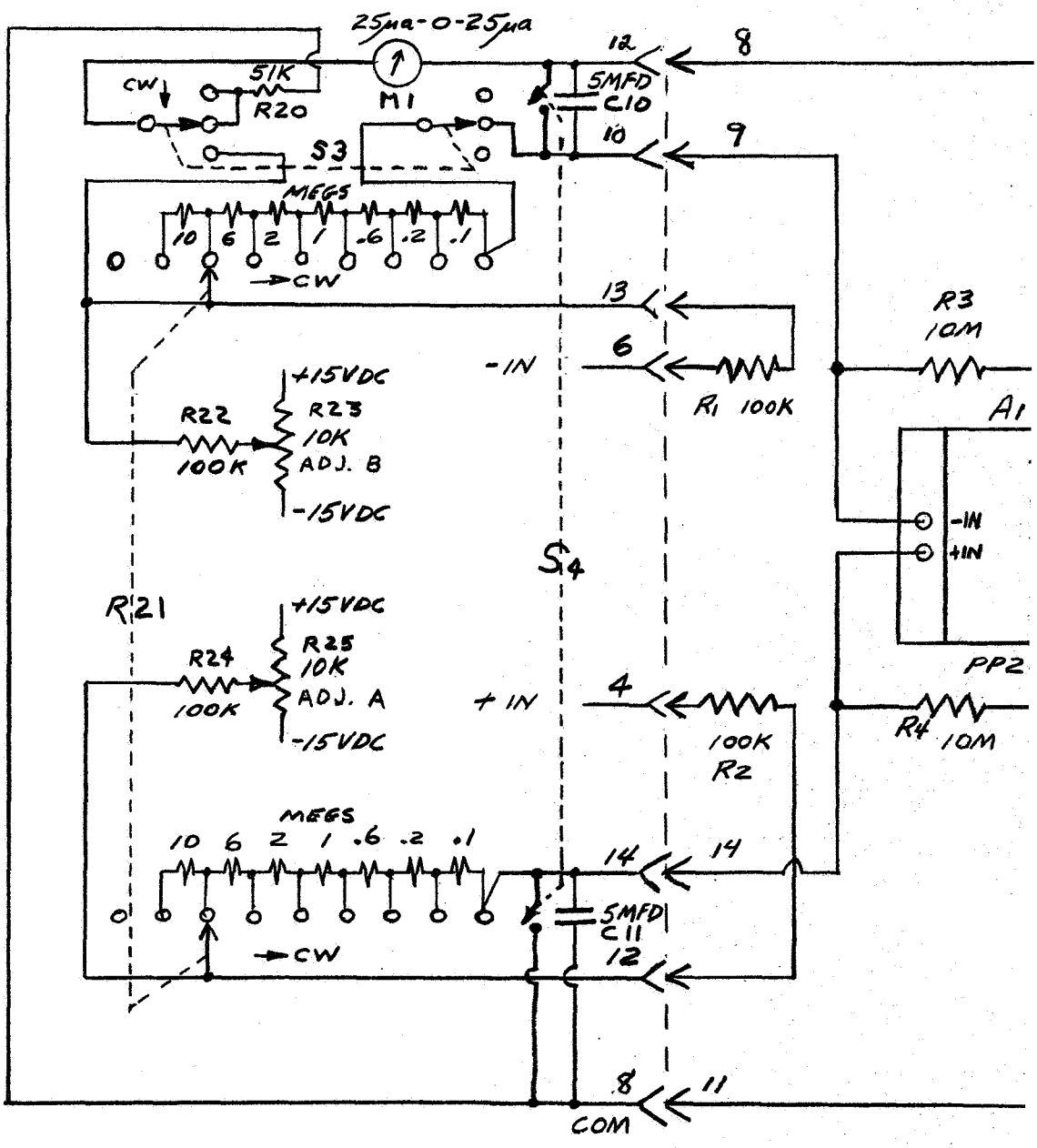
Photograph Of Board 12 - Rear

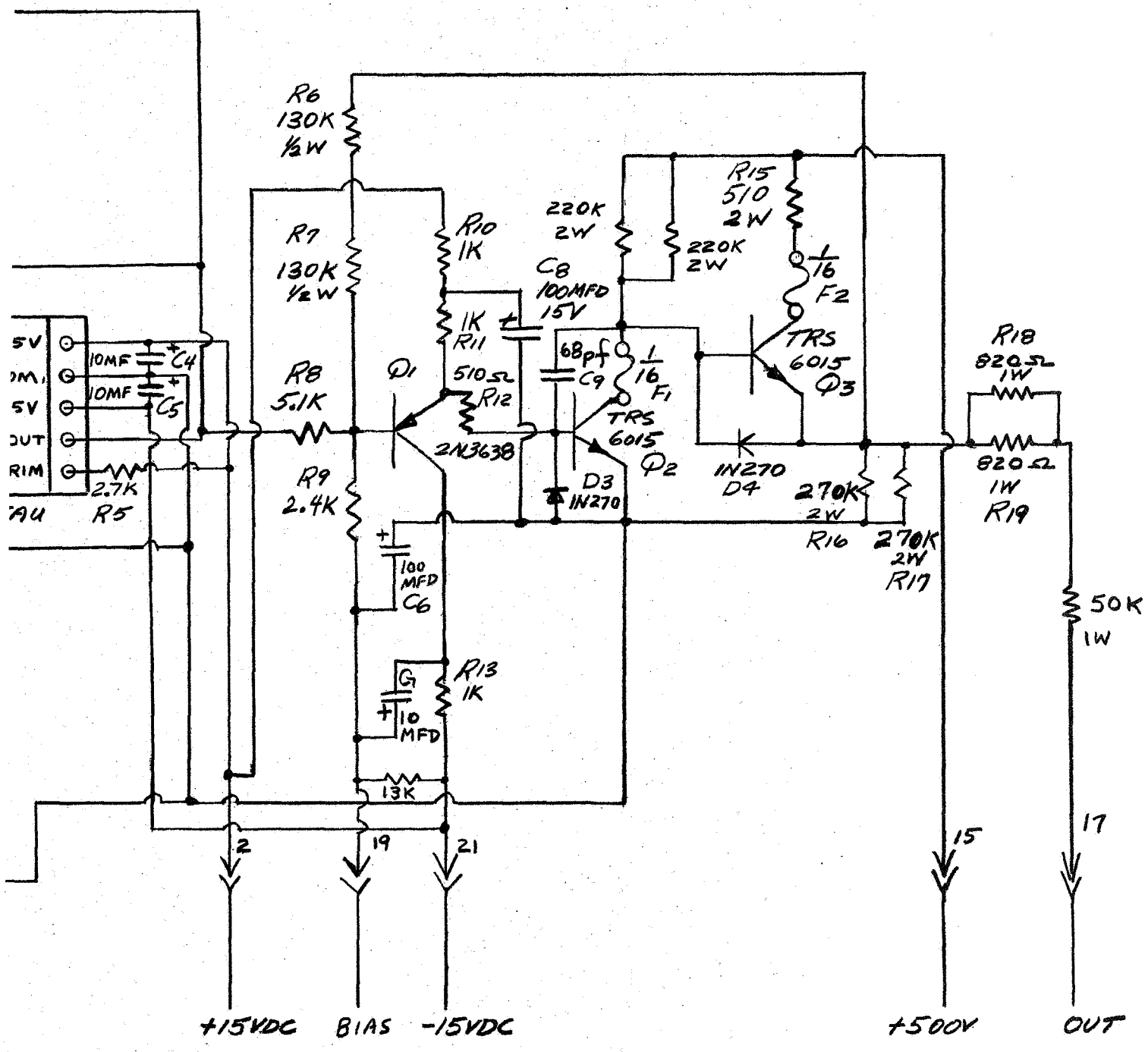


Schematic Of Boards 14, 15

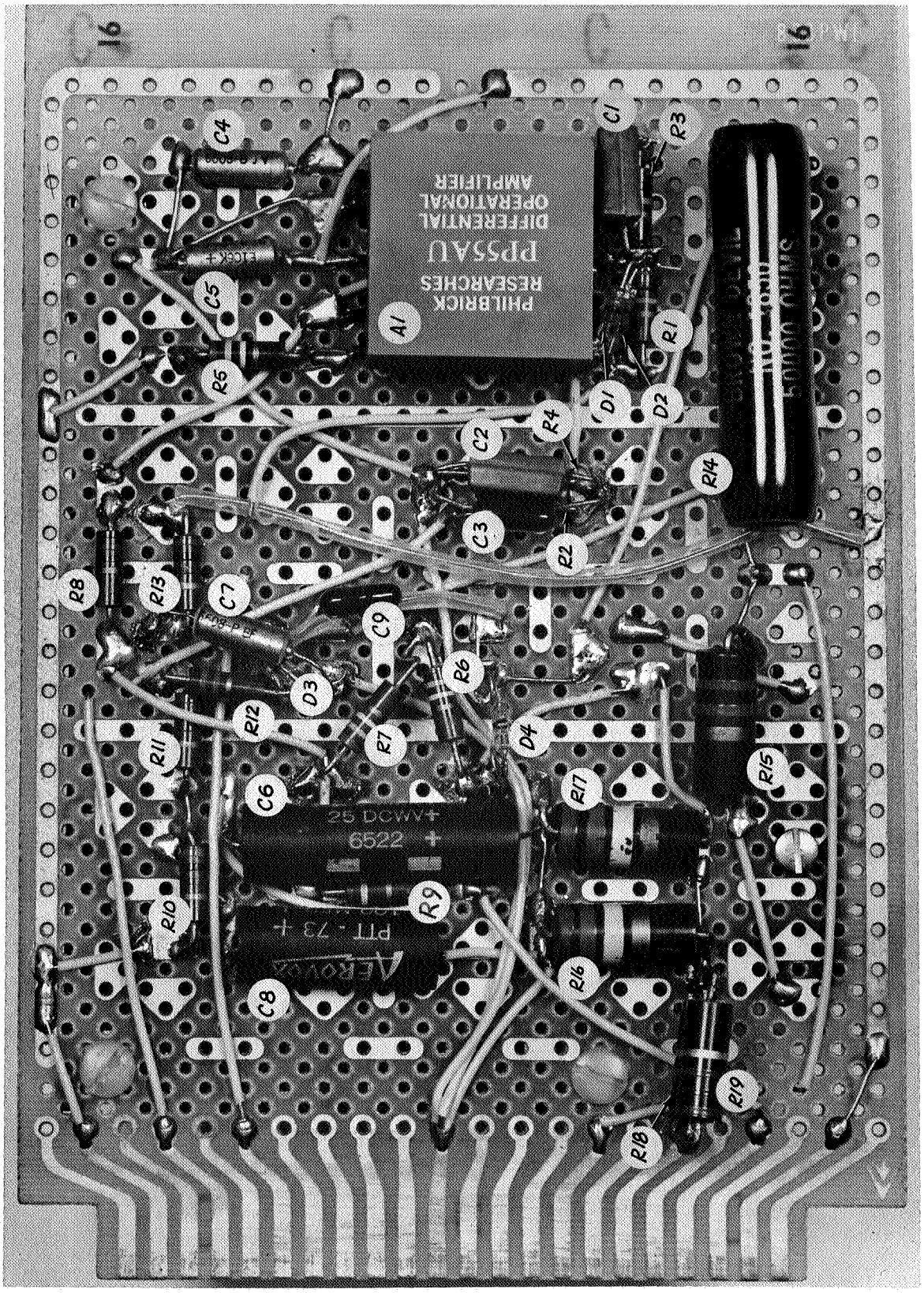


Photograph Of Boards 14, 15

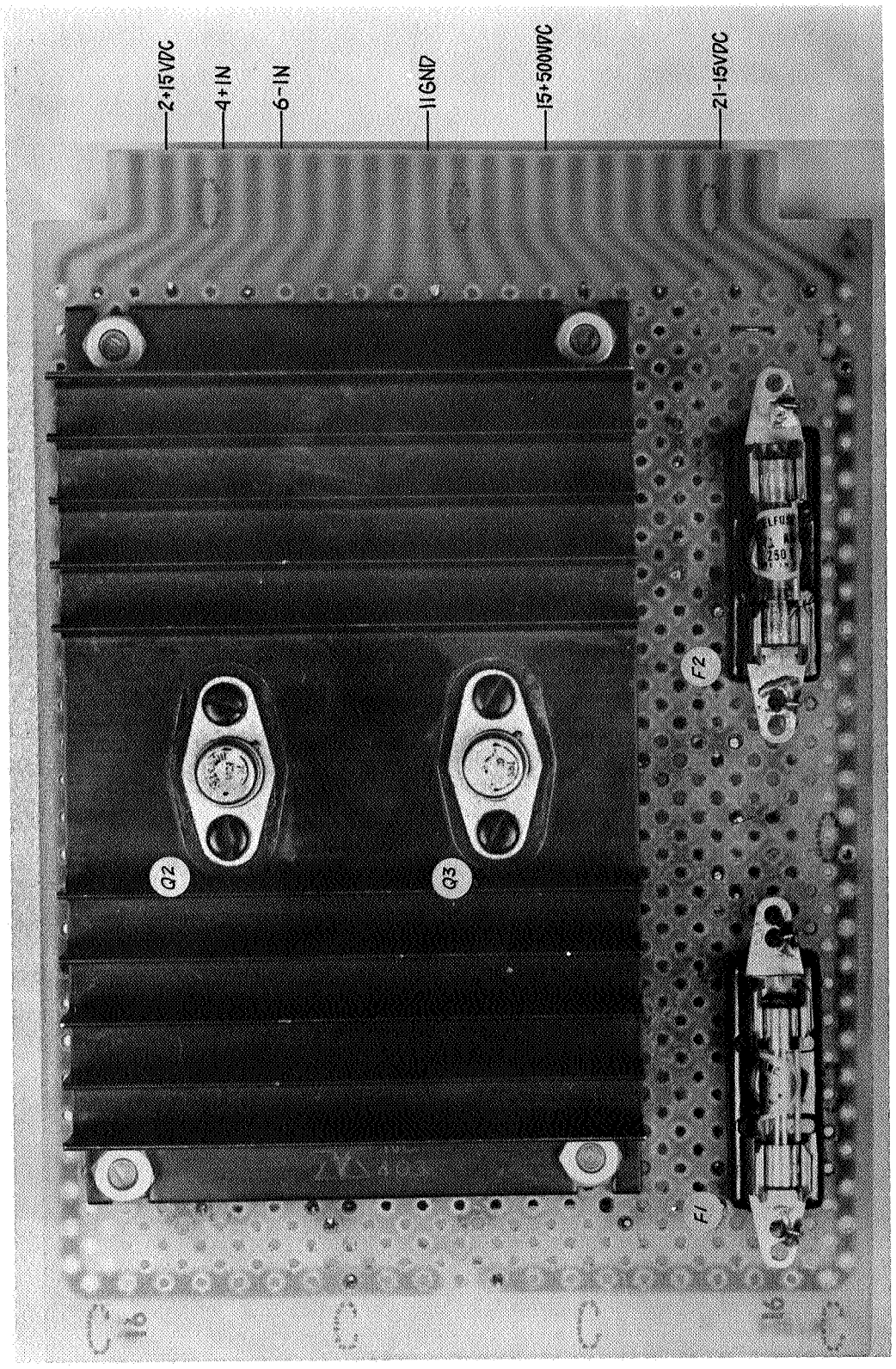

25μa-0-25μa
M1
51K
R20
CW
S3
5MFD
C10
12
8
10
9
MEGS
10 6 2 1 .6 .2 .1
CW
13
R3
10M
6
-IN
R1 100K
A1
+15VDC
R23
10K
ADJ. B
-15VDC
R22
100K
S4
-IN
+IN
R21
+15VDC
R25
10K
ADJ. A
-15VDC
R24
100K
+IN
4
100K
R2
R4 10M
PP2
MEGS
10 6 2 1 .6 .2 .1
14
14
5MFD
C11
CW
12
8
COM
11



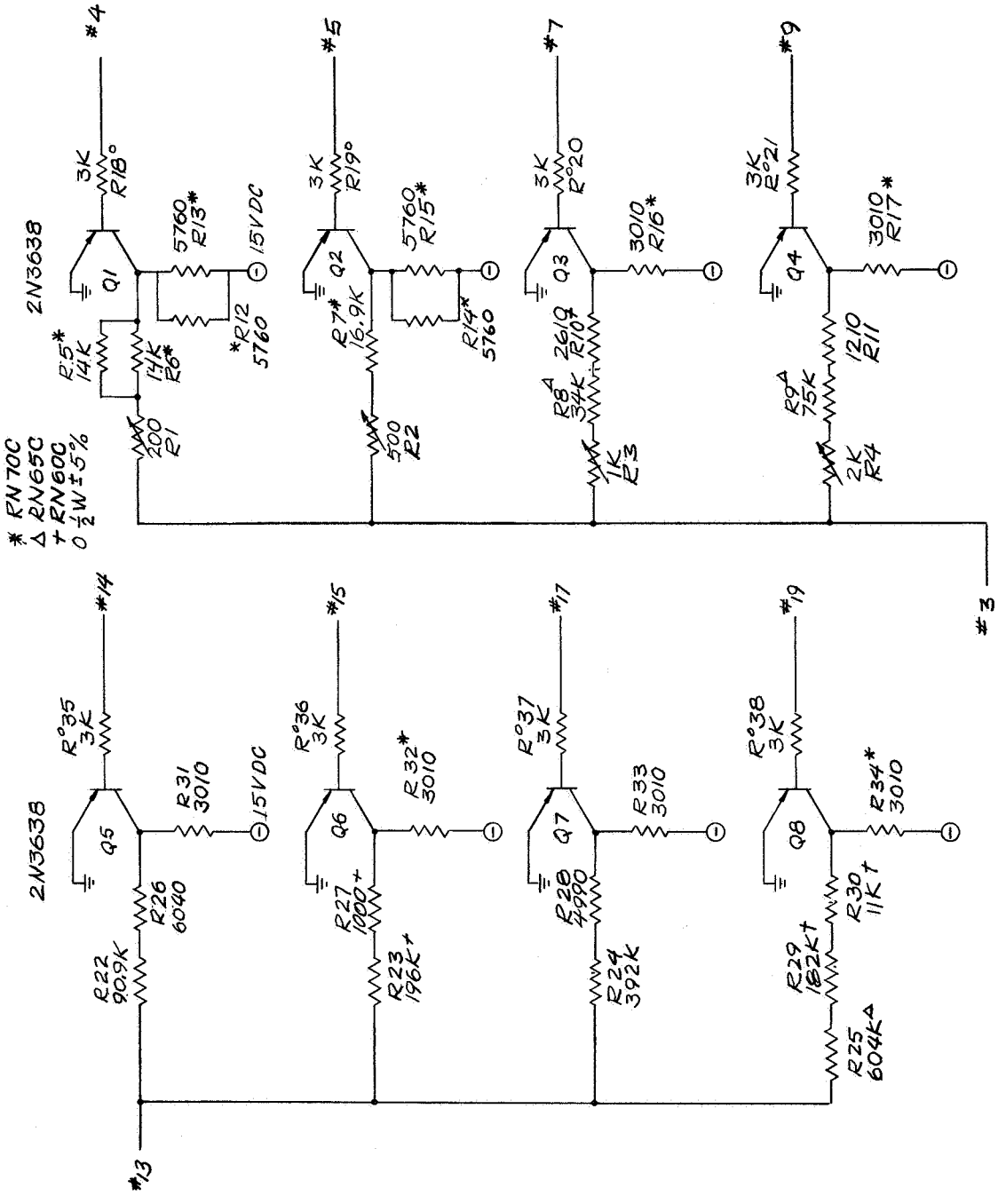
Schematic Of Board 16



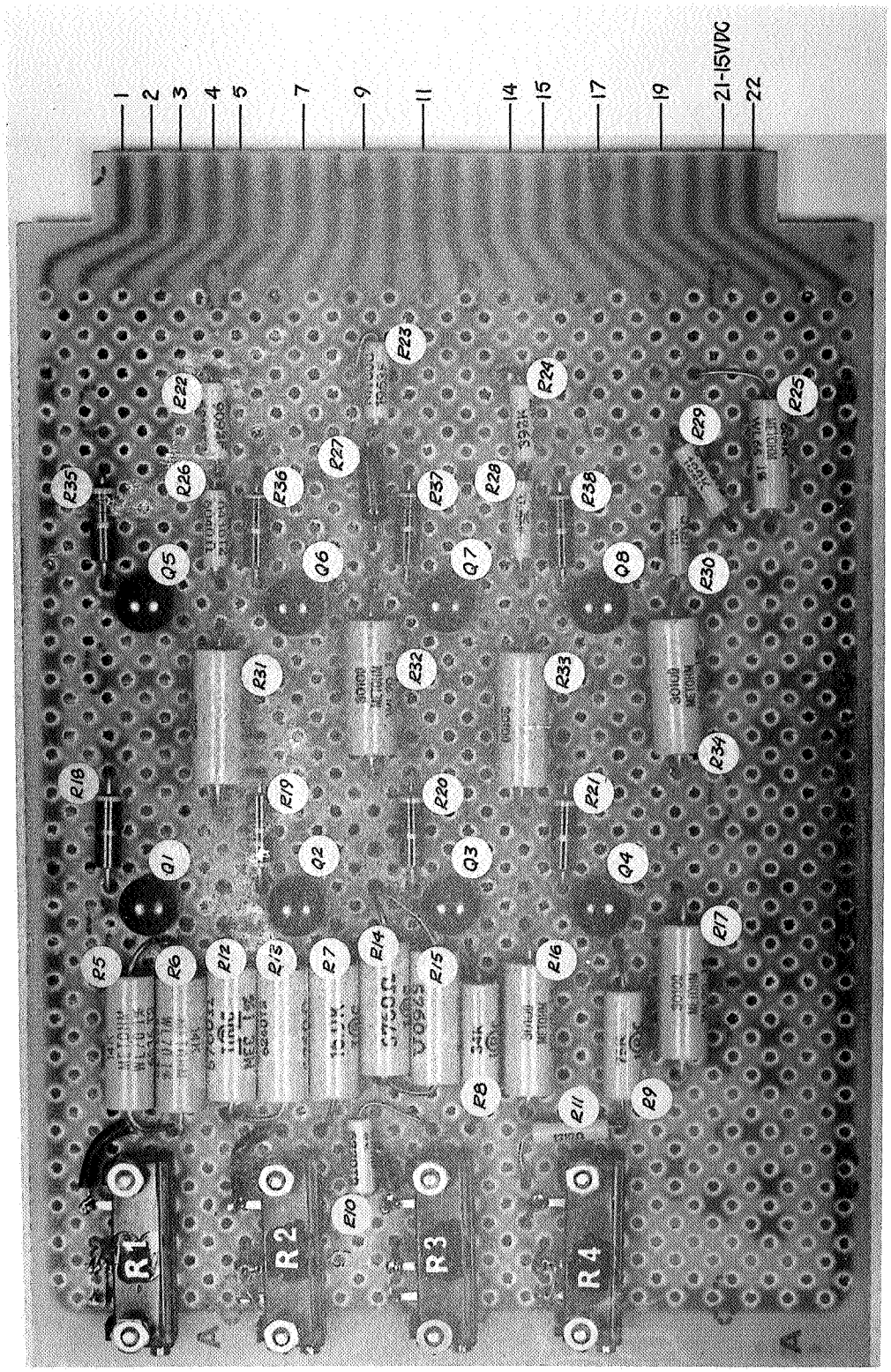
Photograph Of Board 16 - Front



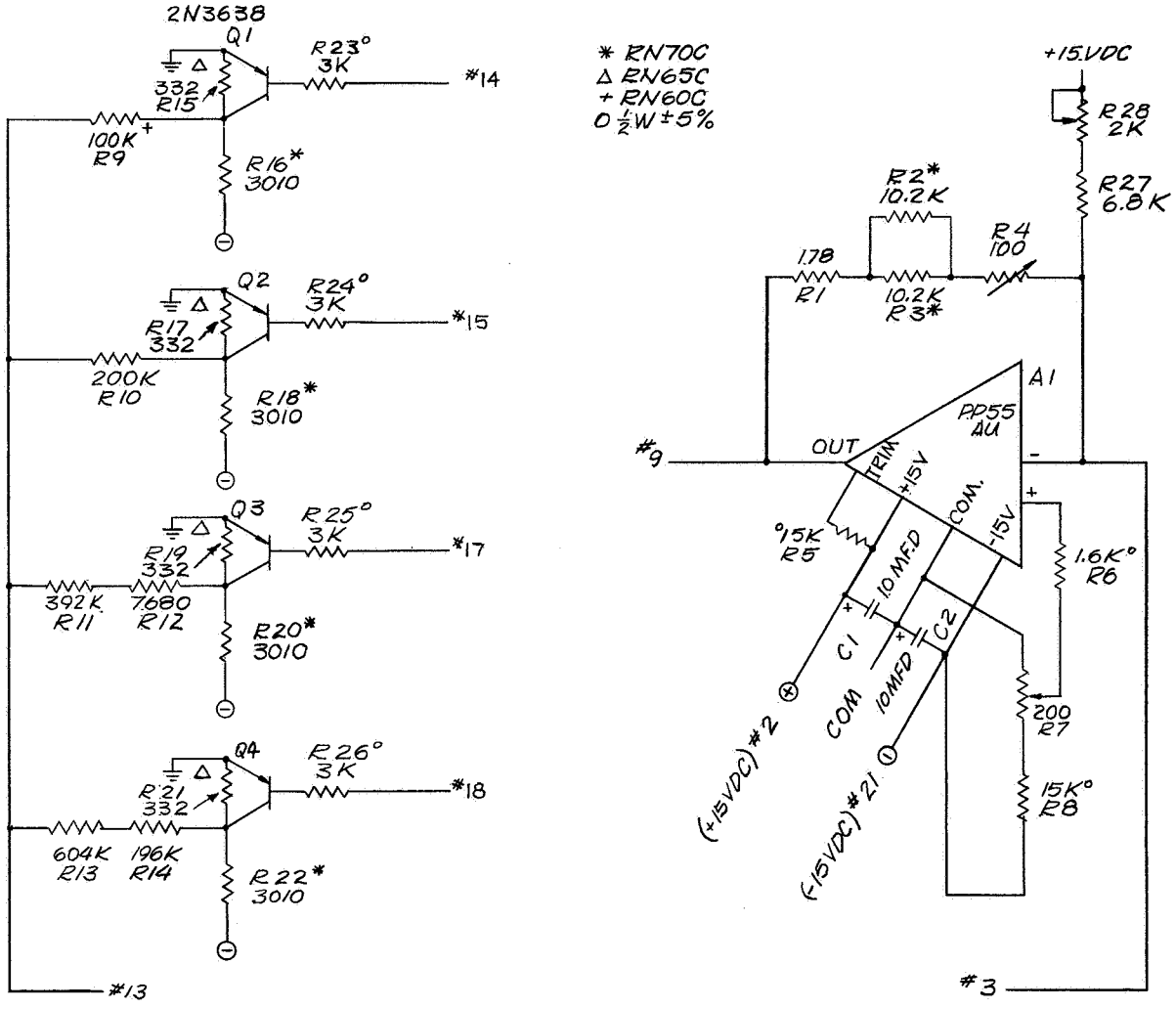
Photograph Of Board 16 - Rear



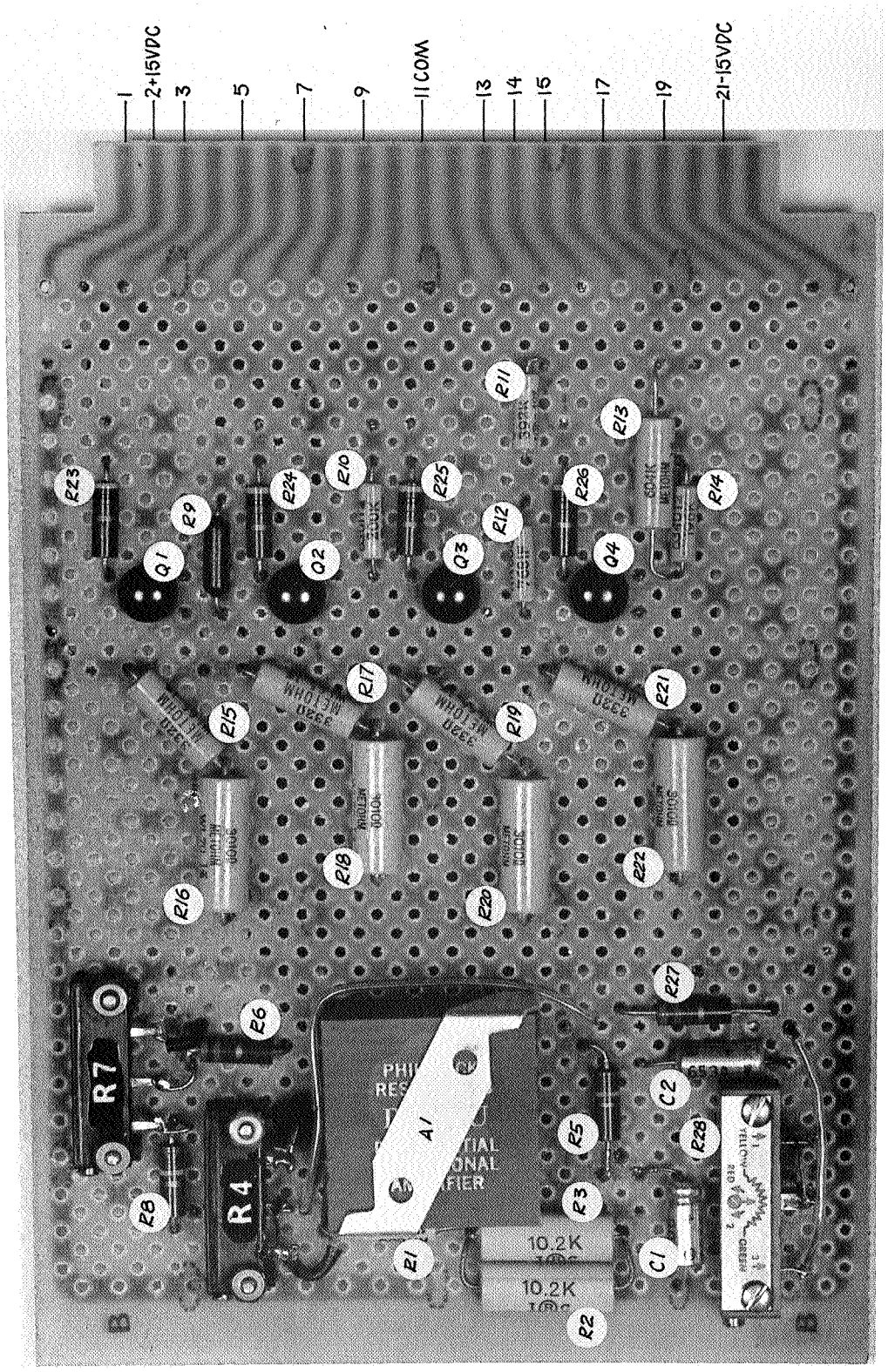
Schematic Of Board A



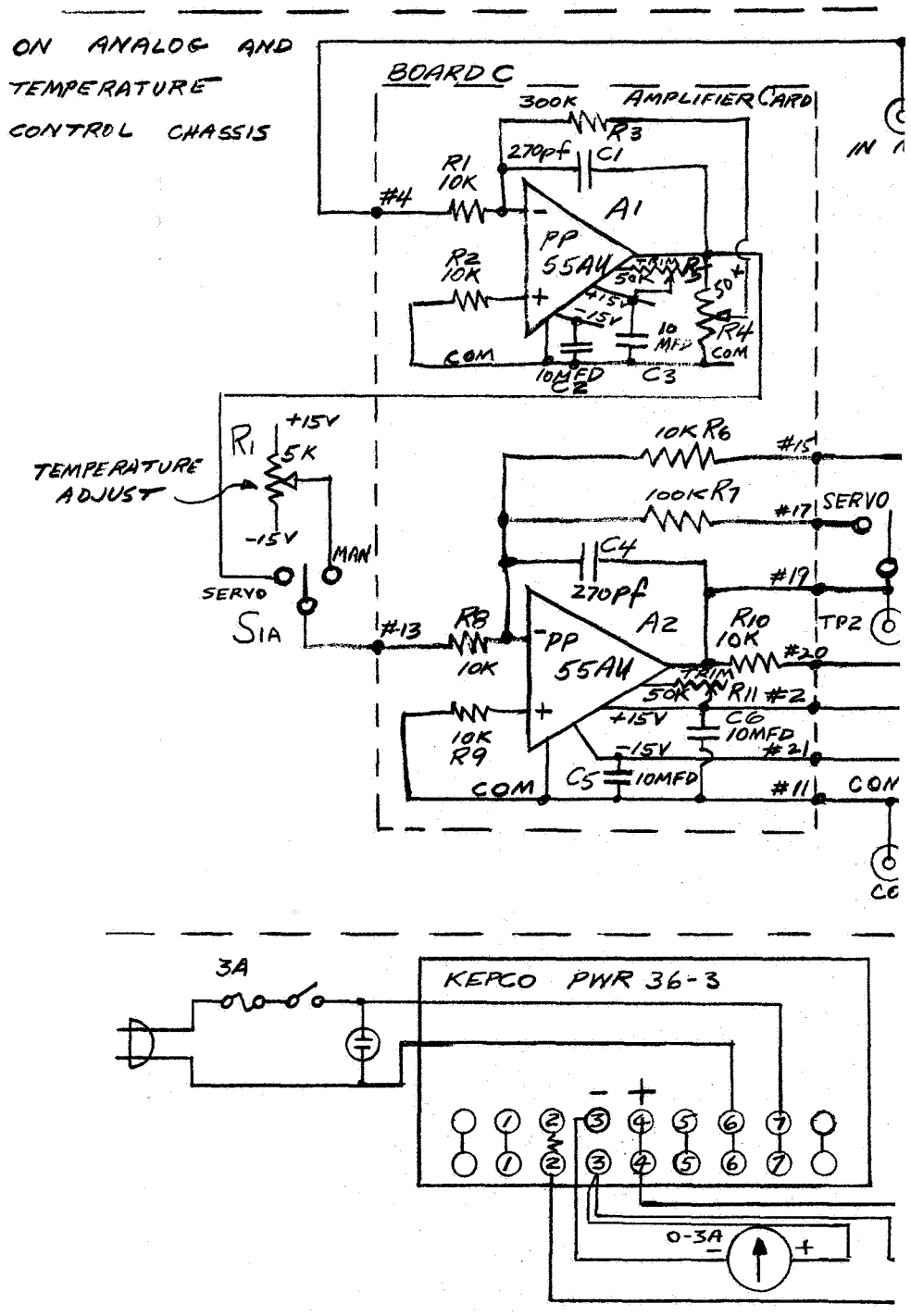
Photograph Of Board A

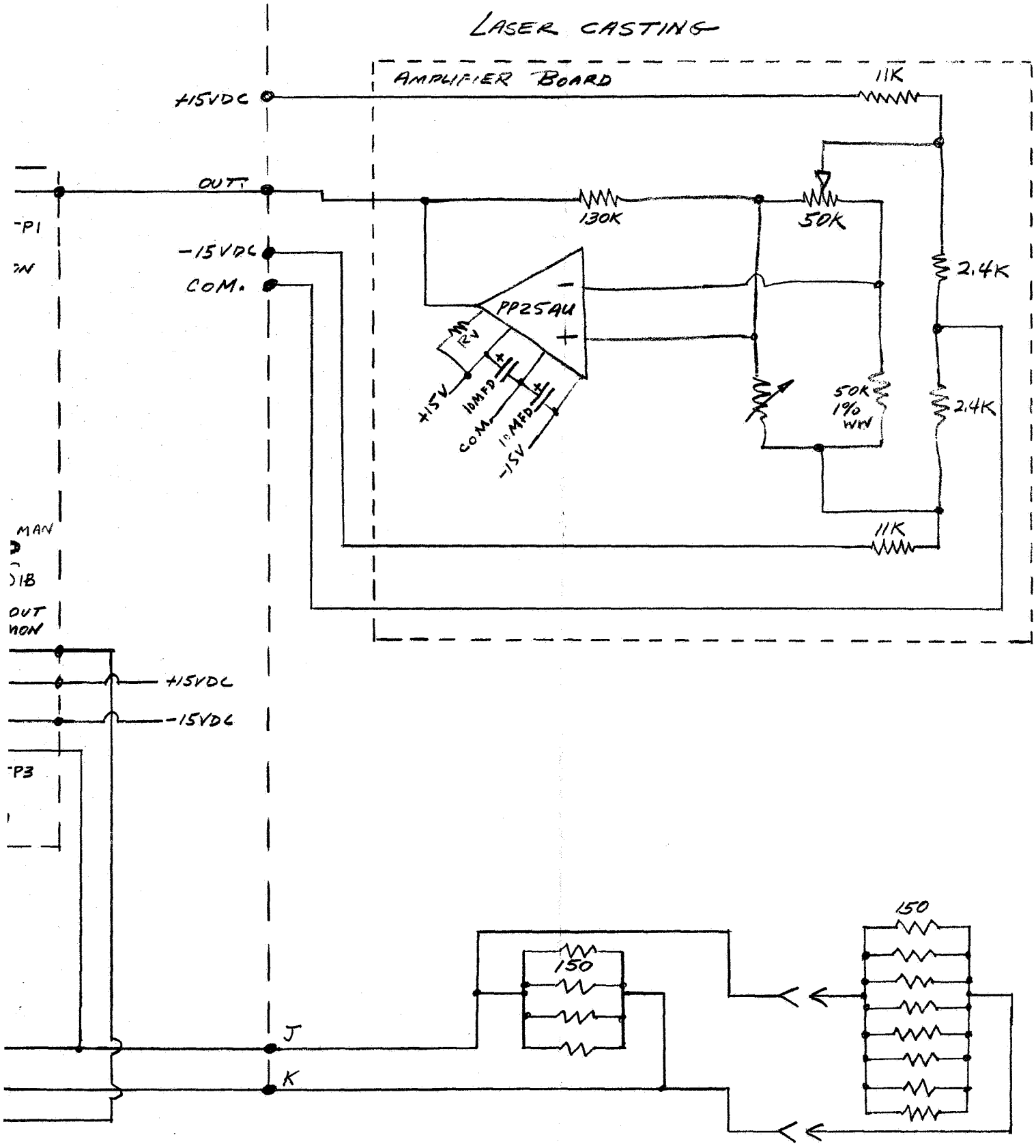


Schematic Of Board B

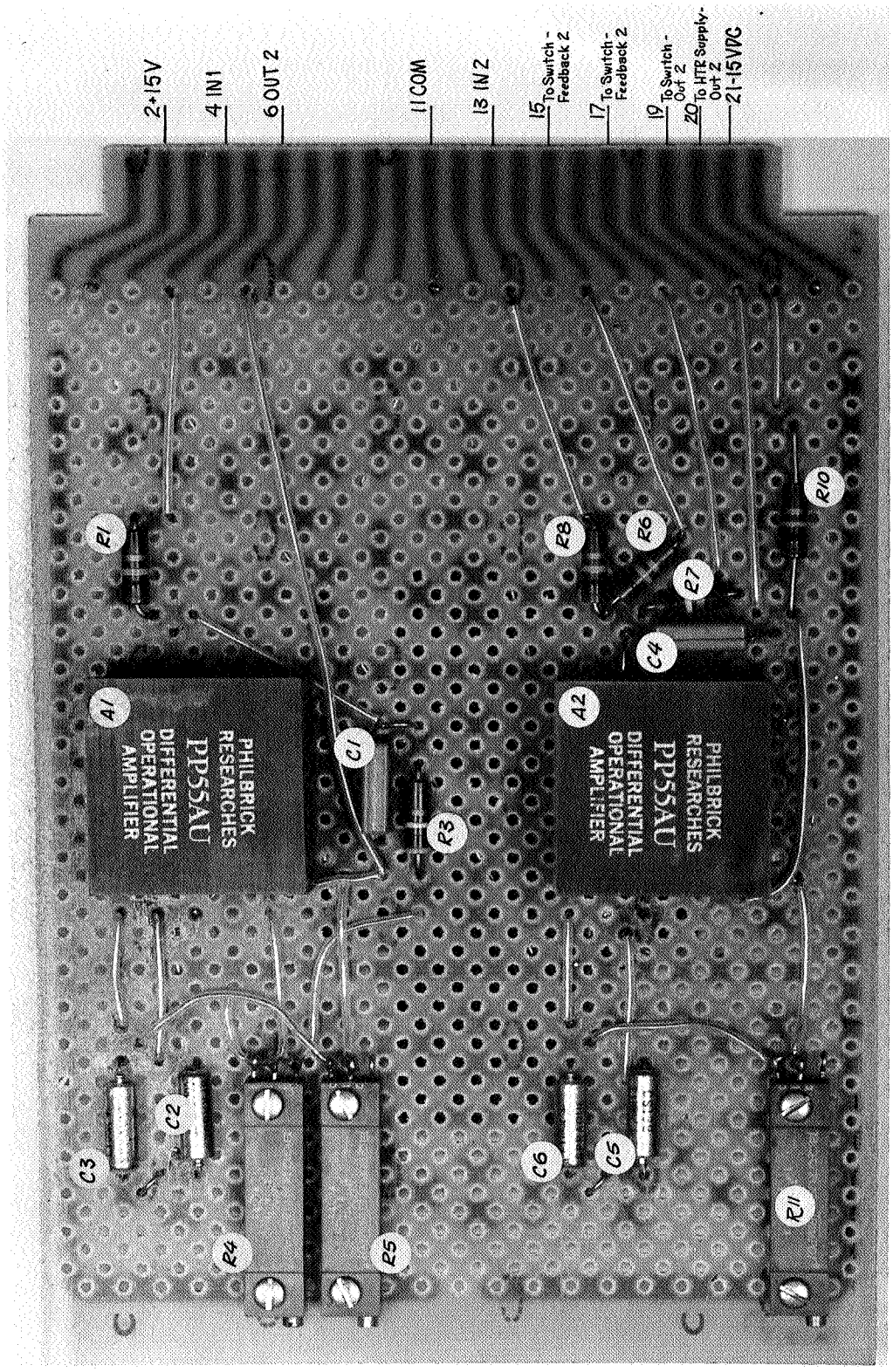


Photograph Of Board B

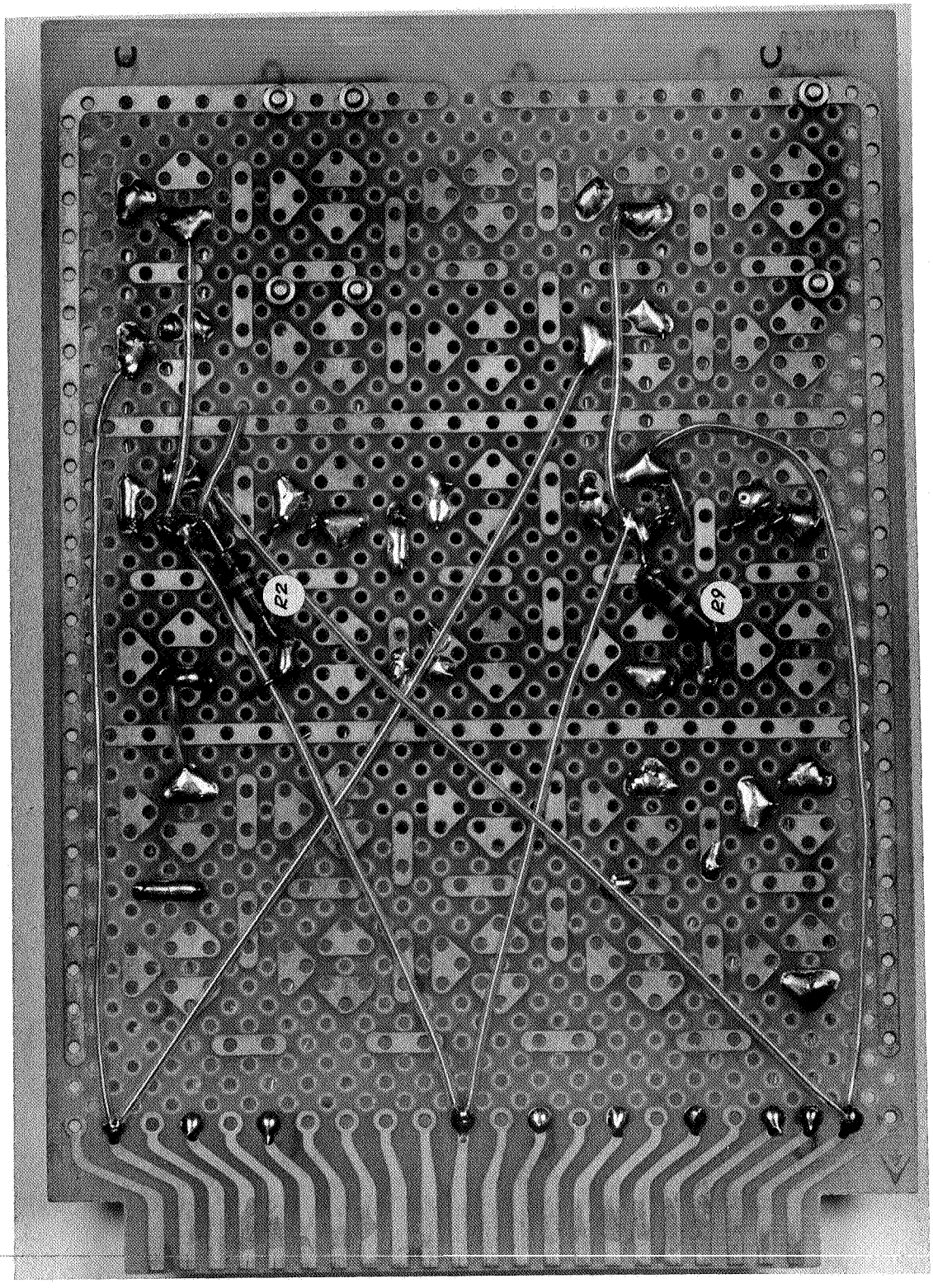

ON ANALOG AND TEMPERATURE CONTROL CHASSIS
BOARD C
AMPLIFIER CARD
300K
R3
270pf
C1
R1
10K
#4
A1
PP
55AH
R2
10K
50K
50
R4
COM
+15V
-15V
10 MFD
10MFD
C2
C3
TEMPERATURE ADJUST
R1
5K
SERVO
MAN
S1A
10K R6
#15
100K R7
#17
SERVO
C4
270pf
#19
#13
R8
10K
A2
R10
10K
TP2
#20
R11 #2
C6
10MFD
#21
R9
C5
10MFD
#11
COM
3A
KEPCO PWR 36-3
0-3A



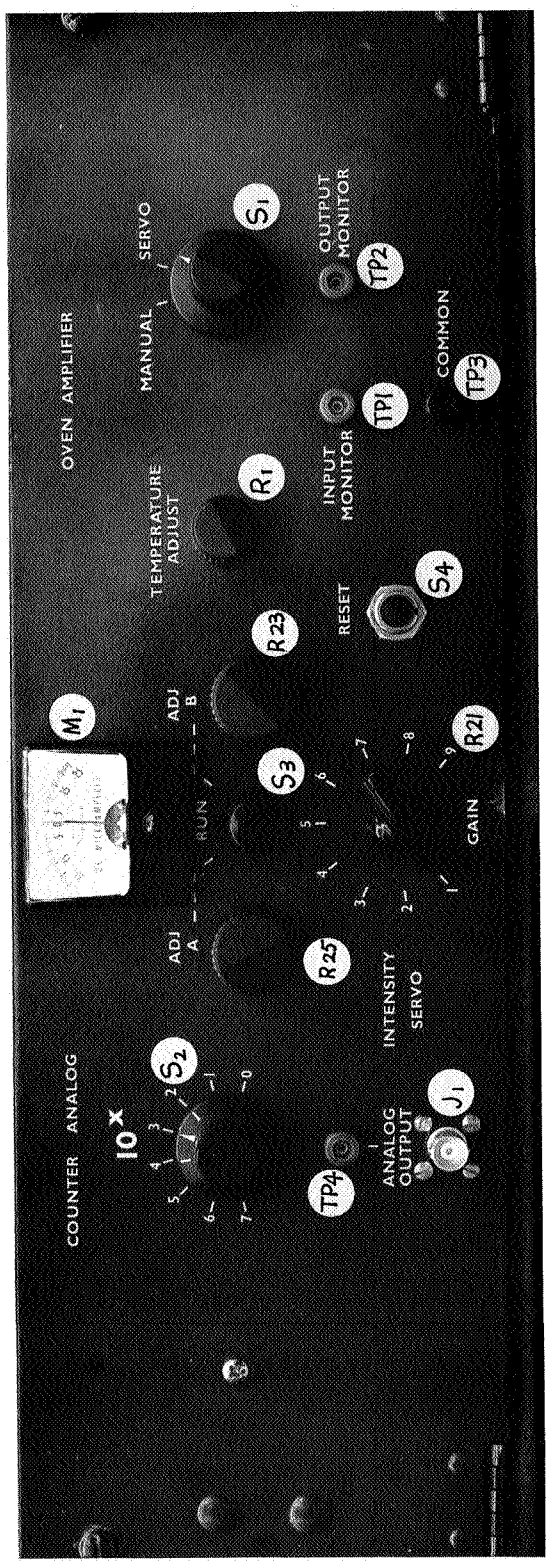
Schematic Of Board C



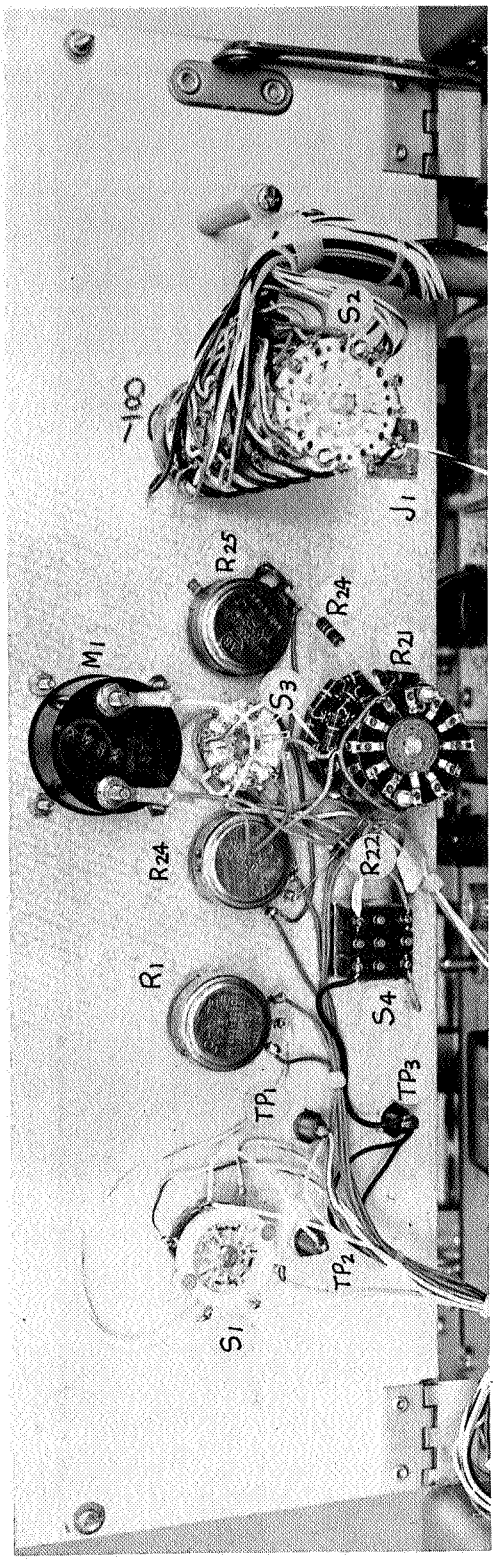
Photograph Of Board C - Front



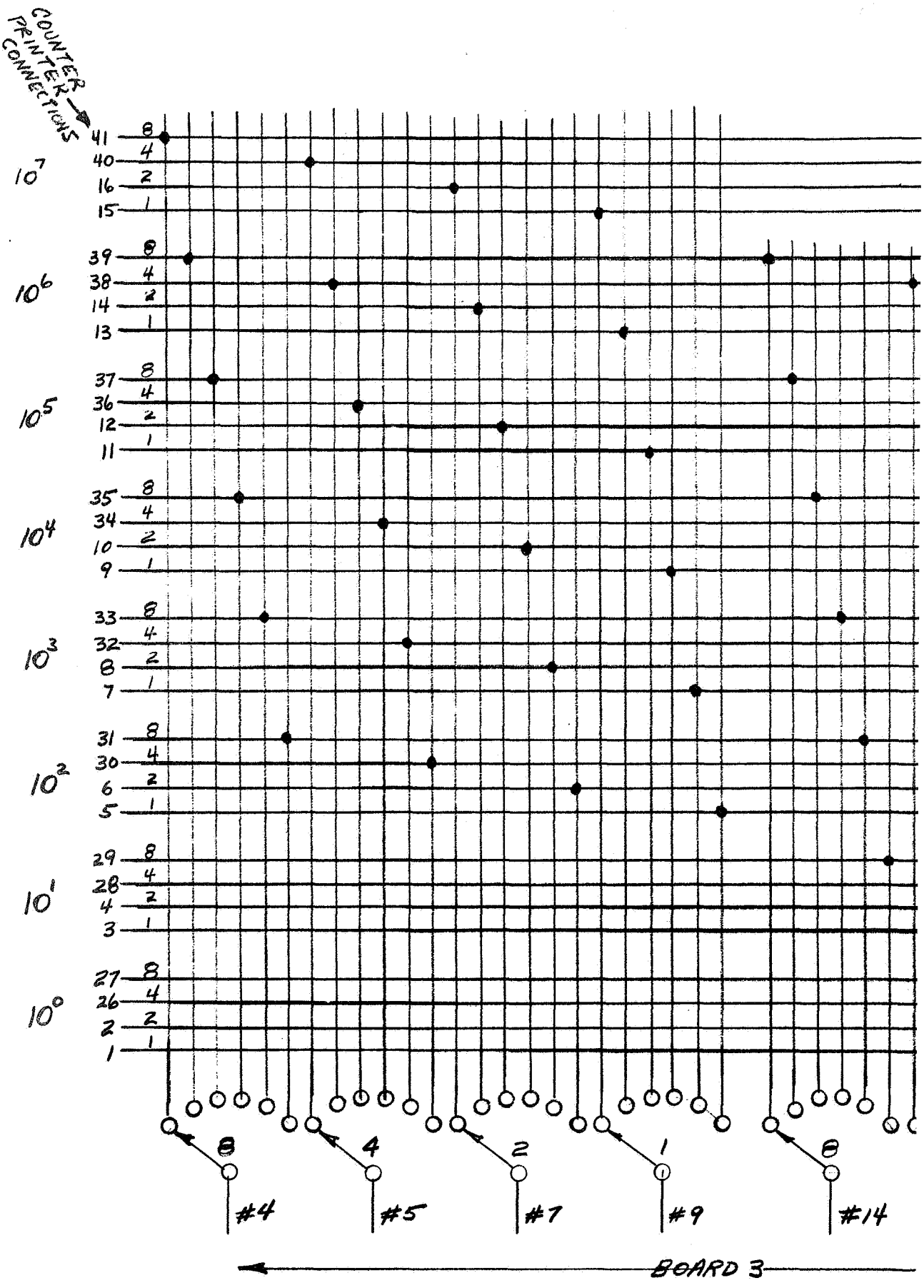
Photograph Of Board C - Rear

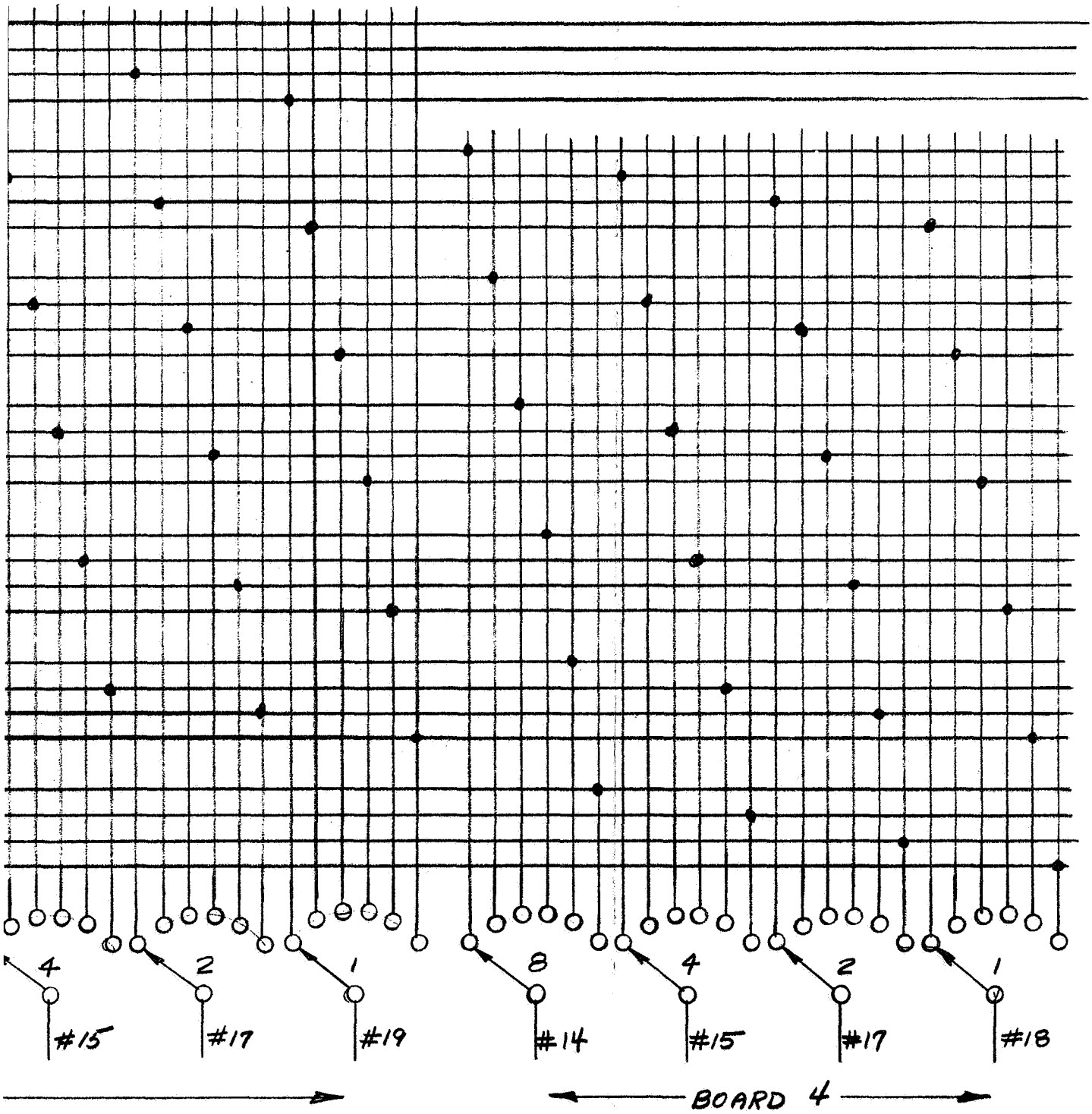


Photograph Of Front Of Analog-Intensity-Temperature Panel



Photograph Of Rear Of Analog-Intensity-Temperature Panel


COUNTER PRINTER CONNECTIONS
10^7
41 8
40 4
16 2
15 1
10^6
39 8
38 4
14 2
13 1
10^5
37 8
36 4
12 2
11 1
10^4
35 8
34 4
10 2
9 1
10^3
33 8
32 4
8 2
7 1
10^2
31 8
30 4
6 2
5 1
10^1
29 8
28 4
4 2
3 1
10^0
27 8
26 4
2 2
1 1
8
4
2
1
8
#4
#5
#7
#9
#14
BOARD 3



Digital-Analog Converter-Interconnection
With CMC

Drawing No. XB 594-0060 [redacted] I-74

BY THEALL DATE 7/6/66 SUBJECT Ring Laser Anode SHEET No. 1 OF 5

CHKD.BY DATE Circuit JOB NO. 26514

XC-594-0040

PART #	TYPE	MFR.	CAT # OR MIL #	VALUE	TOL.	RATING
A1	Amplifier Diff. Solid State	Philbrick	PP55AU			
A2	Amplifier Diff. Solid State	Philbrick	PP55AU			
Q1	Transistor, Silicon, NPN	Motorola	2N3227			
Q2	Transistor, Silicon, PNP	Motorola	2N3743			
Q3	Transistor, Silicon, PNP	Motorola	2N3743			
Q4	Transistor, Silicon NPN	Motorola	2N3227			
Q5	Transistor, Silicon, PNP	Motorola	2N3743			
Q6	Transistor, Silicon, PNP	Motorola	2N3743			
D1	Diode, Silicon	GE	1N914			
D2	Diode, Silicon	GE	1N914			
D3	Diode, Silicon	GE	1N914			
D4	Diode, Silicon	GE	1N914			
D5	Diode, Silicon, Zener	Motorola	1N3014A	180V	±10%	
D6	Diode, Silicon, Zener	Motorola	1N3015A	200V	±10%	

PART #	TYPE	MFR.	CAT # OR MIL #	VALUE	TOL.	RATING
D7	Diode, Silicon, Zener	Motorola	1N3015A	200V	±10%	
D8	Diode, H.V. Stack	RCA	CR212			12KV
D9	Diode, H.V. Stack	RCA	CR212			12KV
D10	Diode, Silicon	GE	1N914			
D11	Diode, Silicon	GE	1N914			
D12	Diode, H.V. Stack	RCA	CR212			12KV
D13	Diode, H.V. Stack	RCA	CR212			12KV
D14	Diode, H.V. Stack	RCA	CR212			12KV
D15	Diode, H.V. Stack	RCA	CR212			12KV
R1	Potentiometer	General Radio	GR974R	100KΩ	±5%	12W
R2	Potentiometer	Allen-Bradley	CMU1021	1KΩ		2W
R3	Potentiometer	General Radio	GR974R	100KΩ	±5%	12W
R4	Potentiometer	Allen-Bradley	CMU1021	1KΩ		2W
R5	Resistor, Comp.	Allen-Bradley	RC20GF	5.1KΩ	±5%	1/2W
R6	Resistor, Comp.	Allen-Bradley	RC20GF	1.5KΩ	±5%	1/2W
R7	Resistor, Comp.	Allen-Bradley	RC20GF	75KΩ	±5%	1/2W
R8	Resistor, Comp.	Allen-Bradley	RC20GF	75KΩ	±5%	1/2W
R9	Resistor, Comp.	Allen-Bradley	RC20GF	11Ω	±5%	1/2W

BY THEALL DATE 7/6/66 SUBJECT Ring Laser Anode SHEET NO. 3 OF 5

CHKD. BY _____ DATE _____ Circuit JOB NO. 26514

XC-594-0040

PART #	TYPE	MFR.	CAT # OR MIL #	VALUE	TOL.	RATING
R10	Resistor, Comp.	Allen-Bradley	RC20GF	5.1KΩ	±5%	1/2 W
R11	Resistor, Comp.	Allen-Bradley	RC20GF	75KΩ	±5%	1/2 W
R12	Resistor, Comp.	Allen-Bradley	RC20GF	75KΩ	±5%	1/2 W
R13	Resistor, Comp.	Allen-Bradley	RC20GF	1.5KΩ	±5%	1/2 W
R14	Resistor, Comp.	Allen-Bradley	RC20GF	11Ω	±5%	1/2 W
R15	Resistor, Comp.	Allen-Bradley	RC20GF	100KΩ	±5%	1/2 W
R16	Resistor, Metallic Film	IRC	MECT2 RN70C	4020Ω	1%	1/2 W
R17	Resistor, Metallic Film	IRC	MECT2 RN70C	100Ω	1%	1/2 W
R18	Resistor, Metallic Film	IRC	MECT2 RN70C	100Ω	1%	1/2 W
R19	Resistor, Metallic Film	IRC	MECT2 RN70C	4020Ω	1%	1/2 W
R20	Resistor, Wire Wound	Ohmite	#1850	50KΩ		20 W
R21	Resistor, Metallic Film	IRC	MECT2 RN70C	4020Ω	1%	1/2 W
R22	Resistor, Metallic Film	IRC	MECT2 RN70C	100Ω	1%	1/2 W
R23	Resistor, Metallic Film	IRC	MECT2 RN70C	100Ω	1%	1/2 W
R24	Resistor, Metallic Film	IRC	MECT2 RN70C	4020Ω	1%	1/2 W

PART #	TYPE	MFR.	CAT # OR MIL #	VALUE	TOL.	RATING
R25	Resistor, Wire-Wound	Ohmite	#1850	50KΩ		20 W
R26	Resistor, Comp.	Allen-Bradley	RC20GF	100KΩ	5%	1/2 W
R27	Resistor, Comp.	Allen-Bradley	RC42GF	220KΩ	5%	2 W
R28	Resistor, Comp.	Allen-Bradley	RC42GF	220KΩ	5%	2 W
R29	Resistor, Comp.	Allen-Bradley	RC20GF	15KΩ	5%	1/2 W
R30	Resistor, Comp.	Allen-Bradley	RC20GF	15KΩ	5%	1/2 W
C1	Capacitor, Electrolytic	Sprague	CS13BE-106K	10MFD	10%	20V
C2	Capacitor, Electrolytic	Sprague	CS13BE-106K	10MFD	10%	20V
C3	Not Assigned					
C4	Capacitor, Mylar	Sprague	2TM-S15	0.015 MFD	±10%	200V
C5	Capacitor, Electrolytic	Sprague	CS13BE-106K	10MFD	10%	20V
C6	Capacitor, Electrolytic	Sprague	CS13BE-106K	10MFD	10%	20V
C7	Not Assigned					
C8	Capacitor, Mylar	Sprague	2TMS-15	0.015 MFD	±10%	200V
M1	Meter	Simpson	1212C	0-15MA		
M2	Meter	Simpson	1212C	25-0-25 μa		
M3	Meter	Simpson	1212C	0-15MA		
J1	Coaxial Jack		UG931/U			5KV
J2	Coaxial Jack		UG931/U			5KV
J3	Coaxial Jack		UG290A/U			50CV

BY THEALL DATE 7/6/66 SUBJECT Ring Laser Anode SHEET NO. 5 OF 5

CHKD.BY DATE Circuit JOB NO. 26514

XC-594-0040

PART #	TYPE	MFR.	CAT # OR MIL #	VALUE	TOL.	RATING
J4	Coaxial Jack		UG290A/U			500V
J5	Coaxial Jack		UG290A/U			500V
J6	Coaxial Jack		UG931/U			5 KV
J7	Coaxial Jack		UG931/U			5 KV
J8	Coaxial Jack		UG290A/U			500V
T1	Variable Trans.	Superior Electric	10B Powerstat			
T2	Trans.	Acme Electric	CC185			
S1	Switch, Toggle SPST					
S2	Switch, Pushbutton SPST	Grayhill	4001			
S3	Switch, Rotary 4 Pole- 8 Pos.	Centralab	JV9035			3000VRMS
F1	Fuse Fuse-Holder	Buss	HJM	3A		
L1	Pilot Lamp Neon 100K	Drake	5200-243 623			

BY ET DATE 6/24/66 SUBJECT Beat Preamplifier SHEET NO. 1 OF 1

CHKD. BY DATE Board 1 XB-594-0046 JOB NO. 26514

Rotation Sensor - Servo

PART #	TYPE	MFR.	CAT. # OR MIL #	VALUE	TOL.	RATING
A1	Amplifier	Philbrick	P25AH			
R1	Resistor, Fixed, Comp.	Allen-Bradley	RC20GF	1K Ω	±5%	1/2W
R2	Resistor, Fixed, Comp.	Allen-Bradley	RC20GF	1K Ω	+5%	1/2W
R3	Resistor, Fixed, Comp.	Allen-Bradley	RC20GF	1K Ω	±5%	1/2W
R4	Resistor, Fixed, Comp.	Allen-Bradley	RC20GF	100K Ω	±5%	1/2W
R5	Resistor, Fixed, Comp.	Allen-Bradley	RC20GF	100K Ω	±5%	1/2W
R6	Resistor, Fixed, Comp.	Allen-Bradley	RC20GF	2.4K Ω	±5%	1/2W
R7	Resistor, Fixed, Comp.	Allen-Bradley	RC20GF	10K Ω	±5%	1/2W
R8	Resistor, Fixed, Comp.	Allen-Bradley	RC20GF	1K Ω	±5%	1/2W
C1	Capacitor	Arco-Elmenco Mica	CM-20-E-102-J	1000 PFD	±5%	500WVDC
C2	Capacitor	Sprague Tantalex	CS13BE106K	10MFD	±10%	20WVDC
C3	Capacitor	Sprague Tantalex	CS13BE106K	10MFD	±10%	20WVDC

BY ET DATE 6/24/66 SUBJECT Squaring Amplifier SHEET NO. 1 OF 3

CHKD. BY DATE Board 2 XB-594-0047 JOB NO. 26514

Rotation Sensor - Servo

PART #	TYPE	MFR.	CAT. # OR MIL #	VALUE	TOL.	RATING
Q1	Transistor, Silicon	Motorola	2N3227			
Q2	Transistor, Silicon	Motorola	2N3227			
Q3	Transistor, Silicon	Motorola	2N3227			
D1	Diode, Germanium	Sylvania	1N270			
D2	Diode, Germanium	Sylvania	1N270			
D3	Diode, Germanium	Sylvania	1N270			
D4	Diode, Germanium	Sylvania	1N270			
D5	Diode, Silicon	Hughes	1N914			
D6	Diode, Silicon	Hughes	1N914			
R1	Resistor, Fixed, Comp.	Allen-Bradley	RC20GF	20K Ω	±10%	1/2W
R2	Resistor, Fixed, Comp.	Allen-Bradley	RC20GF	3.9K Ω	±10%	1/2W
R3	Resistor, Fixed, Comp.	Allen-Bradley	RC20GF	7.5K Ω	±5%	1/2W
R4	Resistor, Fixed, Comp.	Allen-Bradley	RC20GF	1K Ω	±10%	1/2W

BY ET DATE 6/24/66 SUBJECT Squaring Amplifier SHEET NO. 2 OF 3

CHKD. BY DATE Board 2 XB-594-0047 JOB NO. 26514

Rotation Sensor - Servo

PART #	TYPE	MFR.	CAT. # OR MIL #	VALUE	TOL.	RATING
R5	Resistor, Fixed, Comp.	Allen-Bradley	RC20GF	10K Ω	±10%	1/2W
R6	Resistor, Fixed, Comp.	Allen-Bradley	RC20GF	1.3K Ω	±5%	1/2W
R7	Resistor, Fixed, Comp.	Allen-Bradley	RC20GF	100 Ω	±5%	1/2W
R8	Resistor, Fixed, Comp.	Allen-Bradley	RC20GF	1.5K Ω	±5%	1/2W
R9	Resistor, Fixed Comp.	Allen-Bradley	RC20GF	10K Ω	±10%	1/2W
R10	Resistor Fixed, Comp.	Allen-Bradley	RC20GF	1.3K Ω	±5%	1/2W
R11	Resistor, Fixed Comp.	Allen-Bradley	RC20GF	100 Ω	±5%	1/2W
R12	Resistor, Fixed Comp.	Allen-Bradley	RC20GF	1.5K Ω	±5%	1/2W
C1	Capacitor	Arco Elmenco Mica	CM-15-E-271J	270pf	±5%	500WVDC
C2	Capacitor	Sprague Monolythic Non-Pol.	Series (23 5C 15)	2.2 MFD	±20%	25WVDC
C3	Capacitor	Sprague Tantalex	CS13BE-225K	2.2 MFD	±10%	20WVDC
C4	Capacitor	Sprague Tantalex	CS13BE-106K	10 MFD	±10%	20WVDC

BY ET DATE 6/24/66 SUBJECT Squaring Amplifier SHEET No. 3 OF 3

CHKD. BY DATE Board 2 XB-594-0047 JOB NO. 26514

Rotation Sensor - Servo

PART #	TYPE	MFR.	CAT. # OR MIL #	VALUE	TOL.	RATING
C5	Capacitor	Sprague Tantalex	CS13BE106K	10 MFD	±10%	20WVDC
C6	Capacitor	Sprague Tantalex	CS13BE225K			
C7	Capacitor	Sprague Tantalex	CS13BE106K			
C8	Capacitor	Sprague Tantalex	CS13BE106K			

BY ET DATE 6/24/66 SUBJECT Servo Amplifier SHEET No. 1 OF 1

CHKD. BY DATE Board 7 XB-594-0048 JOB NO. 26514

Rotation Sensor - Servo

PART #	TYPE	MFR.	CAT. # OR MIL #	VALUE	TOL.	RATING
A1	Amplifier	Philbrick	PP25AU			
R1	Resistor, Fixed Comp.	Allen-Bradley	RC20GF	1K Ω	±5%	1/2W
R2	Resistor, Fixed Comp.	Allen-Bradley	RC20GF	100K Ω	±10%	1/2W
R3	Resistor, Fixed Comp.	Allen-Bradley	RC20GF	51K Ω	±5%	1/2W
R4	Resistor, Fixed Comp.	Allen-Bradley	RC20GF	100K Ω	±5%	1/2W
R5	Resistor, Fixed Comp.	Allen-Bradley	RC20GF	2.4K Ω	±5%	1/2W
R6	Resistor, Fixed Comp.	Allen-Bradley	RC20GF	2.4K Ω	±5%	1/2W
C1	Capacitor, Tantalex	Sprague	CS13BE106K	10MF	10%	20WVDC
C2	Capacitor, Tantalex	Sprague	CS13BE106K	10MF	10%	20WVDC
C3	Capacitor, Mica	Arco-Elmenco	CM15C120	12pf	±5%	500WVDC

BY ET DATE 6/24/66 SUBJECT Logic One-Shots SHEET NO. 1 OF 3

CHKD. BY DATE Board 8 XB-594-0049 JOB NO. 26514

Rotation Sensor - Servo

PART #	TYPE	MFR.	CAT. # OR MIL #	VALUE	TOL.	RATING
Q1	Transistor, Silicon	Fairchild	2N3638			
Q2	Transistor, Silicon	Fairchild	2N3638			
Q3	Transistor, Silicon	Fairchild	2N3638			
Q4	Transistor, Silicon	Fairchild	2N3638			
Q5	Transistor, Silicon	Fairchild	2N3638			
Q6	Transistor, Silicon	Fairchild	2N3638			
D1	Diode, Silicon	Hughes	1N914			
D2	Diode, Silicon	Hughes	1N914			
D3	Diode, Silicon	Hughes	1N914			
D4	Diode, Silicon	Hughes	1N914			
D5	Diode, Silicon	Hughes	1N914			
D6	Diode, Silicon	Hughes	1N914			
R1	Resistor, Fixed, Comp.	Allen-Bradley	RC20GF	10K Ω	±10%	1/2W
R2	Resistor, Fixed, Comp.	Allen-Bradley	RC20GF	5.1K Ω	±5%	1/2W

BY ET DATE 6/24/66 SUBJECT Logic One-Shots SHEET NO. 2 OF 3

CHKD. BY DATE Board 8 XB-594-0049 JOB NO. 26514

Rotation Sensor - Servo

PART #	TYPE	MFR.	CAT. # OR MIL #	VALUE	TOL.	RATING
R3	Resistor, Fixed, Comp.	Allen-Bradley	RC20GF	2K Ω	±5%	1/2W
R4	Resistor, Fixed, Comp.	Allen-Bradley	RC20GF	51K Ω	±5%	1/2W
R5	Resistor, Fixed, Comp.	Allen-Bradley	RC20GF	10K Ω	±10%	1/2W
R6	Resistor, Pot.	Bourns	30252S-1-503	50K Ω		
R7	Resistor, Fixed, Comp.	Allen-Bradley	RC20GF	5.1K Ω	±5%	1/2W
R8	Resistor, Fixed, Comp.	Allen-Bradley	RC20GF	4.3K Ω	±5%	1/2W
R9	Resistor, Fixed, Comp.	Allen-Bradley	RC20GF	4.3K Ω	±5%	1/2W
R10	Resistor, Fixed, Comp.	Allen-Bradley	RC20GF	75K Ω	±5%	1/2W
R11	Resistor, Fixed, Comp.	Allen-Bradley	RC20GF	7.5K Ω	±5%	1/2W
R12	Resistor, Fixed, Comp.	Allen-Bradley	RC20GF	2K Ω	±5%	1/2W
R13	Resistor, Fixed, Comp.	Allen-Bradley	RC20GF	51K Ω	±5%	1/2W
R14	Resistor, Fixed, Comp.	Allen-Bradley	RC20GF	62K Ω	±5%	1/2W
R15	Resistor, Fixed, Comp.	Allen-Bradley	RC20GF	5.1K Ω	±5%	1/2W

BY ET DATE 6/24/66 SUBJECT Logic One-Shots SHEET NO. 3 OF 3

CHKD. BY DATE Board 8 XB-594-0049 JOB NO. 26514

Rotation Sensor - Servo

PART #	TYPE	MFR.	CAT. # OR MIL #	VALUE	TOL.	RATING
R16	Resistor, Fixed, Comp.	Allen-Bradley	RC20GF	4.3K Ω	±5%	1/2W
R17	Resistor, Fixed, Comp.	Allen-Bradley	RC20GF	4.3K Ω	±5%	1/2W
R18	Resistor, Fixed, Comp.	Allen-Bradley	RC20GF	75K Ω	±5%	1/2W
R19	Resistor, Fixed, Comp.	Allen-Bradley	RC20GF	7.5K Ω	±5%	1/2W
R20	Resistor, Fixed, Comp.	Allen-Bradley	RC20GF	2K Ω	±5%	1/2W
R21	Resistor, Fixed, Comp.	Allen-Bradley	RC20GF	20K Ω	±5%	1/2W
R22	Resistor, Fixed, Comp.	Allen-Bradley	RC20GF	20K Ω	±5%	1/2W
C1	Capacitor, Silvered Mica	Arco-Elmenco	CM-20-E-102J	1000 pf	±5%	500WVDC
C2	Capacitor, Silvered Mica	Arco-Elmenco	CM-20-E-202J	2000 pf	±5%	500WVDC
C3	Capacitor Metall. Paper	Sprague 252	118P1059	1.0 MFD		200VDC
C4	Capacitor, Silvered Mica	Arco-Elmenco		2000 pf		
C5	Capacitor, Metall. Paper	Hopkins-Engr. Co.	1K10104	0.1 MFD		1000VDC

BY ET DATE 6/27/66 SUBJECT Ramp Circuit SHEET NO 1 OF 5

CHKD. BY DATE Board 9 XB-594-0050 JOB NO 26514

Rotation Sensor - Servo

PART #	TYPE	MFR	CAT # OR MIL #	VALUE	TOL.	RATING
Q1	Transistor, Germanium	T.I.	2N404A			
Q2	Transistor, Germanium	T.I.	2N404A			
Q3	Transistor, Silicon	Fairchild	2N3638			
Q4	Transistor, Silicon	Fairchild	2N3642			
Q5	Transistor, Silicon	Fairchild	2N3642			
Q6	Transistor, Germanium	T.I.	2N404A			
Q7	Transistor, Germanium	T.I.	2N404A			
D1	Diode, Silicon	Hughes	1N914			
D2	Diode, Silicon	Hughes	1N914			
D3	Diode, Silicon	Hughes	1N914			
D4	Diode, Silicon	Hughes	1N914			
D5	Diode, Silicon	Hughes	1N914			
D6	Diode, Silicon	Hughes	1N914			
R1	Resistor, Fixed, Comp.	Allen-Bradley	RC20GF	16KΩ	±5%	1/2W

BY ET DATE 6/27/66 SUBJECT Ramp Circuit SHEET NO 2 OF 5

CHKD. BY DATE Board 9 XB-594-0050 JOB NO 26514

Rotation Sensor - Servo

PART #	TYPE	MFR.	CAT # OR MIL #	VALUE	TOL.	RATING
R2	Resistor, Fixed, Comp.	Allen-Bradley	RC20GF	5.1K Ω	±5%	1/2 W
R3	Resistor, Fixed, Comp.	Allen-Bradley	RC20GF	51K Ω	±5%	1/2 W
R4	Resistor, Fixed, Comp.	Allen-Bradley	RC20GF	61K Ω	±5%	1/2 W
R5	Resistor, Fixed, Comp.	Allen-Bradley	RC20GF	75K Ω	±5%	1/2 W
R6	Resistor, Fixed , Comp.	Allen-Bradley	RC20GF	7.5K Ω	±5%	1/2 W
R7	Resistor, Fixed, Comp.	Allen-Bradley	RC20GF	1.3K Ω	±5%	1/2 W
R8	Resistor, Fixed, Comp.	Allen-Bradley	RC20GF	16K Ω	±5%	1/2 W
R9	Resistor, Fixed, Comp.	Allen-Bradley	RC20GF	75K Ω	±5%	1/2 W
R10	Resistor, Fixed , Comp.	Allen-Bradley	RC20GF	7.5K Ω	±5%	1/2 W
R11	Resistor, Fixed , Comp.	Allen-Bradley	RC20GF	1.3K Ω	±5%	1/2 W
R12	Resistor, Fixed, Comp.	Allen-Bradley	RC20GF	16K Ω	±5%	1/2 W
R13	Resistor, Fixed, Comp.	Allen-Bradley	RC20GF	51K Ω	±5%	1/2 W

PART #	TYPE	MFR.	CAT # OR MIL #	VALUE	TOL.	RATING
R14	Resistor, Fixed, Comp.	Allen-Bradley	RC20GF	16K Ω	±5%	1/2 W
R15	Resistor, Fixed, Comp.	Allen-Bradley	RC20GF	16K Ω	±5%	1/2 W
R16	Resistor, Fixed, Comp.	Allen-Bradley	RC20GF	5.1K Ω	±5%	1/2 W
R17	Resistor, Fixed, Comp.	Allen-Bradley	RC20GF	20K Ω	±5%	1/2 W
R18	Resistor, Fixed, Comp.	Allen-Bradley	RC20GF	39K Ω	±5%	1/2 W
R19	Resistor, Fixed, Comp.	Allen-Bradley	RC20GF	39K Ω	±5%	1/2 W
R20	Resistor, Fixed, Comp.	Allen-Bradley	RC20GF	20K Ω	±5%	1/2 W
R21	Resistor, Fixed, Comp.	Allen-Bradley	RC20GF	510 Ω	±5%	1/2 W
R22	Resistor, Fixed, Comp.	Allen-Bradley	RC20GF	510 Ω	±5%	1/2 W
R23	Resistor, Fixed, Comp.	Allen-Bradley	RC20GF	1K Ω	±10%	1/2 W
R24	Resistor, Fixed, Comp.	Allen-Bradley	RC20GF	10K Ω	±10%	1/2 W

PART #	TYPE	MFR	CAT# OR MIL #	VALUE	TOL.	RATING
R25	Resistor, Fixed, Comp.	Allen-Bradley	RC20GF	5.1K Ω	±5%	1/2 W
R26	Resistor, Fixed , Comp.	Allen-Bradley	RC20GF	51K Ω	±5%	1/2 W
R27	Resistor, Fixed, Comp.	Allen-Bradley	RC20GF	30K Ω	±5%	1/2 W
R28	Resistor, Fixed, Comp.	Allen-Bradley	RC20GF	30K Ω	±5%	1/2 W
R29	Resistor, Fixed, Comp.	Allen-Bradley	RC20GF	5.1K Ω	±5%	1/2 W
R30	Resistor, Fixed, Comp.	Allen-Bradley	RC20GF	4.3K Ω	±5%	1/2 W
R31	Resistor, Fixed, Comp.	Allen-Bradley	RC20GF	4.3K Ω	±5%	1/2 W
R32	Resistor, Fixed, Comp.	Allen-Bradley	RC20GF	75K Ω	±5%	1/2 W
R33	Resistor, Fixed, Comp.	Allen-Bradley	RC20GF	7.5K Ω	±5%	1/2 W
R34	Resistor, Fixed, Comp.	Allen-Bradley	RC20GF	2K Ω	±5%	1/2 W
R35	Resistor Fixed Comp.	Allen-Bradley	RC20GF	110 Ω	±5%	1/2 W
R36	Resistor Fixed Comp.	Allen-Bradley	RC20GF	100 Ω	±10%	1/2 W

BY ET DATE 6/27/66 SUBJECT Ramp Circuit SHEET 5 OF 5

CHKD. BY DATE Board 9 XB-594-0050 JOB NO 26514

Rotation Sensor - Servo

PART #	TYPE #	MFR.	CAT # OR MIL #	VALUE	TOL.	RATING
C1	Capacitor Silvered Mica	Arco-Elmenco	CM-20-E 202J	2000 pf	±5%	500WVDC
C2	Capacitor Silvered Mica	Arco-Elmenco	CM-20-E 202J	2000 pf		
C3	Capacitor Metall. Paper	Sprague	121P40591-R552	4.0 MFD	±5%	150 WVDC
C4	Capacitor, Silvered Mica	Arco-Elmenco	CM-20-E-202J	2000 pf	±5%	500WVDC
C5	Capacitor, Dipped Mylar-Paper	Cornell-Dubilier	DPMS 4P25	25 MFD	±10%	400 WVDC
C6	Capacitor, Electro-lytic	Aerovox	PTT-92	10 MFD		50 DCWV
C7	Capacitor, Electro-lytic	Aerovox	PTT-72	50 MFD		15 DCWV

BY ET DATE 6/29/66 SUBJECT Servo Switch SHEET NO. 1 OF 3

CHKD. BY DATE Board 10 XB-594-0051 JOB NO 26514

Rotation Sensor - Servo

PART #	TYPE	MFR	CAT # OR MIL #	VALUE	TOL.	RATING
Q1, Q2	Dual. Diff. Transistor Amplifier, Silicon	Motorola	2N2480			
Q3, Q4	Dual Diff. Transistor Amplifier, Silicon	Motorola	2N2480			
Q5	Transistor, Germanium	T.I.	2N404A			
Q6	Transistor, Germanium	T.I.	2N404A			
Q7	Transistor, Silicon	Fairchild	2N3638A			
Q8	Transistor, Silicon	Fairchild	2N3638A			
Q9	Transistor, Silicon	Fairchild	2N3642			
Q10	Transistor, Silicon	Fairchild	2N1711			
Q11	Transistor, Silicon	Fairchild	2N3642			
D1	Diode, Silicon Zener	Motorola	1N753			
D2	Diode, Silicon	Hughes	1N914			
D3	Diode, Silicon	Hughes	1N914			
D4	Diode, Silicon	Hughes	1N914			

BY ET DATE 6/29/66 SUBJECT Servo Switch SHEET NO 2 OF 3

CHKD. BY DATE Board 10 XB-594-0051 JOB NO 26514

Rotation Sensor - Servo

PART #	TYPE	MFR	CAT # OR MIL #	VALUE	TOL.	RATING
R1	Resistor, Fixed, Comp.	Allen-Bradley	RC20GF	10K Ω	±10%	1/2 W
R2	Resistor, Fixed, Comp.	Allen-Bradley	RC20GF	1.5K Ω	±5%	1/2 W
R3	Resistor, Fixed, Comp.	Allen-Bradley	RC20GF	1.5K Ω	±5%	1/2 W
R4	Resistor, Fixed, Comp.	Allen-Bradley	RC20GF	3K Ω	±5%	1/2 W
R5	Trimpot	Bourns	3067S-1-201	200 Ω		1/2 W
R6	Trimpot	Bourns	3067S-1-202	2K Ω		1/2 W
R7	Resistor, Fixed, Comp.	Allen-Bradley	RC20GF	51 Ω	±5%	1/2 W
R8	Resistor, Fixed, Comp.	Allen-Bradley	RC20GF	62 Ω	±5%	1/2 W
R9	Resistor, Fixed, Comp.	Allen-Bradley	RC20GF	560 Ω	±10%	1/2 W
R10	Resistor, Fixed, Comp.	Allen-Bradley	RC20GF	30K Ω	±5%	1/2 W
R11	Resistor, Fixed, Comp.	Allen-Bradley	RC20GF	43K Ω	±5%	1/2 W
R12	Resistor, Fixed, Comp.	Allen-Bradley	RC20GF	30 Ω	±5%	1/2 W
R13	Resistor, Fixed, Comp.	Allen-Bradley	RC20GF	1.5K Ω	±5%	1/2 W

BY ET DATE 6/29/66 SUBJECT Servo Switch SHEET NO 3 OF 3

CHKD. BY DATE Board 10 XB-594-0051 JOB NO 26514

Rotation Sensor - Servo

PART #	TYPE	MFR	CAT # OR MIL #	VALUE	TOL.	RATING
R14	Resistor, Fixed, Comp.	Allen-Bradley	RC20GF	1.5K Ω	±5%	1/2 W
R15	Resistor, Fixed, Comp.	Allen-Bradley	RC20GF	3K Ω	±5%	1/2 W
R16	Resistor, Fixed, Comp.	Allen-Bradley	RC20GF	3K Ω	±5%	1/2 W
R17	Resistor, Fixed, Comp.	Allen-Bradley	RC20GF	62K Ω	±5%	1/2 W
R18	Resistor, Fixed, Comp.	Allen-Bradley	RC20GF	7.5K Ω	±5%	1/2 W
R19	Resistor, Fixed, Comp.	Allen-Bradley	RC20GF	12K Ω	±10%	1/2 W
R20	Resistor, Fixed, Comp.	Allen-Bradley	RC20GF	10K Ω	±10%	1/2 W
C1	Capacitor, Silvered Mica	Arco-Elmenco	CM-20-E 502J	5000 pfd	±5%	500 WVDC
C2	Capacitor, Electro-lytic	Sprague	CS13BE106K	10MFD	±10%	20 WVDC

BY ET DATE 6/30/66 SUBJECT Storage Ampl. SHEET NO 1 OF 2

CHKD. BY DATE Board 11 XB-594-0052 JOB NO 26514

Rotation Sensor-Servo

PART #	TYPE	MFR	CAT# OR MIL#	VALUE	TOL.	RATING
A1	Amplifier Solid-State Diff.	Philbrick	PP55AU			
R1	Resistor, Fixed, Comp.	Allen-Bradley	RC20GF	10K Ω	±10%	1/2 W
R2	Trimpot	Bourns	3067S-1-502	5K Ω		1/2 W
R3	Resistor, Fixed, Comp.	Allen-Bradley	RC20GF	100K Ω	±5%	1/2 W
R4	Resistor, Fixed, Comp.	Allen-Bradley	RC20GF	1K Ω	±5%	1/2W
R5	Resistor, Fixed, Comp.	Allen-Bradley	RC20GF	10MEG.	±10%	1/2 W
R6	Resistor, Fixed, Comp.	Allen-Bradley	RC20GF	1K Ω	±10%	1/2 W
R7	Resistor, Fixed, Comp.	Allen-Bradley	RC20GF	39K Ω	±5%	1/2 W
R8	Resistor, Fixed, Comp.	Allen-Bradley	RC20GF	12K Ω	±5%	1/2 W
C1	Capacitor, Metall. Paper	Sprague	121P50591 -R552	5.0 Mfd.		150 VDC
C2	Capacitor Metall. Paper	Sprague	121P50591 -R552	5.0 Mfd.		150 VDC

BY ET DATE 6/30/66 SUBJECT Storage Ampl. SHEET NO 2 OF 2

CHKD.BY DATE Board 11 XB-594-0052 JOB NO 26514

Rotation Sensor-Servo

PART #	TYPE	MFR	CAT # OR MIL #	VALUE	TOL.	RATING
C3	Capacitor	Arco-Elmenco	CM-20-E 102J	1000 PFD	±5%	500 WVDC
C4	Capacitor, Electro-lytic	Sprague	CS13BE-106K	10 MFD	10%	20 WVDC
C5	Capacitor, Electro-lytic	Sprague	CS13BE-106K	10 MFD	10%	20 WVDC

BY Theall DATE 6/30/66 SUBJECT Pusher Driver SHEET NO 1 OF 2

CHKD. BY DATE Board 12 XB-594-0053 JOB NO 26514

Rotation Sensor - Servo

PART #	TYPE	MFR	CAT # OR MIL #	VALUE	TOL.	RATING
Q1	Transistor, Silicon	Fairchild	2N3638			
Q2	Transistor, Silicon	Industro	TRS 6015			
Q3	Transistor, Silicon	Industro	TRS 6015			
D1	Diode, Germanium	Sylvania	1N270			
D2	Diode, Germanium	Sylvania	1N270			
R1	Resistor, Fixed, Comp.	Allen-Bradley	RC20GF	2.7K Ω	±5%	1/2 W
R2	Resistor, Fixed, Comp.	Allen-Bradley	RC20GF	2.7K Ω	±5%	1/2 W
R3	Resistor, Fixed, Comp.	Allen-Bradley	RC20GF	2.4K Ω	±5%	1/2 W
R4	Resistor, Fixed, Comp.	Allen-Bradley	RC20GF	1K	±10%	1/2 W
R5	Resistor, Fixed, Comp.	Allen-Bradley	RC20GF	1K	±10%	1/2 W
R6	Resistor, Fixed, Comp.	Allen-Bradley	RC20GF	1K	±10%	1/2 W
R7	Resistor Fixed Comp.	Allen-Bradley	RC20GF	510 Ω	±5%	1/2 W

PART #	TYPE	MFR.	CAT # OR MIL #	VALUE	TOL.	RATING
R8	Resistor, Fixed, Comp.	Allen-Bradley	RC20GF	130K Ω	±5%	1/2 W
R9	Resistor, Fixed, Comp.	Allen-Bradley	RC20GF	130K Ω	±5%	1/2 W
R10	Resistor, Wire Wound	Ohmite Brown Devil	#1850	50K Ω		20 W
R11	Resistor, Comp.	Allen-Bradley	RC42GF	510 Ω	±5%	2W
R12	Resistor, Comp.	Allen-Bradley	RC32GF	820 Ω	±10%	1W
C1	Capacitor, Electro-lytic	Aerovox	PTT 86	100 MFD		25 WVDC
C2	Capacitor, Electro-lytic	Sprague	CS13BE-106K	10 MFD	10%	20 WVDC
C3	AS C1					
C4	Capacitor, Mica	Arco-Elmenco	CM-15-E 620J	62PFD	±5%	500 WVDC
C5	Capacitor, Metall. Paper	Sprague	155P	0.01 MFD		600 WVDC
F1	Fuse 8AG	Little Fuse	Series 36100	1/16A		250 WV
F2	Fuse 8AG	Little Fuse	Series 36100	1/16A		250 WV
	Fuse Holder	Little Fuse	387001			
	Heat Dissipator	Wakefield	NC403K			2°C/W

BY THEALL DATE 6/30/66 SUBJECT Analog Storage SHEET NO. 1 OF 2

CHKD. BY DATE Board 14 JOB NO. 26514

XB-594-0054

PART #	TYPE	MFR.	CAT.# OR MIL #	VALUE	TOL.	RATING
A1	Amplifier, Diff. Solid State	Philbrick	PP25AU			
Q1	Transistor, Germanium	Texas Instrument	2N1808			
Q2	Transistor, Germanium	Texas Instrument	2N1808			
Q3	Transistor, Silicon	Fairchild	2N3642			
Q4	Transistor, Silicon	Fairchild	2N1711			
Q5	Transistor, Silicon	Fairchild	2N1711			
D1	Diode, Silicon	Hughes	1N914			
R1	Resistor, Comp.	Allen-Bradley	RC20GF	5.1KΩ	±5%	1/2 W
R2	Resistor, Comp.	Allen-Bradley	RC20GF	33KΩ	±10%	1/2 W
R3	Resistor, Comp.	Allen-Bradley	RC20GF	12KΩ	±10%	1/2 W
R4	Resistor, Comp.	Allen-Bradley	RC20GF	15KΩ	±10%	1/2 W
R5	Resistor, Comp.	Allen-Bradley	RC20GF	100KΩ	±10%	1/2 W
R6	Resistor, Comp.	Allen-Bradley	RC20GF	100KΩ	±10%	1/2 W
R7	Resistor, Comp.	Allen-Bradley	RC20GF	12KΩ	± 5%	1/2 W
R8	Resistor, Comp.	Allen-Bradley	RC20GF	39KΩ	± 5%	1/2 W

BY THEALL DATE 7/1/66 UBJECT Analog Storage SHEET NO. 2 OF 2

CHKD. BY _____ DATE _____ Board 14 XB-594-0054 JOB NO. 26514

Rotation Sensor - Servo

PART #	TYPE	MFR.	CAT. # OR MIL #	VALUE	TOL.	RATING
C1	Capacitor, Metalized Paper	Sprague	96P10591S2	1.0 MFD	10%	100VDC
C2	Capacitor, Electrolytic	Sprague	CS13BE106K	10 MFD	10%	20WVDC
C3	Capacitor, Electrolytic	Sprague	CS13BE106K	10 MFD	10%	20WVDC
C4	Capacitor, Electrolytic	Sprague	CS13BE106K	10 MFD	10%	20WVDC

BY THEALL DATE 7/1/66 SUBJECT Differential Ampl. SHEET NO. 1 OF 3

CHKD. BY _____ DATE _____ & PZT Driver - Board 16 JOB NO. 26514

XB-594-0055 Rotation Sensor - Servo

PART #	TYPE	MFR.	CAT # OR MIL #	VALUE	TOL.	RATING
A1	Amplifier, Diff. Solid-State	Philbrick	PP55AU			
Q1	Transistor, Silicon	Fairchild	2N3638			
Q2	Transistor, Silicon	Industro	TRS6015			
Q3	Transistor Silicon	Industro	TRS6015			
D1	Diode, Germanium	Sylvania	IN270			
D2	Diode, Germanium	Sylvania	IN270			
D3	Diode, Germanium	Sylvania	IN270			
D4	Diode, Germanium	Sylvania	IN270			
R1	Resistor, Comp.	Allen-Bradley	RC20GF	10KΩ	±5%	1/2 W
R2	Resistor, Comp.	Allen-Bradley	RC20GF	10KΩ	±5%	1/2 W
R3	Resistor, Comp.	Allen-Bradley	RC20GF	10KΩ	±5%	1/2 W
R4	Resistor, Comp.	Allen-Bradley	RC20GF	10KΩ	±5%	1/2 W
R5	Resistor, Comp.	Allen-Bradley	RC20GF	130KΩ	±5%	1/2 W
R6	Resistor, Comp.	Allen-Bradley	RC20GF	130KΩ	±5%	1/2 W
R7	Resistor, Comp.	Allen-Bradley	RC20GF	130KΩ	±5%	1/2 W
R8	Resistor, Comp.	Allen-Bradley	RC20GF	5.1KΩ	±5%	1/2 W
R9	Resistor, Comp.	Allen-Bradley	RC20GF	2.4KΩ	±5%	1/2 W

PART #	TYPE	MFR.	CAT # OR MIL #	VALUE	TOL.	RATING
R10	Resistor, Comp.	Allen-Bradley	RC20GF	1KΩ	±10%	1/2 W
R11	Resistor, Comp.	Allen-Bradley	RC20GF	1KΩ	±10%	1/2 W
R12	Resistor, Comp.	Allen-Bradley	RC20GF	510Ω	± 5%	1/2 W
R13	Resistor, Comp.	Allen-Bradley	RC20GF	1KΩ	±10%	1/2 W
R14	Resistor, Wire Wound	Ohmite	1850 Brown Devil	50KΩ		20 W
R15	Resistor, Comp.	Allen-Bradley	RC42GF	510Ω	± 5%	2 W
R16	Resistor, Comp.	Allen-Bradley	RC42GF	270KΩ	±10%	2 W
R17	Resistor, Comp.	Allen-Bradley	RC42GF	270KΩ	±10%	2 W
R18	Resistor, Comp.	Allen-Bradley	RC32GF	820Ω	±10%	1 W
R19	Resistor, Comp.	Allen-Bradley	RC32GF	820Ω	±10%	1 W
C1	Capacitor, Mica	Arco-Elmenco	CM15E-501J	500PFD	± 5%	500WVDC
C2	Capacitor, Mica	Arco-Elmenco	CM15E-501J	500PFD	± 5%	500WVDC
C3	Capacitor, Mica	Arco-Elmenco	CM15E-301J	300PFD	± 5%	500WVDC
C4	Capacitor, Electrolytic	Sprague	CS13BE-106K	10MFD	±10%	20WVDC
C5	Capacitor, Electrolytic	Sprague	CS13BE-106K	10MFD	±10%	20WVDC
C6	Capacitor, Electrolytic	Aerovox	PTT86	100MFD	±10%	25WVDC
C7	Capacitor, Electrolytic	Sprague	CS13BE-106K	10MFD	±10%	20WVDC

QTY	PART #	TYPE	MFR.	CAT # OR MIL #	VALUE	TOL.	RATING
	C8	Capacitor, Electrolytic	Aerovox	PTT73	100MFD		15WVDC
	C9	Capacitor Mica	Arco-Elmenco	CM-15E-680J	68PFD	±5%	500WVDC
	F1	Fuse 8ag	Little Fuse	Series 36100	1/16A		250V
	F2	Fuse 8ag	Little Fuse	Series 36100	1/16A		250V
2		Fuse Holder	Little Fuse	387001			
1		Heat Dissipator	Wakefield	NC403K			2°C/W

BY Theall DATE 7/1/66 SUBJECT D-A Converter SHEET NO. 1 OF 3

CHKD. BY DATE Board A XB-594-0041 JOB NO. 26514

Rotation Sensor

PART #	TYPE	MFR.	CAT. # OR MIL #	VALUE	TOL.	RATING
Q1	Transistor, Silicon	Fairchild	2N3638			
Q2	Transistor, Silicon	Fairchild	2N3638			
Q3	Transistor, Silicon	Fairchild	2N3638			
Q4	Transistor, Silicon	Fairchild	2N3638			
Q5	Transistor, Silicon	Fairchild	2N3638			
Q6	Transistor, Silicon	Fairchild	2N3638			
Q7	Transistor, Silicon	Fairchild	2N3638			
Q8	Transistor, Silicon	Fairchild	2N3638			
R1	Trimpot	Bourns	3067S-1-201	200 Ω		1/2W
R2	Trimpot	Bourns	3067S-1-501	500 Ω		1/2W
R3	Trimpot	Bourns	3067S-1-102	1000 Ω		1/2W
R4	Trimpot	Bourns	3067S-1-202	2K Ω		1/2W
R5	Resistor Metall. Film	Ward-Leonard	WL70 RN70C	14K Ω	1%	1/2W
R6	Resistor Metall. Film	Ward-Leonard	WL70 RN70C	14K Ω	1%	1/2W
R7	Resistor Metall. Film	IRC	MEC T2 RN70C	16.9K Ω	1%	1/2W
R8	Resistor Metall. Film	IRC	MEB T2 RN65C	34K Ω	1%	1/4W

BY Theall DATE 7/1/66 SUBJECT D-A Converter SHEET NO. 2 OF 3

CHKD. BY DATE Board A XB-594-0041 JOB NO. 26514

Rotation Sensor

PART #	TYPE	MFR.	CAT.# OR MIL #	VALUE	TOL.	RATING
R9	Resistor Metall. Film	IRC	MEB T2 RN65C	75K Ω	1%	1/4W
R10	Resistor Metall. Film	IRC	MEA T2 RN60C	2610 Ω	1%	1/8W
R11	Resistor Metall. Film	IRC	MEA T2 RN60C	1210 Ω	1%	1/8W
R12	Resistor, Metall. Film	IRC	RN70C MECT2	5760Ω	1%	1/2W
R13	Resistor, Metall. Film	IRC	RN70C MEC T2	5760Ω	1%	1/2W
R14	Resistor, Metall. Film	IRC	RN70C MEC T2	5760 Ω	1%	1/2W
R15	Resistor, Metall. Film	IRC	RN70C MEC T2	5760 Ω	1%	1/2W
R16	Resistor, Metall. Film	Ward Leonard	WL70 RN70	3010 Ω	1%	1/2W
R17	Resistor, Metall. Film	Ward Leonard	WL70 RN70	3010 Ω	1%	1/2W
R18	Resistor, Comp.	Allen-Bradley	RC20GF	3K Ω	5%	1/2W
R19	Resistor, Comp.	Allen-Bradley	RC20GF	3K Ω	5%	1/2W
R20	Resistor, Comp.	Allen-Bradley	RC20GF	3K Ω	5%	1/2W
R21	Resistor, Comp.	Allen-Bradley	RC20GF	3K Ω	5%	1/2W
R22	Resistor, Metall. Film	IRC	MEAT2 RN60C	90.9K Ω	1%	1/8W
R23	Resistor, Metall. Film	IRC	MEAT2 RN60C	196K Ω	1%	1/8W
R24	Resistor, Metall. Film	IRC	MEAT2 RN60C	392K Ω	1%	1/8W
R25	Resistor, Metall. Film	Ward-Leonard	WL65 RN65	604K Ω	1%	1/4W

BY Theall DATE 7/1/66 SUBJECT D-A Converter SHEET NO. 3 OF 3

CHKD. BY DATE Board A XB-594-0041 JOB NO. 26514

Rotation Sensor

PART #	TYPE	MFR.	CAT.# OR MIL #	VALUE	TOL.	RATING
R26	Resistor, Metall. Film	IRC	MEAT2 RN60C	6040 Ω	1%	1/8W
R27	Resistor, Metall. Film	IRC	MEAT2 RN60C	1K Ω	1%	1/8W
R28	Resistor, Metall. Film	IRC	MEAT2 RN60C	4990 Ω	1%	1/8W
R29	Resistor, Metall. Film	IRC	MEAT2 RN60C	182K Ω	1%	1/8W
R30	Resistor, Metall. Film	IRC	MEAT2 RN60C	11K Ω	1%	1/8W
R31	Resistor Metall. Film	Ward-Leonard	WL70 RN70C	3010 Ω	1%	1/2W
R32	Resistor, Metall. Film	Ward-Leonard	WL70 RN70C	3010 Ω	1%	1/2W
R33	Resistor, Metall. Film	Ward-Leonard	WL70 RN70C	3010 Ω	1%	1/2W
R34	Resistor, Metall. Film	Ward-Leonard	WL70 RN70C	3010 Ω	1%	1/2W
R35	Resistor, Comp.	Allen-Bradley	RC20GF	3K Ω	5%	1/2W
R36	Resistor, Comp.	Allen-Bradley	RC20GF	3K Ω	5%	1/2W
R37	Resistor, Comp.	Allen-Bradley	RC20GF	3K Ω	5%	1/2W
R38	Resistor, Comp.	Allen-Bradley	RC20GF	3K Ω	5%	1/2W

BY THEALL DATE 7/5/66 SUBJECT DA Converter SHEET NO. 1 OF 3

CHKD. BY DATE Board B JOB NO. 26514

XB-594-0042

PART #	TYPE	MFR.	CAT # OR MIL #	VALUE	TOL.	RATING
A1	Amplifier, Diff. Solid-State	Philbrick	PP55AU			
Q1	Transistor, Silicon, PNP	Fairchild	2N3638			
Q2	Transistor, Silicon, PNP	Fairchild	2N3638			
Q3	Transistor, Silicon, PNP	Fairchild	2N3638			
R1	Resistor, Metal Film	IRC	MEAT2 RN60C	178Ω	1%	1/8 W
R2	Resistor, Metal Film	IRC	MECT2 RN70C	10.2KΩ	1%	1/2 W
R3	Resistor, Metal Film	IRC	MECT2 RN70C	10.2KΩ	1%	1/2 W
R4	Trimpot	Bourns	3067S-1-101	100Ω		1/2 W
R5	Resistor Comp.	Allen-Bradley	RC20GF	15KΩ	5%	1/2 W
R6	Resistor Comp.	Allen-Bradley	RC20GF	1.6KΩ	5%	1/2 W
R7	Trimpot	Bourns	3067S-1-201	200Ω		1/2 W
R8	Resistor, Comp.	Allen-Bradley	RC20GF	15KΩ	5%	1/2 W
R9	Resistor, Metallic Film	IRC	MEAT2 RN60C	100KΩ	1%	1/2 W
R10	Resistor, Metallic Film	IRC	MEAT2 RN60C	200KΩ	1%	1/2 W
R11	Resistor, Metallic Film	IRC	MEAT2 RN60C	392KΩ	1%	1/2 W

PART #	TYPE	MFR.	CAT # OR MIL #	VALUE	TOL.	RATING
R12	Resistor, Metallic Film	IRC	MEAT2 RN60C	7680Ω	1%	1/8 W
R13	Resistor, Metallic Film	Ward-Leonard	WL65 RN65	604KΩ	1%	1/4 W
R14	Resistor, Metallic Film	IRC	MEAT2 RN60C	196KΩ	1%	1/8 W
R15	Resistor, Metallic Film	Ward-Leonard	WL65 RN65	332Ω	1%	1/4 W
R16	Resistor, Metallic Film	Ward-Leonard	WL70 RN65	3010Ω	1%	1/2 W
R17	Resistor, Metallic Film	Ward-Leonard	WL65 RN65	332Ω	1%	1/4 W
R18	Resistor, Metallic Film	Ward-Leonard	WL70 RN70	3010Ω	1%	1/2 W
R19	Resistor, Metallic Film	Ward-Leonard	WL65 RN65	332Ω	1%	1/4 W
R20	Resistor, Metallic Film	Ward-Leonard	WL70 RN70	3010Ω	1%	1/2 W
R21	Resistor, Metallic Film	Ward-Leonard	WL65 RN65	332Ω	1%	1/4 W
R22	Resistor, Metallic Film	Ward-Leonard	WL70 RN70	3010Ω	1%	1/2 W
R23	Resistor, Comp.	Allen-Bradley	RC20GF	3KΩ	5%	1/2 W
R24	Resistor, Comp.	Allen-Bradley	RC20GF	3KΩ	5%	1/2 W
R25	Resistor, Comp.	Allen-Bradley	RC20GF	3KΩ	5%	1/2 W
R26	Resistor, Comp.	Allen-Bradley	RC20GF	3KΩ	5%	1/2 W

BY THEALL DATE 7/5/66 SUBJECT DA Converter SHEET NO. 3 OF 3

CHKD BY _____ DATE _____ Board B JOB NO. 26514

XB-594-0042

PART #	TYPE	MFR.	CAT # OR MIL #	VALUE	TOL.	RATING
R27	Resistor, Comp.	Allen-Bradley	RC20GF	6.8KΩ	5%	1/2 W
R28	Trimpot	Bourns	273-1-202	2KΩ	5%	1/4 W
C1	Capacitor, Electro-lytic	Sprague	CS13BE-106K	10MFD	10%	20WVDC
C2	Capacitor, Electro-lytic	Sprague	CS13BE-106K	10MFD	10%	20WVDC

BY THEALL DATE 7/5/66 SUBJECT Temperature Control SHEET NO. 1 OF 2

CHKD. BY DATE Amplifier Board C JOB NO. 26514

XB-594-0056

PART #	TYPE	MFR.	CAT. # OR MIL #	VALUE	TOL.	RATING
A1	Amplifier Diff. Solid-State	Philbrick	PP55AU			
A2	Amplifier Diff. Solid-State	Philbrick	PP55AU			
R1	Resistor, Comp.	Allen-Bradley	RC20GF	10K Ω	5%	1/2W
R2	Resistor, Comp.	Allen-Bradley	RC20GF	10K Ω	5%	1/2W
R3	Resistor, Comp.	Allen-Bradley	RC20GF	300KΩ	5%	1/2W
R4	Trimpot	Bourns	3052S-1-503	50K Ω		1W
R5	Trimpot	Bourns	3052S-1-503	50K Ω		1W
R6	Resistor, Comp.	Allen-Bradley	RC20GF	10KΩ	5%	1/2W
R7	Resistor, Comp.	Allen-Bradley	RC20GF	100KΩ	5%	1/2W
R8	Resistor, Comp.	Allen-Bradley	RC20GF	10K Ω	5%	1/2W
R9	Resistor Comp.	Allen-Bradley	RC20GF	10K Ω	5%	1/2W
R10	Resistor Comp.	Allen-Bradley	RC20GF	10K Ω	5%	1/2W
R11	Trimpot	Bourns	3052S-1-503	50KΩ		1W
C1	Capacitor, Mica	Arco-Elmenco	CM-15-E-271J	270PF	±5%	500WVDC
C2	Capacitor, Electro-lytic	Sprague	CS13BE-106K	10MFD	10%	20WVDC
C3	Capacitor, Electro-lytic	Sprague	CS13BE-106K	10MFD	10%	20WVDC

BY THEALL DATE 7/5/66 SUBJECT Temperature Control SHEET NO. 2 OF 2

CHKD. BY DATE Amplifier Board C JOB NO. 26514

XB-594-0056

PART #	TYPE	MFR.	CAT. # OR MIL #	VALUE	TOL.	RATING
C4	Capacitor	Arco-Elmenco	CM-15-E 271J	270PF	±5%	500WVDC
C5	Capacitor, Electro-lytic	Sprague	CS13BE-106K	10MFD	10%	20WVDC
C6	Capacitor, Electro-lytic	Sprague	CS13BE-106K	10MFD	10%	20WVDC

APPENDIX II

MEASUREMENT OF SATURATION INDUCED OPTICAL NONRECIPROCITY IN A RING LASER PLASMA

BY
P. H. LEE
AND
J. G. ATWOOD

(Reprinted from IEE Journal of Quantum Electronics)

THE PERKIN-ELMER CORPORATION
Electro-Optical Division

INTERIM

NEW TECHNOLOGY REPORT

NASA Contract: NAS 8-11669

October 14, 1965

Perkin-Elmer Sales Order: 26514

GENERAL

The items discussed in the New Technology section of this report are forerunners of a more detailed discussion to be submitted in the Final Report, required as a contractually deliverable item. It is the intention, since this is a research-type contract, to meet our Final New Technology Report requirements by submitting the Final Report due under the contract.

The work to be described below was performed by Paul Lee and Gordon Dueker of the Perkin-Elmer Corporation.

The new devices and technology developed under the contract fall into the following general classes:

A. Investigation of materials for use in ring lasers;

B. Optical devices and techniques;

C. Electronic controls for lasers;

D. Mode control of ring lasers.

Descriptions of items in each category are developed below.

NEW TECHNOLOGY

A. Investigation of Materials for Use in Ring Lasers

1. Factor of Merit for Faraday Rotation

Control of light in a ring laser cavity is often done by rotating the plane of polarization utilizing the Faraday effect in a transparent substance. However, many glasses have too much loss,

from bulk scatter or absorption, to allow operation at all within the laser cavity. Fused silica, which has minimum losses, also has low Faraday rotation. In attempting to find a better material, several different types of glass were obtained from optical stores, and polished on parallel faces approximately one inch apart. The samples were placed at Brewster's angle inside the resonator of a 7.5 meter perimeter ring laser with a single 80cm x 4mm diameter plasma tube. Of the 6 samples prepared, only 2, namely, F-2 and SK-16 would operate. Scatter was estimated visually in comparison to that in fused silica. Reduction in power output was noted relative to the unmodified laser.

Schott Glass Type #	Fraction of Power Relative to no Sample	Estimated Relative Scatter
BAK - 1	0	Not observed
BAK - 2	0	Not observed
SK - 2	0	Not observed
SK - 4	0	Not observed
SK - 16	0.01	5 x
F - 2	0.1	2 x

Table I.

2. Optical Homogeneity

Fused silica is supplied by the manufacturer in several forms. The two most common for fabrication of laser components are rectangular slabs or ingots, and cylindrical rods. Interferometric examination of both showed several fringes of optical path difference per centimeter of aperture, concentrated mostly near the outer surface of the cast shape. Annealing of the material according to the manufacturers' instructions produced no measurable change. It was concluded that the path difference was due to density gradients produced during the casting. Critical parts for laser applications, where multiple passes of light through the material occur, should be fabricated from sections of large ingots avoiding the outer cast surfaces.

3. Anti-Reflection Coatings

In many instances, it is desired to operate a laser plasma tube with circularly polarized light in the plasma or to be able to choose the plane of polarization at random. Conventional design of tubes utilizes end windows set at Brewster's angle to the beam, and does not allow this freedom. During the program, two laser tubes were constructed having windows perpendicular to the beam, and with anti-reflection coatings on both surfaces. The coatings were double-layer, MgF_2 - CeF_3 films. In order to have enough excess gain to operate as a laser, it was necessary to have reflection losses below about 1/2 percent total. This was achieved by selection of the best coatings from a number of trials. The tubes with these coated windows operated as linear lasers with reasonable gain, and produced unpolarized light. The life of both tubes was short, not exceeding four hours of operating time. In contrast, extended storage time of several months had no apparent detrimental effect. Further investigation is required to determine the causes of the limited life.

B. Optical Devices and Techniques

1. Brewster's Angle Flat Plate Coupler

A device which provides efficient coupling of energy from a linear F-P laser into a ring type of resonator is shown in Figure 1.

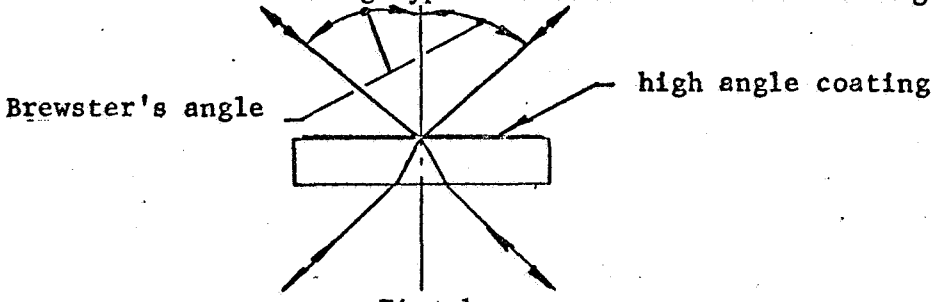


Fig. 1

The beam entering and leaving the uncoated surface of the plate may be the operating path of a conventional linear laser, and negligible loss will occur at the Brewster surface. On the coated side, the emerging rays can be utilized to align a ring laser, with the plate as one of the permanent mirrors of the ring. After alignment, the plate serves as one exit port of the ring, with no spurious back reflections. The dielectric coating must be designed for operation at the angle corresponding to Brewster's angle in fused silica (55° 33' for 6328Å) and for the amount of transmission desired.

2. Shovel-nose Prisms

A second means of coupling to ring lasers is shown in Figure 2 where it is desirable to have beams at a narrow angle to each other.

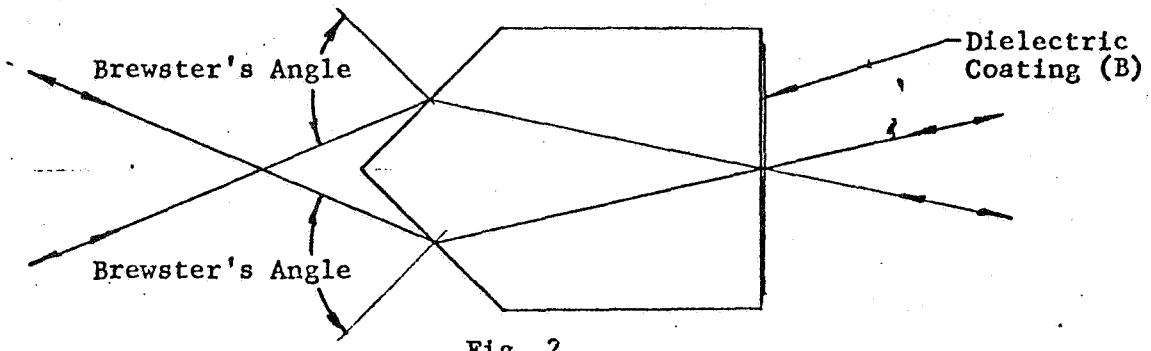


Fig. 2

Beams enter from the right at a small angle (10 to 15 degrees) away from normal incidence, and leave at the left through a Brewster's angle surface. The angles between the beams can be chosen within limits, to fit various geometries of ring lasers and a curved surface may be used at (B) as the focusing element. Because of the low-loss Brewster surfaces, either side may be placed inside a ring laser resonator.

3. Unit Beam Combiner

To gain information about the phase and frequency of the contracirculating beams in a ring laser, it is often necessary to combine them in some type of interferometer. The combining must be done in a stable structure which does not introduce spurious phase shifts itself, and which does not couple energy from one beam to the other inside the laser cavity. A structure meeting these requirements is shown in Figure 3. It is specifically designed to work with the output prisms described in paragraph 2, but could be modified to work at other angles. All input and exit surfaces are at Brewster's angle to the beams. The partially reflecting surface coating is at a cemented interface and is protected from damage.

Three mechanical motions are required to align the beams. They are: side-wise translation (a), which serves to bring the beams to the same point on the partially reflecting surface; rotation (b) about the point of intersection of the beams, in the horizontal plane, and rotation (c) about the same point, but in the vertical plane. The

latter two motions are sufficient to make the beams collinear after they have been made to intersect at the beam-splitting surface.

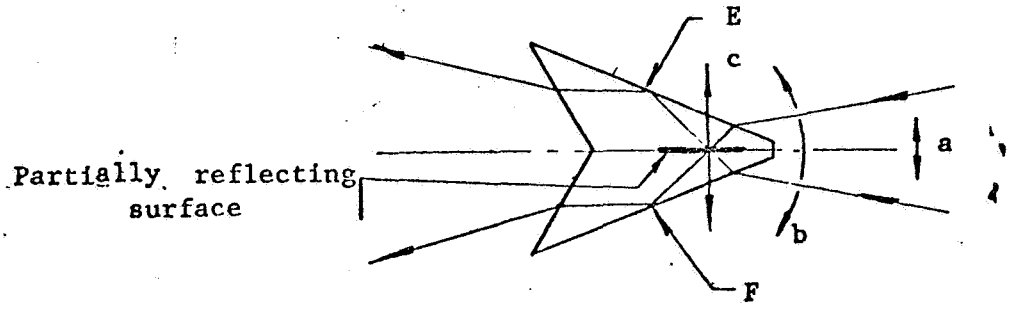


Fig. 3

A total internal reflection of each pair of combined beams occurs at points E & F. This allows the beams to be extracted at Brewster's angle, and avoids ghost reflections from the surfaces.

4. Non-Reciprocal Gain Control

In a ring laser the two contra-circulating beams may have differing intensities because of residual Faraday rotation and other secondary non-reciprocal effects. To correct such effects, or to deliberately emphasize them, a non-reciprocal gain control was designed. Figure 4 shows a sketch of the element.

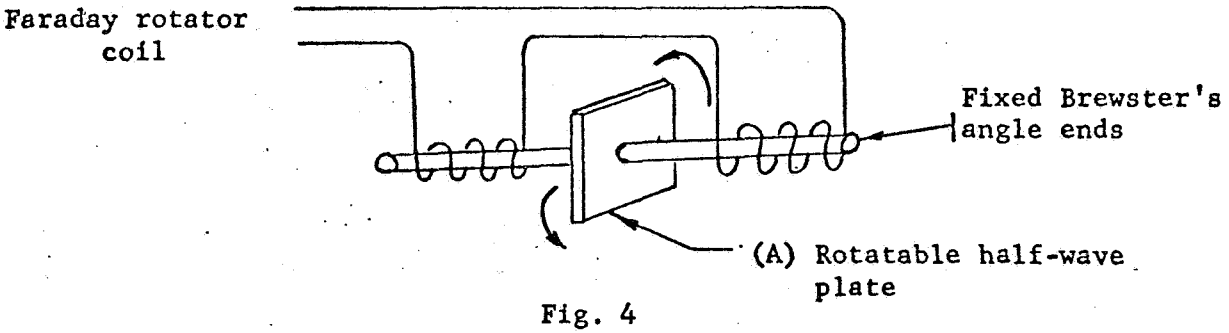


Fig. 4

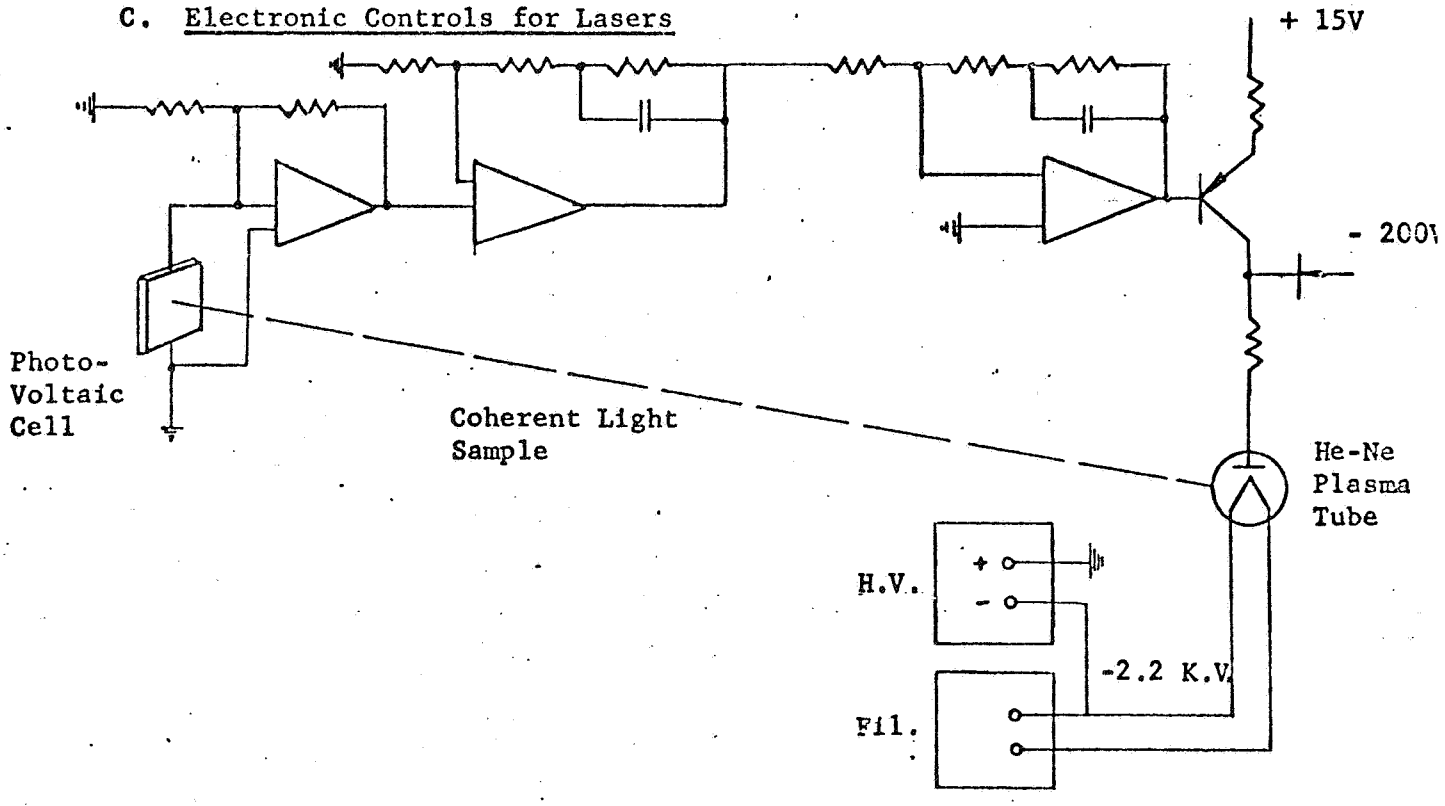
At (A) is a crystal quartz half-wave retardation plate in a rotatable mount. On either side of the half-wave plate are fused silica rods with Brewster's angle ends, and on them is wound a solenoid for producing non-reciprocal Faraday rotation. In operation, a reciprocal loss is introduced into both beams, by rotating the half-wave plate, which rotates the plane of polarization away from that established by the Brewster's angle surfaces elsewhere in the ring.

By passing current through the coil, one beam is then rotated in the direction of better alignment to the Brewster surfaces, while the contra-circulating beam is further mis-aligned.

5. Beam Diameter Control

A constantly recurring problem in ring laser design is loss caused by scattering and optical inhomogeneity of materials needed inside the resonator. The problem is even more critical in ring than in linear lasers because only half as many passes are made through the active medium by the light. A partial solution to the problem is found by using properly spaced curved mirrors to control the beam diameter in the laser cavity. If, for instance, two mirrors are spaced apart by the sum of their focal lengths, a converging beam will be produced between them, while essentially parallel beams may be maintained elsewhere in the system. Critical components may be inserted near the focus, where the beam cross-section is a minimum. Other combinations of spacing and focal lengths may also be used to enlarge or decrease the cross-section of the beam inside the cavity.

C. Electronic Controls for Lasers



1. Laser Intensity Regulator

Laser beam intensity was regulated with an electronic loop closed to the laser anode current. In one system, a photovoltaic cell coupled laser output to an amplifier chain which used a high voltage PNP transistor as laser anode driver. Net loop gain was 46 db, breaking at 1 kc and 10 kc to fall into zero db at 100 kc. Beam intensity fluctuations were held within one part per thousand. Use of small integrated feedback amplifiers combines compactness and gain stability in the signal portion of the loop.

D. Mode Control in Ring Lasers

1. Variable Couplers

When a requirement arises for coupling energy into or out of a ring laser cavity it is often desirable to have the amount of coupling variable. Such requirements may include longitudinal mode control, alignment of other systems, and frequency or phase control. It is an additional advantage if the coupler does not deviate the beam into which it is inserted. A coupler having both these features is shown in Figure 5.

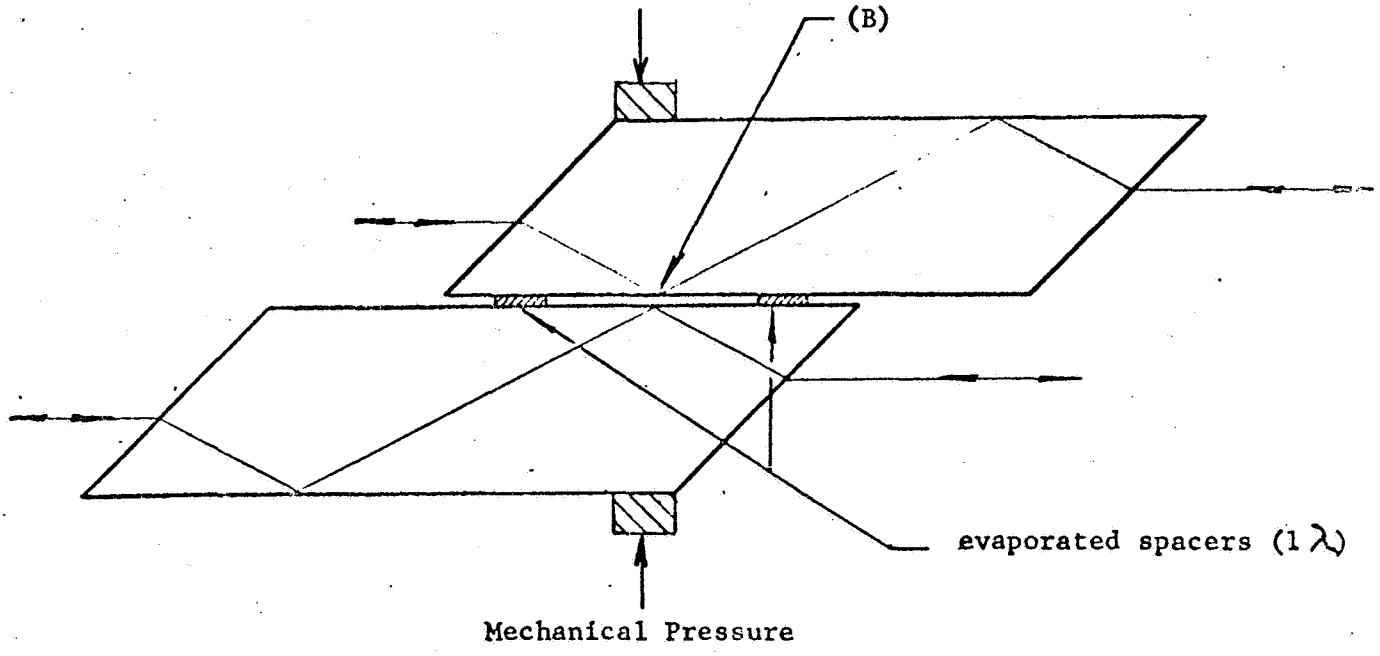


Fig. 5

The laser beam enters either prism at Brewster's angle and is totally internally reflected twice at opposite faces. At the adjacent TIR surfaces at (B) the prisms may be placed so close to contact (of the order of 1 wave or less) that the total internal reflection is partially frustrated, and energy is transferred across the gap from one prism to the other. The amount of coupling can be varied from zero to almost 100% by changing the gap width mechanically or electrically for automatic remote control. Prism geometry is such that minor motion of the device does not deviate either beam.

2. 3-Mirror Fabry-Perot

Linear Fabry-Perot lasers have been operated with a third internal mirror in the form of a half Brewster's angle prism, as shown in Figure 6.

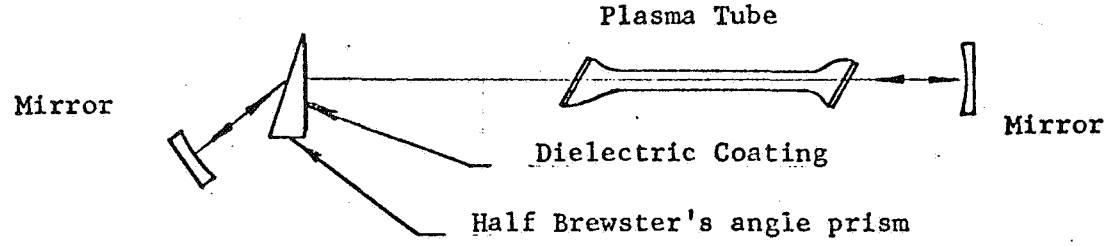


Fig. 6

By placing the rear surface of the internal mirror at Brewster's angle, reflection losses are avoided. The prism may be mounted on a slide providing motion perpendicular to the plane of the drawing, in which case the prism may be moved to bring surfaces of differing reflectivity into position in the beam.

Robert S. Peeters
New Technology Officer

RSP:ejw

Reprinted from IEEE JOURNAL OF *QUANTUM ELECTRONICS*
Vol. QE- 2, Number 8, August 1966
Pp. 235-243
Copyright 1966, and reprinted by permission of the copyright owner
PRINTED IN THE U.S.A.

N67-35629 (NASA-CR-88193) DEVELOPMENT AND FABRICATION OF RING LASER SYSTEMS. P. H. Lee (Perkin-Elmer Corp.) Dec. 1966. pp. 178 1/16
unclas

5B1—Measurement of Saturation Induced Optical Nonreciprocity in a Ring Laser Plasma

P. H. LEE AND J. G. ATWOOD

Abstract—**When a gas laser plasma is illuminated by unequally intense laser beams traveling in opposing directions, its index of refraction becomes significantly nonreciprocal. We have studied this effect by measuring the beat frequency between the counter-rotating beams in a 6328Å He–Ne ring laser under controlled conditions.**

Frequency locking was effectively eliminated by using a Faraday effect beat frequency bias element. The measured beat frequency became a strong function of two independent parameters: the ring resonator tuning and the beam intensity difference.

A second Faraday effect element was introduced to control nonreciprocal losses within the ring resonator. Servo loops controlling both the total laser intensity and the intensity ratio between the counterrotating beams permitted direct measurement of the nonreciprocal gain caused by saturation, or hole burning. The effects observed are contained in Aronowitz' theoretical description of ring lasers.

Manuscript received May 2, 1966. This worked was supported in part by the Air Force Avionics Laboratory, AVTL, Wright-Patterson Air Force Base, Dayton, Ohio, under contract AF33(615)-2059, and by the National Aeronautics and Space Administration, George C. Marshall Space Flight Center, Huntsville, Ala., under contract NAS8-11669. This paper was presented at the 1966 International Quantum Electronics Conference, Phoenix, Ariz.

The authors are with the Research Department, The Perkin Elmer Corporation, Norwalk, Conn.

Introduction

IN THE FIRST published paper suggesting applications of the ring laser, Rosenthal[1] saw the device as a generally useful detector of optical path nonreciprocity. This is inequality of optical path length around the ring resonator when it is traversed in opposite directions. He suggested its use not only as a rotation-sensor, but also for detection of magneto-optic effects and optical path nonreciprocities of other origin.

In the experiments described here, we have used a ring laser to observe optical nonreciprocity in a gaseous laser active medium. The nonreciprocity we see in this

[1] A. H. Rosenthal, "Regenerative circulatory multiple-beam interferometry for the study of light-propagation effects," *J. Opt. Soc. Amer.*, vol. 52, pp. 1143–1148, October 1962.

experiment is caused by saturation of the inverted population by the two opposite traveling light waves in the ring laser.

The effect is interesting for several reasons. First, it is a way of studying the interaction of light with matter in a configuration which is uniquely simple theoretically. It is so because in the limit where the laser is operated in a pure traveling-wave mode, the entire active medium is subject to a constant uniform intensity of illumination. We were able in some of these experiments to approach this mode of operation.

Second, the saturation induced nonreciprocity in the gas is interesting because it represents a major potential source of error in ring laser rotation sensors.

In our experiments, we have broadened the application of the ring laser to measure more than the nonreciprocity of optical path length. We have measured the nonreciprocity of optical transmittance, as well. This was done by introducing into the ring an optical component which gave us control over the nonreciprocity of transmittance.

With the apparatus we used we could thus control both the real and imaginary parts of the complex index of refraction within the ring resonator. These could be controlled separately for each of the two directions of traversal.

Using this tool, we were able to measure directly the depth and profile of a hole burned in the Doppler broadened gain curve. This was done together with a direct measure of the dispersive effect of the same hole on the ring laser's beat frequency.

The apparatus used was an experimental breadboard laser not intended for rotation sensing, but rather for testing new measurement techniques and new magneto-optic components.

Experimental Apparatus

The measurements were made using the apparatus shown in Fig. 1.

The 6328Å ring laser consisted of an isosceles triangle with base angles of 21°, and a perimeter of about 70 cm. It included as refracting elements a single dc excited plasma tube with silica Brewster angle windows at each end, a silica Faraday rotation element for introducing a nonreciprocity of optical path length, and another silica magneto-optic element for introducing nonreciprocity of transmission. At the 21° angles, dielectric coated mirrors, one flat and one 120 cm concave radius, completed the ring.

The perimeter of the ring was scanned through several orders by a piezoelectric actuator which moved the flat mirror.

The area of the ring was about 135 cm^2. The optical path around the perimeter was such that the measured frequency spacing between longitudinal modes was 368 MHz. In all experiments the ring oscillated in a TEM_{00} transverse mode, and never in more than one longitudinal mode in each direction. The light was plane polarized with the electric vector horizontal.

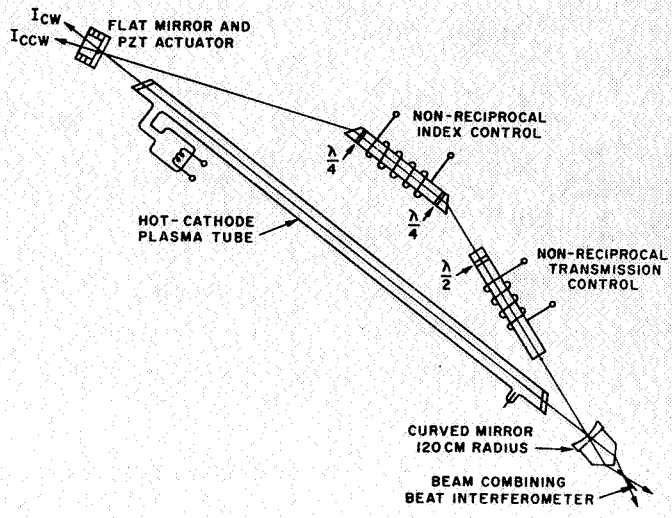


Fig. 1. Schematic diagram of ring laser.

The sensitivity to angular rotation in the ring was calculated to be 10^5 Hz/rad/s. The plane of the ring was horizontal and stationary with respect to the laboratory at 41.75°N latitude. Hence, the rotational frequency splitting induced by the earth's rotation rate was 5 Hz. This amount was negligible compared to the nominal 50 kHz splitting magneto-optically introduced in these experiments.

The beat frequency was observed by interfering the clockwise and the counterclockwise beams transmitted by the concave mirror, detecting the resultant beat on a photomultiplier. The intensities of the clockwise and counterclockwise beams transmitted through the flat mirror were observed with two photomultipliers. The intensity of the sum of clockwise and counterclockwise beams was measured with a silicon solar cell.

The components in the ring were as follows.

A. Plasma Tube

The tube was of glass having 1.5-mm inner bore and 22.5 cm of active length. It had 0.2-cm-thick fused silica end windows at Brewster's angle. The tube was dc excited with a servo controlled current between 3 and 7 mA. It had a heated oxide-coated cathode.

The plasma tube was filled with a 7-to-1 ratio mixture of He^3 and of Ne^{22} which was at best 99.97 percent isotopically pure. The total pressure filled was 3 torr.

B. Laser Power Control

The laser power output could be controlled (or servoed) by controlling the laser plasma anode current. This was delivered by an electronic current source with output current proportional to a remote voltage input signal.

C. Nonreciprocal Transmission Control

The difference between the power levels of the clockwise and counterclockwise beams could be adjusted (or servo controlled) by changing the current in the solenoid

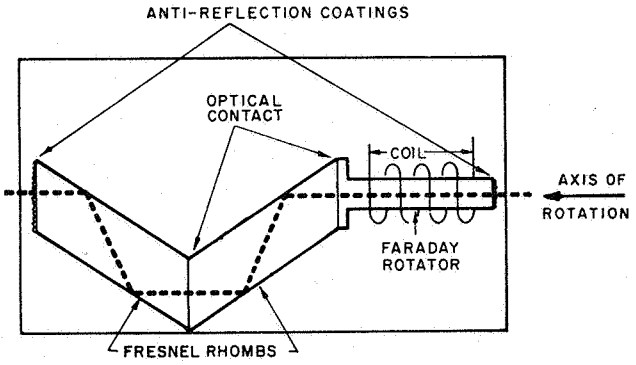


Fig. 2. Nonreciprocal transmission control diagram.

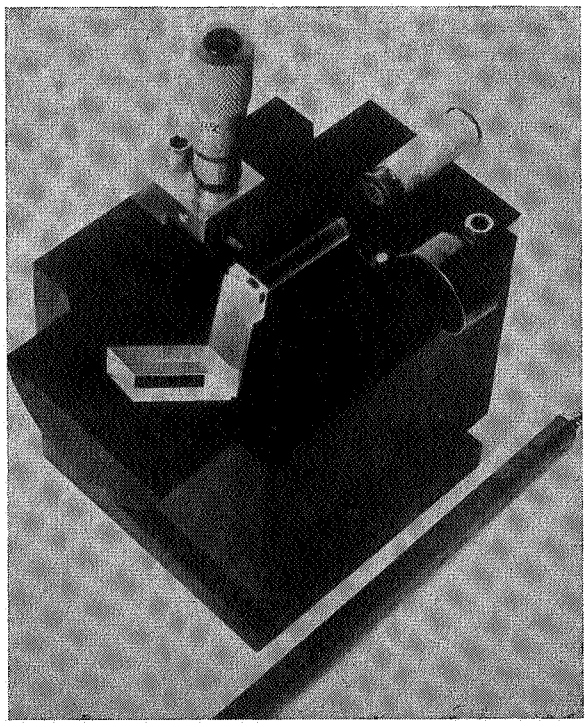


Fig. 3. Nonreciprocal transmission control (exploded view). The micrometer rotates the whole structure and thereby the $\lambda/2$ retardation element.

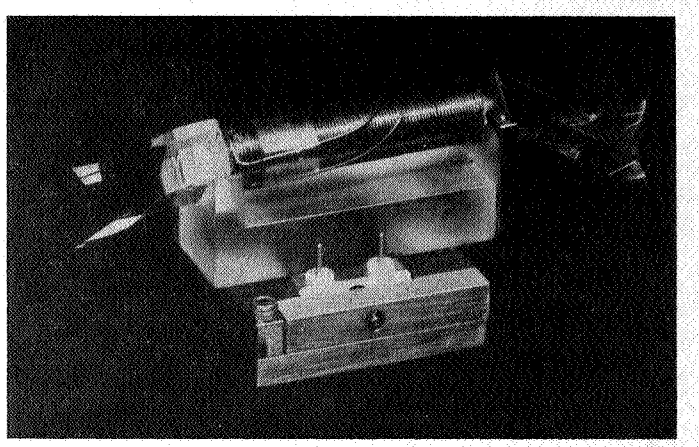


Fig. 4. Nonreciprocal index control (bizarre bar).

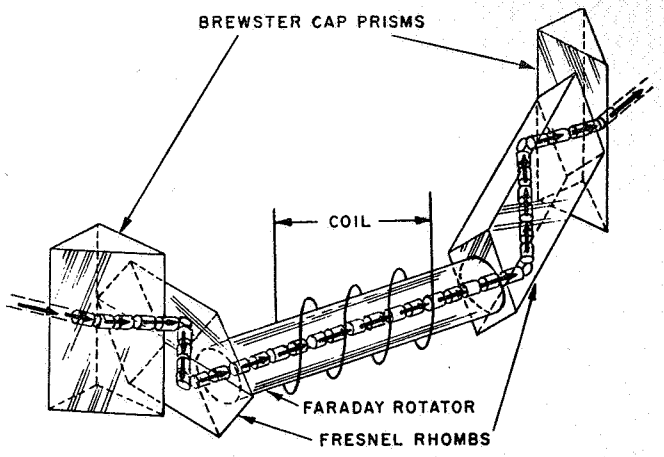


Fig. 5. Nonreciprocal index control (bizarre bar). Material: fused silica. Net beam deviation is a refraction through 42°. Reflection deviations cancel.

generating a longitudinal magnetic field in the device shown in Fig. 2.

This unit consists of a mechanically rotatable half-wave retardation element composed of two Fresnel rhombs in tandem, followed by a magneto-optic Faraday rotator. It functions as follows. The Fresnel rhombs rotate the plane of polarization of the clockwise and counterclockwise beams reciprocally. The magneto-optic element rotates the planes of polarization of the clockwise and counterclockwise beams nonreciprocally. For fixed settings of rhomb angle and solenoid current, these rotations add for one direction of circulation and subtract for the other. The direction for which they subtract is transmitted with lower loss. The direction for which they add suffers higher losses at the Brewster's angle surfaces in the resonator.

A photograph of the unit is shown in Fig. 3. The optical parts are constructed entirely of fused silica. The end faces of the nonreciprocal transmission element are a few degrees off normal to the beam. They are dielectric coated for low reflection loss. With this unit we could conveniently produce nonreciprocal transmission of 10^{-3}. This was large enough to extinguish one direction of propagation while the other oscillation continued with useful intensity.

D. Nonreciprocal Index Control

The frequency splitting between the clockwise and counterclockwise modes of the ring laser was controlled by changing the current in the solenoid of a second magneto-optic element shown in Fig. 4. This device functions as follows. The plane polarized clockwise and counterclockwise light beams enter the Fresnel rhombs through attached Brewster's angle faces, and are converted to circularly polarized light by two total internal reflections inside the material. Then, as shown in Fig. 5, the beams pass through a section of fused silica in a longitudinal magnetic field generated by current in a surrounding solenoid. In this section the index of refraction is nonreciprocal for the two directions of propagation of circularly polarized light.

With this unit we could conveniently produce nonreciprocal optical path length of $\pm 10^{-3}\lambda$, causing mode splittings of ± 350 kHz in this ring resonator. Fifty kHz

was sufficient to eliminate completely all mode-locking effects between the two directions of circulation except when intensity competition occurs at the center of the Doppler line.

The stability of the frequency splitting introduced by this device was about ±25 Hz.

E. Perimeter Tuning Control

The mean frequency of the clockwise and counterclockwise modes was tunable through the Doppler line by a piezoelectric actuator which could move the flat mirror over a full range of ±3 orders. Its frequency response permitted saw-tooth scanning of the mean laser frequency at repetition rates from 0 to 5 kHz. Typical scan rate was 2 GHz/s. The frequency sweep voltage was displayed on the horizontal trace of an oscilloscope, permitting us to plot on the oscilloscope screen various laser performance parameters as a function of mean laser frequency. In all these plots, the longitudinal mode spacing and the center of the Doppler line could be clearly identified. Hence, direct measurements of laser frequency with respect to the Doppler line could be made. We used these controls to study several properties of single mode ring lasers.

Observation of the Competition Effect Under Nondegenerate Conditions

As a single-mode, isotopically pure ring laser is tuned through its Doppler line, an instability occurs near the Doppler line center. During this instability, one of the two directions of circulation goes out and the other gets brighter. This effect, which has long been observed experimentally by us and others, has been theoretically described by Aronowitz[2] and Gyorffy and Lamb.[3] It can be explained as the result of competition between the two beams for stimulated emission from the group of excited atoms in the Doppler distribution having nearly zero component of velocity along the beam.

In ring lasers with small nonreciprocal optical path length bias and no control over nonreciprocal transmission, the competition effect often appears erratic because it is masked by two degeneracies. One is degeneracy of optical frequencies, which leads to phaselocking of the clockwise and counterclockwise oscillations. The other is a degeneracy of the clockwise and counterclockwise transmission which permits random nonreciprocal environmental disturbances to determine which beam will win the competition.

When this double degeneracy is removed by enough nonreciprocal transit time to eliminate phase locking, and by enough controlled nonreciprocal transmission to override random disturbances, the competition effect becomes consistent and reproducible.

The oscilloscope photos in Figs. 6, 7, and 8 show the

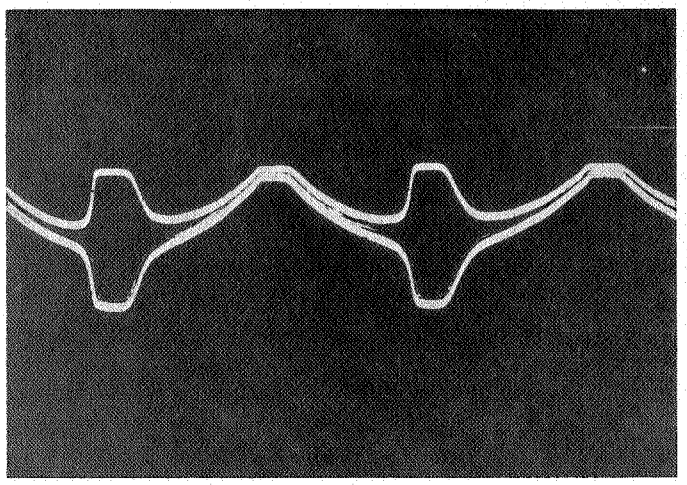


Fig. 6. Intensity competition at line center. The oscillogram showing the simultaneous variation of clockwise and counterclockwise power output vs. linear perimeter sweep over more than two orders. Zero power is at the top of the traces. Power increases downward. The laser goes out between orders where the Doppler broadened gain falls below threshold. One beam is extinguished in the competition near the line center. Sweep direction is left to right at 5 GHz/s. The pattern repeats at the longitidinal mode spacing of 368 MHz. Beat frequency bias is 50 kHz and nonreciprocal transmission is 0.5×10^{-4}.

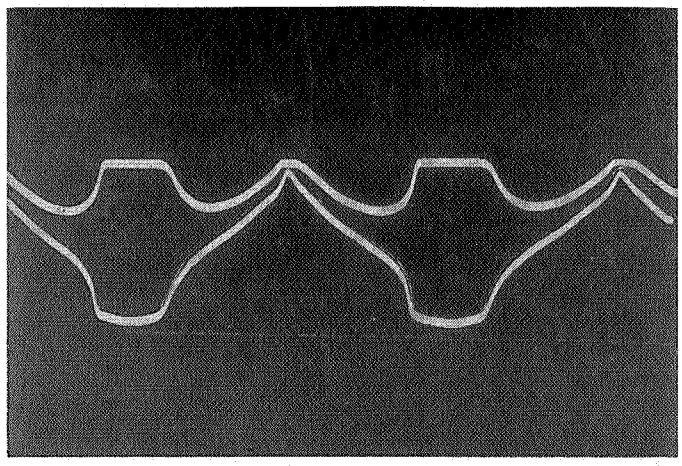


Fig. 7. Effect of increased nonreciprocal transmission on competition. The same conditions as Fig. 6 except that the nonreciprocal transmission ratio is twice as large. The ratio of beam powers is farther from unity at all frequencies and extinction occurs over a wider frequency range.

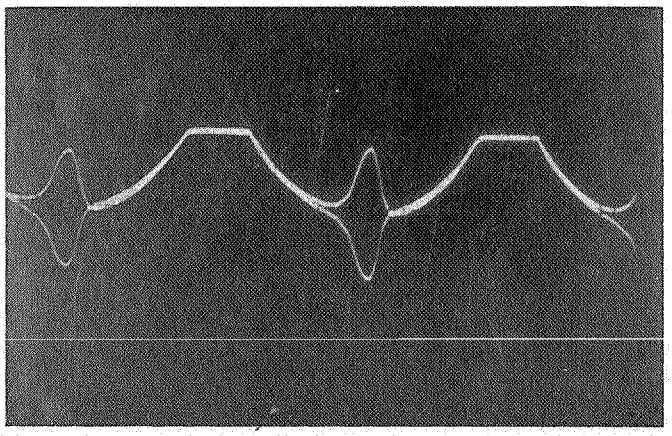


Fig. 8. Competition effect with near minimum nonreciprocal transmission. Otherwise the same conditions as Fig. 6 and Fig. 7 except just enough nonreciprocal transmission to override disturbances. The 50-kHz beat bias prevents complete extinction at the line center. Hence, the linewidth and asymmetry of the effect can be seen.

[2] F. Aronowitz, "Theory of a traveling-wave optical maser," *Phys. Rev.*, vol. 139, pp. A635–A646, August 2, 1962.
[3] B. Gyorffy and W. E. Lamb, Jr., private communication.

effect. In all these photos, a 50 kHz-bias eliminates mode locking and the plasma anode current is held constant. Thus, we see the Doppler-population-dependent variation of power with laser frequency is present in both beams except at the center of the Doppler line. Here, one beam is extinguished and the power in the other beam increases by the amount missing from the extinguished beam.

In Fig. 6 the nonreciprocal transmission ratio is about 0.5×10^{-4}. It causes extinction of the weak beam over 37 MHz. For greater ratios the extinction occurs over a wider frequency range, as shown in Fig. 7, where a transmission ratio of 1.0×10^{-4} causes extinction over 78 MHz.

As the transmission ratio approaches unity, but is just sufficiently nonreciprocal to override disturbances, we see that the large beat frequency bias prevents the total extinction of the weaker beam. This is shown in Fig. 8.

Operating in this last condition permits us to observe the true linewidth and profile of the competition effect. It has a linewidth at half-height of about 30 ± 2 MHz in the laser we used.

Note that the line profile is unsymmetrical. This is a real effect not dependent on scanning conditions. We observed it in all our experiments. The peak is skewed about 8.5 ± 2 MHz to the high frequency side of the center of its base.

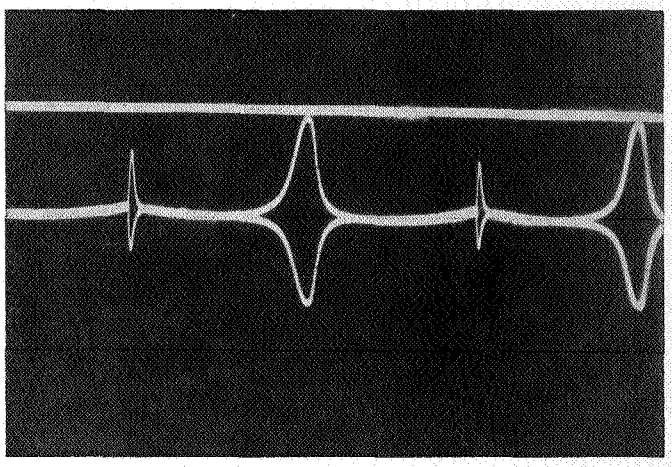


Fig. 9. Competition when Doppler gain effect is removed by sum power servo stabilization. Lower traces are simultaneous power in CW and CCW output beams (increasing downward). Upper trace is zero power line. Competition nearly to extinction appears near the Doppler line center. Longitudinal modes switch at the order ends. Note the otherwise constant and equal output powers.

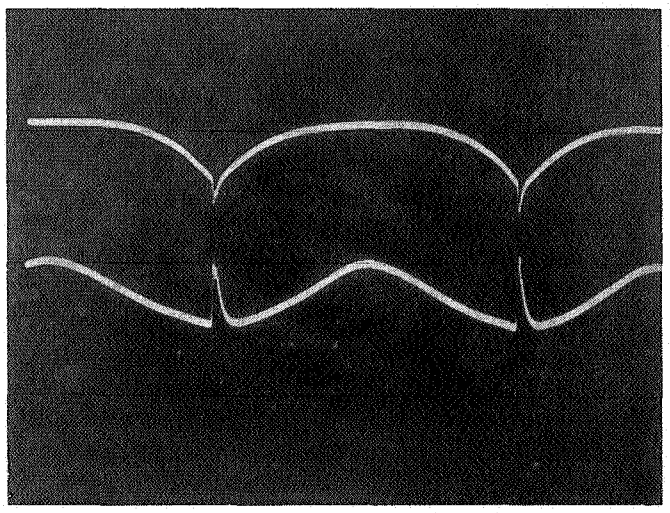


Fig. 10. Variation in servo error signals with perimeter tuning scan. Maximum currents downward. *Upper trace:* total beam power control error needed to remove normal Doppler gain variation. *Lower trace:* beam power ratio control error signal showing a peak at the Doppler line center with an apparent linewidth of 225 MHz. This signal represents the nonreciprocity of transmission needed to restore the ratio of beam powers to 0.59. Oscilloscope frequency response was reduced by high-pass RC filters with a 2×10^{-4} second time constant.

Operation with Beam Power Servo Controlled

A. Total Beam Power Control Servo System

The sum of the power levels of the two beams in the resonator could be servo controlled by varying the laser plasma anode current with an error signal derived from the sum of the currents in the corresponding photomultipliers. The loop gain of this power control was greater than 40 dB and flat with frequency from dc to 30 kHz, falling at 6 dB/octave above this.

Figure 9 shows operation using this control, with just enough small fixed nonreciprocal transmission introduced to override disturbances. The beam powers are equal and constant with frequency except in the center of the Doppler line, where the competition occurs as before.

The error signal of this servo represents the additional pumping of the plasma required to maintain a constant flow of power into the combined output beams. The pumping current varied as the laser frequency was tuned through the Doppler line, having its minimum current at the maximum of this line as shown in Fig. 10.

B. Beam Power Ratio Control Servo

The ratio between the power levels of the clockwise and counterclockwise beams could be servo controlled by varying the current in the nonreciprocal transmission control with an error signal derived from the difference of the currents in the corresponding photomultipliers. The servo holds this difference to a null.

To control the power ratio between the beams, we put a calibrated optical density filter into one beam ahead of the photomultiplier. To maintain the null of photomultiplier currents, the nonreciprocal transmission control adjusts the ratio between beam powers to be equal to the transmittance of the filter. The error in the ratio is small if the loop gain is large.

The loop gain of this ratio control varied from 10 to 40 dB over the resonator tuning range used. The nonreciprocal transmission control current varies as the laser frequency is tuned through the Doppler line, having its minimum current at the maximum of this line, as shown in Fig. 10.

C. Clamping of Hole Populations

Studies of the optical effects of saturation of laser plasmas are often made difficult by variation of the beam power levels during the experiment. The two servos described above make these measurements simple and

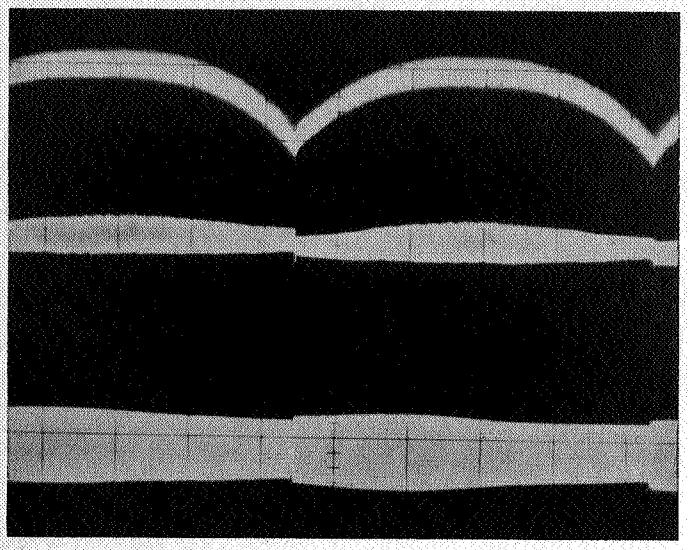


Fig. 11. Beam ratio servo preserves beat at Doppler line center. *Upper traces:* sum power servo error signal. Low-pass filter removed. *Middle trace:* power ratio error signal. Low-pass filter removed. *Lower trace:* 50-kHz beat frequency envelope. These traces show two effects. First, the beat frequency is strong and continuous through the Doppler line center, showing that the intensity ratio servo has eliminated competition. Second, they show a high-frequency oscillation on the beam power servo error signals which was often present but did not influence the average value of the signals. It is filtered out in most of the other traces in this paper.

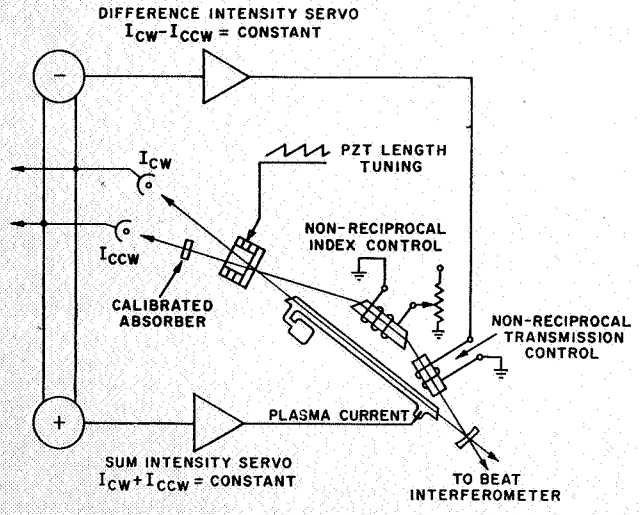


Fig. 12. Block diagram of experimental apparatus. The two servos in combination maintain both the clockwise and counterclockwise hole populations at preset constants throughout a perimeter scan across the Doppler line. Using balanced photocells, the calibrated absorber shown sets the power ratio between the clockwise and counterclockwise beams.

direct by even removing power variation with scan of mean laser frequency through the Doppler line.

Because the resonator losses are naturally constant with laser tuning, and the total optical power output is clamped by the total beam power control, the total beam power servo in effect clamps the sum of the hole populations caused by the clockwise and counterclockwise beams to a fixed value independent of the tuning of the laser resonator through the Doppler line. Because the ratio between the optical power outputs of clockwise and counterclockwise beams also is clamped by the power ratio servo, we have in effect held constant each individual hole population, one of which feeds power to the clockwise and the other to the counterclockwise beam. Thus, each hole population is separately held to a fixed value, independent of the tuning of the laser resonator through the Doppler line.

D. Stable Operation at the Doppler Band Center

The loop gain of the intensity ratio servo is sufficiently high so that when it is used, the competition effect at the Doppler line center is removed. We can then scan the mean laser frequency through the center of the Doppler line, maintaining constant any desired intensity of the clockwise and counterclockwise beams independently. In addition, because the 50-kHz mean beat frequency bias removes phase locking between the two beams, the beat amplitude is constant as we scan through the center of the Doppler line. This is shown in Fig. 11. Figure 12 shows the apparatus used.

Observation of Saturation Induced Nonreciprocity

Operating with a 50-kHz mean beat frequency bias, and with the intensity sum servo and the intensity ratio servo both controlling the beam powers, we scanned the mean laser frequency through the Doppler line.

During this scan, we measured the beat frequency variations about its mean using a Hewlett-Packard model 5244L Counter, followed by a Hewlett-Packard 581A, Digital-to-Analog Converter. The analog signal, actually a measure of the time to count 1000 periods of the beat signal, was plotted on the same oscilloscope with the intensity sum servo error signal, which regularly serves to identify the mode spacing and Doppler line center.

A typical result is shown in Fig. 13. We have observed a variation in the beat frequency of as much as ± 12 kHz, about the mean 50-kHz bias. The presence of this large variation in the beat frequency implies a correspondingly large power and frequency dependent nonreciprocity in the optical path length around the ring for the clockwise and counterclockwise beams.

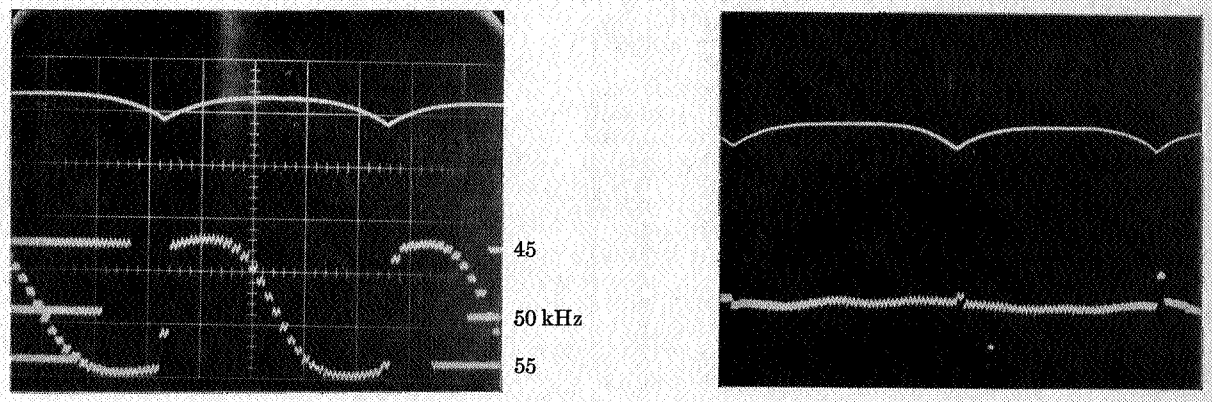
This saturation-induced optical path length nonreciprocity has the following properties.

1) It varies with mean laser frequency as the dispersion curve associated with an absorption line, centered on the Doppler line.

2) Its magnitude is dependent on the powers of the clockwise and counterclockwise beams. It is nearly zero when the beam powers are equal. It reverses when the strong and weak beams exchange.

3) It is independent of the amount of the beat frequency bias. Reversing the 50-kHz bias direction has no effect on the amount and direction of the absolute frequency shift.

The optical path length nonreciprocity is always accompanied by a variation in the nonreciprocal transmission control current. This is also dependent on beam power and independent of beat frequency bias. The shape of this current variation is shown in Fig. 10. The scan



(a) (b)

Fig. 13. Beat frequency variation vs. perimeter tuning. These traces show the nonreciprocal index effect. Peaks of the upper traces mark Doppler line centers. Lower traces show variation of the beat frequency as the laser is tuned through the Doppler line center. (a) Beam power ratio of 0.59, $\Delta f = \pm 6$ kHz. (b) With 10 times scale expansion, the nonreciprocal dispersion goes to zero for a beam power ratio of 1.00.

TABLE I
MEASUREMENTS OF SATURATION INDUCED NONRECIPROCITY

Average Beam Intensity In Gas, W/cm²		Observed Nonreciprocity		Bandwidth
Strong Beam	Weak Beam	Peak-to-Peak Shift in Beat Frequency kHz	Peak-to-Peak Change in Nonreciprocal Transmission	Peak to Peak of Dispersion Curve MHz
0.55	0.33	9.0	3.6×10^{-4}	—
0.34	0.20	12.0	2.2×10^{-4}	220
0.30	0.286	1.3	—	—
0.21	0.13	8.5	—	—
0.17	0.10	9.0	—	216
0.16	0.016	25.0	3.6×10^{-4}	—
0.147	0.147	0.0	—	—
0.13	0.077	7.0	—	240

range in this figure does not show the full height of the Lorentzian.

This nonreciprocity is explainable as the effects of gain and dispersion associated with two hole populations of unequal strength symmetrically placed in the Doppler velocity distribution.

Table I shows a summary of measured nonreciprocities as a function of beam powers. In reducing the data, the beam power outside the resonator was corrected by the exit mirror transmittance to calculate the beam intensity in W/cm² in the gas. The average beam area was taken as that of a circle of 0.04-cm radius, the calculated radius to the $1/e$ intensity in the Gaussian mode.

Nonreciprocity of path length is expressed as the peak-to-peak change in the observed beat frequency shift of the dispersion curves.

Nonreciprocity of gain in the gas is expressed as the peak-to-peak change in nonreciprocal transmission required to maintain a fixed ratio between weak and strong beams, as the Doppler line is scanned.

The nonreciprocal transmission was calculated from the measured solenoid current, the tabulated Verdet constant of silica, and the measured angles between the plane of the Fresnel rhomb and the planes of polarization in the resonator before and after the rhomb was rotated.

Discussion of Results

The general nature of the effects we observe are predicted in the published theory. For the free running case, without servo controls, the behavior of the sum of the two beam powers is approximately that which can be obtained from Aronowitz,[2] including the existence of competition effects. However, the frequency range over which it occurs appears broader. Our results operating through the center of the Doppler line with a variety of beam powers under servo control, so that the intensity instability is removed, show in addition that no rapid change in plasma-pumping current is required to maintain constant beam sum through the competition region.

Nonreciprocal Gain of the Plasma

The variation in nonreciprocal transmission required to preserve a fixed beam power ratio can be obtained from Aronowitz' equations as follows.

In our experiments, the maximum optical frequency scan was ±184 MHz from the Doppler line center. The dispersion peaks were measured at between ±100 MHz and ±120 MHz. The Doppler linewidth factor, Ku = 900 MHz. Therefore, at the points of measurement, the normalized frequency differences of Aronowitz' notation are as follows:

$$\xi_i = (\omega_i - \omega_0)/Ku \cong 0.125$$

$$\eta \cong \gamma_{ab}/Ku \cong 0.125.$$

Also, since the beat frequency is never more than 60 kHz,

$$|\xi_1 - \xi_2| < 10^{-4}.$$

We may thus make the approximations that $\exp(-\xi_1^2) \cong \exp(-\xi_2^2) \cong 1$, $Z(\xi_1) \cong Z(\xi_2)$. With these simplifications, and taking the difference of Aronowitz' equations (42) and (43), we obtain

$$\frac{1}{Q_1} - \frac{1}{Q_2} \cong \frac{A\pi^{1/2}}{\epsilon_0}[(I_2 - I_1)(1 - L(\xi))]. \quad (1)$$

Here, Q_1 and Q_2 are the cold resonator Q's for clockwise and counterclockwise beams, and $L(\xi)$ is a Lorentzian function defined as

$$L(\xi) = [1 + (\xi/\eta)^2]^{-1}. \quad (2)$$

A is a factor containing the inverted population density $\bar{N}(t)$ and the transition dipole moment μ_{ab}:

$$A = |\mu_{ab}|^2\bar{N}(t)/\hbar Ku. \quad (3)$$

I_1 and I_2 are dimensionless intensities:

$$I_i = |\mu_{ab}|^2E_i^2/2\hbar^2\gamma_a\gamma_b. \quad (4)$$

The action of the nonreciprocal transmission servo is to force the equation

$$\frac{1}{Q_1} - \frac{1}{Q_2} = i(t)M \quad (5)$$

where $i(t)$ is the current in the nonreciprocal transmission control and M the factor relating current to transmittance difference. During the scan, A is made slowly varying with frequency as can be seen by the relatively constant error signal of beam power sum servo. Hence, a plot of $i(t)$ should reflect a Lorentzian band of twice the natural linewidth, γ_{ab}, with amplitude proportional to the beam power difference. This is essentially what we see in Fig. 10.

Nonreciprocal Refractive Index

Similarly, starting with the simplified versions of Aronowitz' frequency equations (44) and (45) and subtracting,

$$\delta\omega = 2\Omega + \frac{\pi^{1/2}A}{\epsilon_0}(I_2 - I_1)(\xi/\eta)L(\xi). \quad (6)$$

Here $\delta(\omega)$ is the beat frequency and 2Ω is the bias on the beat frequency.

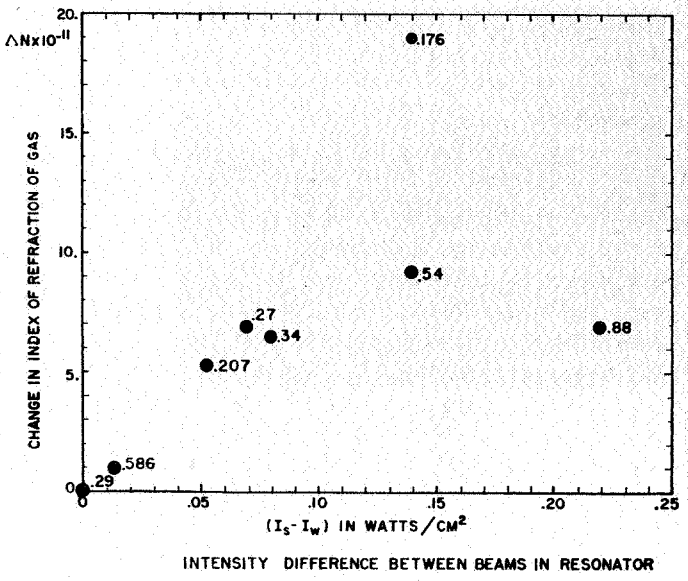


Fig. 14. Measured refractive index nonreciprocity vs. beam intensity difference. The corresponding beam intensity sum is written beside each point.

Again, A is made a slowly varying function by the sum servo. Hence, a plot of the beat frequency vs. mean laser frequency should show a dispersion curve of linewidth $2\gamma_{ab}$. The observed linewidth is seen to range between 210 to 240 mHz. This suggests a γ_{ab} for the transition of about 112 ± 8 mHz.

The peak-to-peak beat frequency shift should be proportional to beam power difference. The plot of Fig. 14 shows this very roughly. Here, the frequency shift is converted to nonreciprocity of refractive index in the gas.

The plot shows a general tendency for the nonreciprocal refractive index to be proportional to $I_2 - I_1$. The value of the sum of the intensities, $I_1 + I_2$, is written beside each point.

Scatter in the data is attributable in part to fluctuation from run to run in the exact value of the Q's of the resonator.

In an effort to see how small the nonreciprocal dispersion could be held, if desired, we balanced the beam intensities as well as we could. The minimum beat frequency excursion we could maintain was about 100 Hz.

We compared the measured nonreciprocal gain of the holes with the measured dispersions they produce for consistency as follows. We eliminate A from (6) using (1). This yields the relation

$$\delta\omega = 2\Omega + \frac{\omega}{2}\left[\frac{1}{Q_1} - \frac{1}{Q_2}\right]\frac{\xi}{\eta}\left[\frac{L(\xi)}{1 - L(\xi)}\right]. \quad (7)$$

Converting the measured nonreciprocal transmittance ΔT, of the whole path length L, to normalized units via the relation

$$\left[\frac{1}{Q_1} - \frac{1}{Q_2}\right] = \frac{\lambda}{2\pi L}\Delta T, \quad (8)$$

substituting into (7) and evaluating the difference of beats for $\xi = \pm\eta$, we calculated the peak-to-peak shift of beat frequency. This was 7 kHz at a beam power difference for which we measure 9 kHz.

Conclusion

In the use of ring lasers as rotation sensors, the magnitude of nonreciprocal dispersion effects we observe could be a source of major error. For example, in the ring we used, the nonreciprocity of transmittance would need to be maintained less than 10^{-7} to cause an error of less than 1 earth's rotation rate anywhere in the Doppler line. Our experiment showed that there were environmental disturbances of nonreciprocal transmission much larger than this. It appears, therefore, that the performance of ring lasers as rotation sensors will be affected by how well errors caused by nonreciprocal dispersion can be controlled in practice.

In these experiments, we had only rough control over the total cold Q of the ring resonator. We did not measure it accurately. The results suggest, however, that if accurate cold Q measurements were made, and the laser were protected from dust and misalignment to maintain the Q constant from run to run, the method described here could be used for measuring the dipole moment of laser transitions.

Acknowledgment

The authors thank W. E. Lamb, Jr., and A. Javan for helpful discussions, and G. W. Dueker and C. E. Theall for engineering the optical and electronic components used.